Identification of *in vivo* interactions of insulin receptor substrate 1 in murine liver

I n a u g u r a l - D i s s e r t a t i o n

zur

Erlangung des Doktorgrades

der Mathematisch-Naturwissenschaftlichen Fakultät

der Universität zu Köln

vorgelegt von

Nina Vanessa Wegner

aus Köln

Köln

2011

Berichterstatter: Prof. Dr. Jens Brüning
Prof. Dr. Günter Schwarz

Tag der mündlichen Prüfung: 24. Oktober 2011

“Causarum enim cognitio cognitionem eventorum facit.”

Die Kenntnis der Ursachen bewirkt die Erkenntnis der Ergebnisse.

Marcus Tullius Cicero (106-43 BC) in Topica

Contents

Contents 5

Figure index 9

Table index 11

Abstract 12

Zusammenfassung 13

1 Introduction 15

1.1 Obesity 15

1.2 Type 2 diabetes mellitus 17

1.3 Insulin signaling 18

1.3.1 Systemic effects of insulin 18

1.3.2 Molecular features of insulin signal transduction 20

1.3.3 Role of insulin receptor substrates in insulin signaling 22

1.3.4 Molecular basis of insulin resistance 24

1.4 Proteomic studies in the context of insulin signaling 30

1.5 Objectives 32

2 Materials and methods 34

2.1 Molecular biology techniques 34

2.1.1 General considerations 34

2.1.2 Cloning PCR 34

2.1.3 DNA sequencing 35

2.1.4 Gel extraction 36

2.1.5 Red E/T Recombination 36

2.1.6 Transformation of competent bacteria 36

2.1.7 Purification of plasmid DNA 36

2.1.8 TOPO TA cloning 37

2.1.9 Ligation 37

2.1.10 Linearization 37

2.1.11 Phenol chloroform extraction 37

2.1.12 Preparation of ES cell DNA 38

2.1.13 Restriction digest of genomic DNA 38

2.1.14 Southern blot 38
2.1.15 Isolation of genomic mammalian DNA 39
2.1.16 Genotyping PCR 39
2.2 Cell Culture Techniques 40
2.2.1 ES cell culture 40
2.2.2 ES cell transfection 40
2.2.3 Microinjection into blastocysts 41
2.2.4 In-vitro cre recombination 41
2.2.5 Fluorescence Microscopy 42
2.2.6 siRNA transfection 42
2.2.7 In-vitro insulin signaling 42
2.3 Animal Experiments 43
2.3.1 Animal care 43
2.3.2 Mouse models 43
2.3.3 Measurement of body weight and liver weight 43
2.3.4 Analysis of body composition 43
2.3.5 Collection of blood samples 43
2.3.6 Glucose tolerance test 44
2.3.7 Insulin tolerance test 44
2.3.8 Extraction of sample material 44
2.3.9 In-vivo insulin signaling 44
2.4 Protein Analysis 45
2.4.1 Organ lysis 45
2.4.2 Streptavidin affinity purification 45
2.4.3 Protein gel electrophoresis 46
2.4.4 Western Blot 46
2.4.5 In-gel trypsin digest 48
2.4.6 Desalting 48
2.4.7 Nano-LC-ESI-MS/MS mass spectrometry 49
2.5 Data Analysis 49
2.5.1 Label-free quantitative analysis 49
2.5.2 General calculations and analysis 49
2.5.3 Statistical methods 49

3 Results 50
3.1 Generation of the targeting vector 50
3.2 Generation of ROSA-CAGS-IRS1-TapTag mice 52
3.2.1 ES cell targeting 52
3.2.2 Transgenic mice 53
3.2.3 Physiological verification 54
3.3 Phenotypic analysis of ROSA-CAGS-IRS1-TapTag mice 55
3.3.1 Body weight 55
3.3.2 Body composition 56
3.3.3 Epigonadal fat pad weight 56
3.3.4 Blood glucose levels 57
3.3.5 Glucose tolerance 59
3.3.6 Insulin tolerance 60
3.3.7 Influence of IRS1 on metabolic phenotype 61
3.4 Proteomic analysis of IRS1 interactions 62
3.4.1 Sample generation 62
3.4.2 Verification of insulin signaling 63
3.4.3 Streptavidin affinity purification 63
3.4.4 Mass spectrometry and label-free quantification 65
3.4.5 Immunodetection of putative IRS1 interaction partners 77
3.5 Role of 14-3-3ε interaction with IRS1 79
4 Discussion 81
4.1 Implications of transgenic expression of IRS1-TapTag on the metabolic phenotype 81
4.2 IRS1 interactions 82
4.2.1 Phosphatidylinositol-3 kinase interaction 83
4.2.2 14-3-3 protein interaction 84
4.2.3 Novel mechanism for the modulation of IRS1 serine phosphorylation 85
4.2.4 Lyn protein interaction 86
4.2.5 Nuclear protein interactions 87
4.2.6 Mitochondrial protein interactions 87
4.2.7 Metabolic protein interactions 88
4.2.8 Cytoskeletal protein interactions 89

4.3 Affinity purifications and their limitations 89
4.4 Implications for insulin resistance 90
5 Perspectives 92
6 Supplemental Data 93
7 References 114

Acknowledgements 131

Statement / Erklärung 132

Figure index

Figure 1: Development of age-standardized mean BMI (black line) and 95% uncertainty intervals (shaded area) between 1980 and 2008; rearranged from (*1*)..... 16
Figure 2: The insulin signal transduction pathway..... 21
Figure 3: Comparison of protein structures of mouse insulin receptor substrates; from (*85*). 23
Figure 4: Known serine phosphorylation sites on IRS1 and IRS2 and the respective kinases inducing the phosphorylation; from (*99*). 27
Figure 5: Scheme of the pCTAPneokana construct, containing the TapTag sequence and a FRT (ellipses) flanked resistance cassette under the control of prokaryotic Pgb2 and eukaryotic PGK promoters. 50
Figure 6: Gene Targeting strategy for the homologous recombination of the ROSA-CAGS-IRS1-TapTag targeting vector into the ROSA26 locus and modified locus after cre-mediated excision of the loxP flanked stop signal..... 51
Figure 7: Southern Blot results for three individual ES cell clones. 52
Figure 8: Verification of functional integration of the ROSA-CAGS-IRS1-TapTag construct in transfected ES cells. 53
Figure 9: Chimeric mouse with an estimated 95% chimerism..... 53
Figure 10: Western blot of hepatic endogenous IRS1 and the elongated IRS1-TapTag in a mouse heterozygous for IRS1-TapTag. 54
Figure 11: Western blot of IRS1 expression in selected issues. 54
Figure 12: Average body weight of female IRS1-TapTag mice and controls over the course of 13 weeks..... 55
Figure 13: Average body weight of male IRS1-TapTag mice and controls over the course of 13 weeks. 56
Figure 14: Average body fat content of IRS1-TapTag mice and controls at the age of 20 weeks. 56
Figure 15: Average epigonadal fat pad weight of IRS1-TapTag mice and controls at the age of 16 weeks. 57
Figure 16: Average blood glucose of female mice with ad libitum access to the respective diet..... 57
Figure 17: Average blood glucose of male mice with ad libitum access to the respective diet. 58
Figure 18: Average blood glucose of fasted mice at the age of 12 weeks. 58

Figure 19: Blood glucose levels of female mice in response to a bolus injection of glucose in a glucose tolerance test. 59
Figure 20: Blood glucose levels of male mice in response to a bolus injection of glucose in a glucose tolerance test..... 60
Figure 21: Blood glucose levels of female mice in response to a bolus injection of insulin in an insulin tolerance test. 61
Figure 22: Blood glucose levels of male mice in response to a bolus injection of insulin in an insulin tolerance test..... 61
Figure 23: Scheme of different conditions applied for a set of 24 mice..... 62
Figure 24: Western blot analysis of protein lysates used for affinity purifications and subsequent mass spectrometry analysis. 63
Figure 25: Representative Western blot of input, unbound protein fraction, wash fractions and biotin eluate of a streptavidin affinity purification. 64
Figure 26: Western blot analysis of biotin eluates of affinity purification..... 64
Figure 27: Coomassie gradient gels with all 24 biotin eluates prepared for subsequent mass spectrometry analysis. 65
Figure 28: Scatter plot of identified interacting proteins after NaCl and insulin treatment. 66
Figure 29: Scatter plot of identified interacting proteins for NCD- and HFD-fed mice.... 67
Figure 30: Scatter plot of IRS1 interacting proteins, significantly changed between NCD and HFD. 68
Figure 31: Scatter plot of IRS1 interacting proteins, significantly changed between NaCl and insulin treatment..... 71
Figure 32: Label-free quantification of bait protein IRS1 (A) and identified subunits of the known interacting protein phosphatidylinositol 3-kinase. 75
Figure 33: Label-free quantification of members of the 14-3-3 protein family. 76
Figure 34: Label-free quantification of tyrosine-protein kinase Lyn..... 77
Figure 35: Western blot analysis of putative IRS1 interaction partners in IRS1-TapTag liver lysates and eluates after streptavidin purification. 78
Figure 36: Western blot analysis of Hepa 1-6 cells. Content of the indicated proteins in control cells and after 14-3-3ε siRNA knockdown. 80
Figure 37: Role of 14-3-3ε and possible role of 14-3-3ζ/δ in the modulation of serine/threonine kinases PKC and QSK. 86

Table index

Table 1: Primers used for cloning PCRs. Sequences in 5'-3' direction. 34
Table 2: Sequencing primers used for verification of insert IRS1-TapTag DNA. 35
Table 3: Primers used for genotyping PCRs. 40
Table 4: Antibodies used for immunodetection of proteins, with dilution applied and the ordering information. 47
Table 5: Amino acid sequence of the components of the TapTag, streptavidin binding peptide (SBP) (*172*) and calmodulin binding peptide (CBP) (*173*). 50
Table 6: IRS1 interacting proteins identified in biotin eluates of affinity purifications, which significantly varied between NaCl controls and insulin-treated mice… 68
Table 7: IRS1 interacting proteins identified in biotin eluates of affinity purifications, which significantly varied between NCD controls and mice fed HFD..... 71
Table 8-S: List of proteins potentially interacting with IRS1, which were identified in biotin eluates derived from TapTag liver lysates of affinity purifications. 93

Abstract

The development of obesity, insulin resistance and type 2 diabetes is highly interlinked. In the past, differential phosphorylation and protein interaction of the insulin receptor substrates (IRS) have been identified in the regulation of insulin signaling. However, the exact molecular changes on the IRS protein network that occur upon insulin resistance have yet to be determined completely.

In this study, a transgenic mouse model was generated featuring a streptavidin binding peptide tag allowing for IRS1 affinity purification in the liver and the assessment of *in vivo* interactions of IRS1 in diet-induced obesity and insulin signaling. To this end, affinity purification of hepatic streptavidin binding peptide-tagged IRS1 was performed and subsequent mass spectrometry and label-free quantification of the results led to the identification of 809 putative IRS1 interactions. Of the interacting proteins, association of 53 was reduced on HFD in the non-insulin stimulated state. Comparing the different diets upon insulin signaling, IRS1 association of 31 proteins was increased in NCD-fed mice, while in HFD-fed mice only 18 proteins were increasingly associated with IRS1.

Notably, the association of p110α and β with the IRS1-p85 complex was increased upon insulin treatment in NCD-fed mice. However, this effect was blunted on HFD, indicating a reduced insulin signaling capacity in HFD-fed mice and a contribution to the development of insulin resistance.

A tendency towards increased Lyn association with IRS1 upon HFD may likely lead to the development of insulin resistance, as for Fyn, a kinase related to Lyn, a regulation of energy expenditure and fatty acid oxidation has been described previously.

Moreover, 14-3-3 proteins ε, α/β, γ, η and ζ/δ increasingly interacted with IRS1 upon insulin signaling in NCD conditions, however on HFD interaction was reduced to levels seen in the non-insulin stimulated state. In this context, 14-3-3 proteins seem to serve as adaptor proteins regulating the association of kinases with IRS1, a mechanism that may affect the signaling functionality of IRS1 and thereby contribute to insulin resistance upon diet-induced obesity.

IRS1 interaction with two serine/threonine kinases, protein kinase C (PKC) and salt inducible kinase 3 (QSK) was identified in this study. IRS1-PKC interaction has been described previously in connection with 14-3-3 interaction. QSK, however, is a novel interacting protein of IRS1, which has been shown to also interact with 14-3-3 proteins. These findings strongly suggest that not only PKC-, but also QSK-mediated regulation of insulin signaling at the level of IRS1 may contribute to insulin resistance.

Zusammenfassung

Die Grundlagen zur Entstehung von Adipositas, Insulinresistenz und Typ 2 Diabetes sind stark verzahnt. Bisher wurde unter anderem das differenzielle Auftreten von Insulin Rezeptor Substrat (IRS)-spezifischen Phosphorylierungen und Proteininteraktionen für die Regulierung der Insulin Signaltransduktion verantwortlich gemacht. Jedoch sind die zugrundeliegenden molekularen Veränderungen des IRS Proteinnetzwerkes während einer Insulinresistenz noch weitgehend unbekannt.

In dieser Arbeit wurde ein transgenes Mausmodell generiert, welches es erlaubt, IRS1 spezifisch per fusioniertem Streptavidinbindepeptid aufzureinigen und *in vivo* Interaktionen von IRS1 zu charakterisieren. Speziell wurde der veränderte Zustand bei ernährungsinduzierter Adipositas und Insulinbehandlung in der Leber untersucht. Dazu wurde die Streptavidin-Affinitäts-Aufreinigung von hepatischem IRS1 in Kombination mit Massenspektrometrie durchgeführt. Eine anschließende markierungsfreie Quantifizierung der Ergebnisse führte zur Identifizierung von 809 putativen Interaktionspartnern von IRS1. Basal war die Assoziation von 53 dieser Proteine bei fettreicher Diät (FD) reduziert. Vergleiche zwischen normaler Diät (ND) und FD ergaben zudem, dass die Assoziation von 31 Proteinen mit IRS1 nach Insulingabe bei ND erhöht war, während nach Insulingabe bei FD nur 18 Proteine verstärkt mit IRS1 assoziiert waren.

Insbesondere war die Interaktion von p110α und β mit IRS1 nach Insulingabe bei ND erhöht. Jedoch blieb dieser Effekt bei FD aus, was auf eine reduzierte Insulinsignaltransduktion bei FD hinweist und darauf schließen lässt, dass die Regulation von p110 einen Beitrag zur Entstehung von Insulinresistenz leistet.

Für die Tyrosin-Proteinkinase Lyn wurde eine Tendenz zu verstärkter Assoziation mit IRS1 bei FD festgestellt, was möglicherweise zur Entstehung von Insulinresistenz beitragen kann. Fyn, eine verwandte Kinase von Lyn, ist dafür bekannt, Energieaufwand und Fettsäureoxidation zu regulieren.

Darüber hinaus interagieren die 14-3-3 Proteine ε, α/β, γ, η und ζ/δ nach Insulingabe bei ND verstärkt mit IRS1. Allerdings war diese Interaktion bei FD reduziert. In diesem Zusammenhang scheinen die 14-3-3 Proteine als Adapterproteine zu fungieren, die die Assoziation von Kinasen mit IRS1 regulieren, und so schließlich sowohl die Funktionalität von IRS1, als auch adipositasinduzierte Insulinresistenz beeinflussen.

Zwei Serin/Threoninkinasen, Proteinkinase C (PKC) und salt inducible kinase 3 (QSK) wurden in dieser Arbeit als IRS1-Interaktionspartner identifiziert. Die Interaktion von IRS1 und PKC in Verbindung mit 14-3-3 wurde bereits in der Literatur beschrieben. QSK ist jedoch bisher nicht als Interaktionspartner von IRS1 bekannt und interagiert zusätzlich mit 14-3-3.

Diese Ergebnisse weisen stark auf einen ähnlichen Mechanismus von PKC- und QSK-vermittelter Regulation der Insulinsignaltransduktion auf der Ebene von IRS1 hin, welche schließlich zur Entstehung der Insulinresistenz beitragen kann.

1 Introduction

1.1 Obesity

Among the variety of non-communicable pathologies, obesity and associated health syndromes play an increasingly important role in society.

According to the World Health Organization (WHO), worldwide, obesity has increased more than 2 fold since 1980 and today affects as many as 200 million men and nearly 300 million women (*1*). Additionally, 1.5 billion adults over the age of 20 were overweight in 2008 and approximately 43 million children under the age of five were overweight in 2010 (*2*).

In Germany, 70% of all men and 50% of all women are overweight. Alarmingly, although in Germany the percentage of overweight people has remained stable over the last 20 years, an increasing number of obese patients has been recorded during this period (*3*).

Although rather a surrogate characteristic, the body-mass index (BMI) is widely used and accepted as a measure of adiposity. The BMI is calculated by the ratio of body weight in kilograms to square of height in meters. Per WHO definition, a BMI above 25 kg/m^2 indicates overweight, while a BMI above 30 kg/m^2 demarcates obesity (*2*).

Besides the BMI, waist-to-hip ratio (WHR) may be used to estimate pathological levels of body fat. The WHR leads to a more accurate approximation of risk related to cardiovascular disease than BMI, as here, not only the amount of fat but also its distribution throughout the body plays a determining role (*4*).

Recently, extensive comparative analysis of long-term developments of body mass index in 199 countries with over 9 million participants has revealed a worldwide increase of BMI by 0.4 kg/m^2 per decade for men and 0.5 kg/m^2 per decade for women since 1980 (*1*). The highest BMI among high-income countries was detected in the United States of America with comparable increases of male and female BMI. Analysis of BMI in Germany also revealed a modest constant increase since 1980, which was more pronounced in men than in women (Figure 1). These data suggest that increasing BMI and obesity will further affect societies around the world for the next decades.

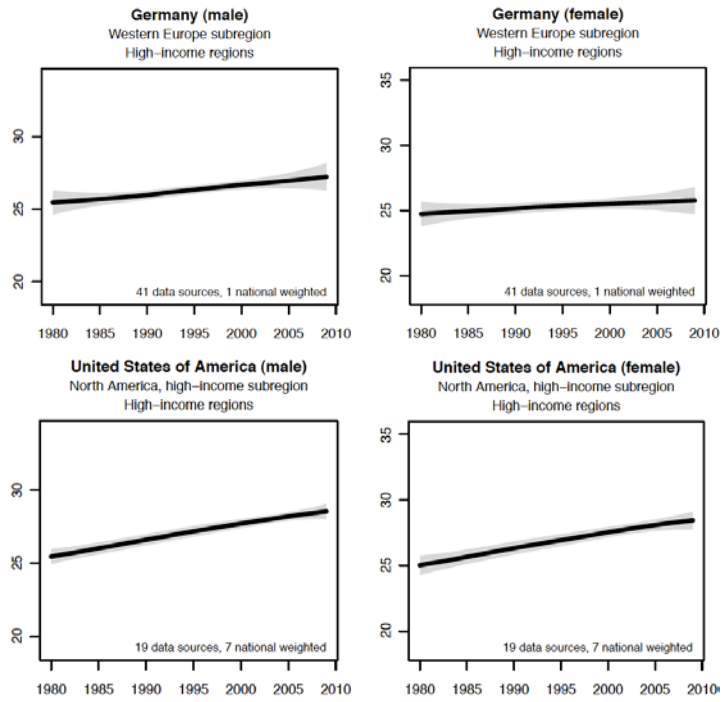

Figure 1: Development of age-standardized mean BMI (black line) and 95% uncertainty intervals (shaded area) between 1980 and 2008. Results shown for males and females in Germany and the United States of America; rearranged from (*1*).

Despite this, at the same time obesity is one of the most neglected risk factors for various diseases. In addition to the obvious overall reduced quality of life related to obesity, numerous studies support the finding that obesity, but also overweight, lead to the development of various comorbid diseases. For example, the development of insulin resistance and resulting type 2 diabetes mellitus is largely based on overweight and obesity (*5*). Yet, also cardiovascular disease, myocardial infarction and cerebral infarction are known to coincide with increased body weight (*4, 6, 7*). Furthermore, obesity related cancers, osteoarthritis and psychological disturbance are found with increased incidence among obese patients (*8*). Taken together, several studies conclude drastic decreases in life expectancy and increases in early mortality due to obesity and overweight (*9-11*).

Major causes of overweight and obesity include a trend towards a sedentary lifestyle with an overall decrease in physical activity, and excess intake of food rich in macronutrients (*12*). These environmental factors, together with polygenic variations, steer society towards an increased BMI attributing to the majority of all cases of obesity. In contrast, monogenic mutations, like leptin deficiencies, leptin receptor deficiencies (*13*) or melanocortin receptor mutations cause less than 5% of all cases of severe obesity (*14, 15*).

1.2 Type 2 diabetes mellitus

Diabetes mellitus is one of the most common metabolic disorders (*16*). In Germany, diabetes occurs in almost 6% of men and almost 5% of women, however the prevalence remained stable between 1990 and 2005 (*17*).

Worldwide, more than 220 million people suffer from diabetes and similar to estimates for obesity, the WHO predicts a dramatic rise in diabetic patients and in diabetes related deaths over the next two decades (*18*). Prevalence of diabetes rises with increasing age, increasing body mass index, increasing sedentary behavior and decreasing education (*17*).

Most data sources do not distinguish between type 1 and type 2 diabetes mellitus (*19*), however, WHO estimates attribute more than 95% of all diabetes cases to type 2 diabetes mellitus (*20*).

While type 1 diabetes is an early-onset autoimmune disease by which insulin-producing β-cells in the islets of Langerhans are destroyed (*21*), generally type 2 diabetes occurs later in life (*22*) and while type 1 diabetes is characterized by an absolute deficiency in the hormone insulin (*21*), type 2 diabetes leads to relative insulin deficiency. However, both type 1 and type 2 diabetes result in severe hyperglycemia. Depending on the fasting state, human normoglycemic blood glucose levels in whole blood range from 60 to 140 mg/dL (3.3 mmol/L to 7.8 mmol/L). In contrast, in uncontrolled diabetic patients hyperglycemia can reach more than 270-360 mg/dL (15-20 mmol/L). General recommendations refer to maximum values of 126 mg/dL (7 mmol/L) for fasting blood glucose, while after a meal a short-term maximum of 180 mg/dL (10 mmol/L) is tolerated.

The development of insulin resistance as a major characteristic of type 2 diabetes (*16, 23*) is mainly influenced by increased body weight (*17*), but also progressive β-cell dysfunction begins before onset of the disease and plays a determining role for the progression of type 2 diabetes (*24*). Insulin resistance is initially compensated by an increased insulin secretion and proliferation in the pancreatic β-cells, however, this eventually leads to β-cell failure (*25, 26*).

Further, type 2 diabetes may include impaired glucose tolerance, leading to either normal or increased insulin response in mild cases of glucose intolerance, or decreased insulin response in severe cases of glucose intolerance (*27*). Fatal complications including kidney failure, neuropathy, retinopathy, dermopathy, increased risk of atherosclerosis and stroke (*28*) occur secondary to insulin resistance and glucose intolerance, determining the severity of the disease.

The most obvious strategies for treatment and possibly even prevention of type 2 diabetes include extensive changes in lifestyle, i.e. a healthier diet (*29*) and regular physical activity (*30*). Indeed, nutrition and exercise seem to regulate insulin receptor expression (*31*), increasing insulin functionality.

Nonetheless, medicinal treatment is available. Besides the administration of insulin also sulfonylurea, thiazolidinedione and the biguanid metformin, which improve insulin release, insulin sensitivity and glucose uptake, respectively, are used to ameliorate the effects of diabetes (*32-34*).

1.3 Insulin signaling

1.3.1 Systemic effects of insulin

Following a meal, blood glucose levels are elevated, and more glucose enters pancreatic β-cells through insulin-independent glucose transporters 2 (GLUT2) (*35*). Upon increasing intracellular glucose, adenosine triphosphate (ATP) is produced, which leads to the closure of ATP-sensitive K_{ATP} channels, shutting down potassium exchange through the membrane and resulting in its depolarization. In turn, opening voltage-gated calcium channels facilitate Ca^{2+} influx, which triggers exocytosis of secretory granules containing insulin. Finally, secretion into the circulation occurs (*36*). These granules are preformed and reside at the cell membrane, enabling an immediate response to the acute insulin demand after meals.

Through the bloodstream, insulin targets its various metabolic target tissues like skeletal muscle, white adipose tissue and the liver through the insulin receptor. Among those major targets, adipocytes show the highest expression of insulin receptor, while in comparison, expression in hepatocytes and skeletal muscle cells is approximately 30% and 10%, respectively (*37, 38*). Nevertheless, only a small fraction of glucose clearance from the blood can be attributed to white adipose tissue, whereas skeletal muscle takes up the largest amount of blood glucose of approximately 70% (*38-40*). The insulin receptor is furthermore expressed in brain, heart, kidney, pulmonary alveoli, pancreas, placenta, various blood cells, and fibroblasts (*41*).

As a result of anabolic insulin signaling, uptake of glucose is increased in peripheral organs, like white adipose tissue and skeletal muscle, where it can be utilized or stored (*42*).

Except for the intestine and kidney, where glucose uptake is also facilitated via sodium-linked glucose transporters, which act against concentration gradients (*43*), other

tissues mainly utilize glucose transporters, which carry glucose along the concentration gradient. This second class of glucose transporters comprises five known transporter proteins, i.e. glucose transporters 1-5 (*38*).

Among those, GLUT4 is the only insulin-dependent glucose transporter and expression is localized to insulin responsive tissues, like skeletal muscle, cardiac muscle and adipose tissue, whereas GLUT1, GLUT2, GLUT3 and GLUT5 are independent of insulin and differ in their kinetic properties as well as distribution (*38*).

Neurons and the placenta are organs with high glucose demand, which explains the presence of GLUT3, exhibiting the highest affinity for glucose among the glucose transporters. GLUT2 has only low affinity to glucose and is localized in hepatocytes and pancreatic β-cells, but also kidney and small intestinal epithelium take up glucose via GLUT2. GLUT1 on the other hand, is expressed on various cell types, with high expression in brain, erythrocytes, and endothelial cells. GLUT5 has the lowest glucose affinity and a higher affinity for fructose. GLUT5 can be found on small intestinal cells, sperm, kidney, brain, adipose tissue cells and muscle (*38*).

In white adipose tissue, where energy is stored in the form of newly synthesized lipids, glycolysis is increased upon insulin signaling, leading to increased formation of glycerol-3-phosphate used for triglyceride synthesis (*44*). To support this effect, anti-catabolic actions of insulin reduce lipolysis (*45*), thus reducing the amount of non-esterified fatty acids circulating to the liver (*46*). In addition, insulin signaling increases glucose uptake into adipocytes via an intensified expression and translocation of GLUT4 and also GLUT1 expression is regulated by insulin (*38, 45*).

As in adipose tissue, in skeletal muscle, insulin signaling likewise leads to an increased expression and translocation of GLUT4 (*38*). Furthermore, insulin stimulates the synthesis of hexokinase II and pyruvate kinase, increasing glycolysis and formation of ATP (*47*). Generation of glycogen storage from glucose is a key feature in skeletal muscle, which is also elevated upon insulin signaling contributing to the regulation of blood glucose levels (*48, 49*).

Moreover, in the liver glycolysis and the formation of ATP are increased upon insulin signal transduction, whereas glycogenolysis and gluconeogenesis are blocked (*50, 51*). Further, insulin facilitates glycogen synthesis and increases biosynthesis of hexokinase IV, which enhances glycolysis in response (*52*). Overall, the liver contributes substantially to the control of blood glucose by the regulation of hepatic glucose production.

The secretion of glucagon by pancreatic α-cells leads to an increase in blood glucose and thus is inhibited by insulin and elevated blood glucose levels (*53*). As up to 75% of hepatic glucose production is determined by glucagon in order to counteract decreasing amounts of blood glucose (*54*), the inhibition of glucagon secretion by insulin indirectly reduces hepatic glucose production in the liver (*55*).

In summary, utilization of stored energy is inhibited upon insulin action, and glucose, lipid and protein release from tissues is decreased (*42*). By action of insulin, less gluconeogenic amino acids are released from fat and muscle and therefore less of those precursors are available for glucose production in the liver (*56*).

In addition to insulin's effects on peripheral organs, insulin signaling also affects the central nervous tissue. However, rather than influencing metabolic pathways, insulin here seems to act on numerous regulatory pathways, for example regulating appetite or affecting the reward centers of the brain (*57*).

1.3.2 Molecular features of insulin signal transduction

The peptide hormone insulin binds to the membrane-bound insulin receptor via its two extracellular α-subunits and thereby triggers a conformational change on the two intracellular β-subunits of the receptor (*58*). In turn, this conformational change facilitates the autophosphorylation of the insulin receptor on a maximum of seven tyrosine residues thereby activating its tyrosine kinase abilities (*59, 60*). Proteins containing phosphotyrosine binding (PTB) domains then interact with the receptor (*61-64*) and are phosphorylated on tyrosine residues, while being localized to the plasma membrane through pleckstrin homology (PH) domains (*63, 64*). Among those proteins, the insulin receptor substrates (IRS) play a prominent role, as proteins like the p85 subunit of phosphatidylinositol-3 kinase (PI3K) or growth factor receptor bound protein 2 (Grb2) interact with the phosphorylated IRS proteins via their src homology 2 (SH2) domains (*65, 66*).

Further downstream, signaling branches off at the level of the IRS proteins into the PI3K-pathway (*67*) and the Ras/Raf mitogen-activated protein kinase (MAPK)-pathway (*68, 69*), related to metabolic and proliferative regulation, respectively (Figure 2).

The metabolic PI3K-pathway is initiated by binding of the regulatory p85 subunit of the PI3K to IRS proteins (*66, 70*). The catalytic p110 subunit of PI3K then transforms phosphatidylinositol-4,5-bisphosphate (PIP2) into phosphatidylinositol-3,4,5-trisphosphate (PIP3), which activates phosphoinositide dependent kinase 1 (PDK1) (*71*). Subsequently, protein kinase B (Akt) is activated by phosphorylation on serine and threonine residues

(*72*) and the PI3K-pathway diverges into several branches leading to the repression of lipolysis, the de-repression of glycogen synthesis, and protein synthesis (*73*). Furthermore, PDK1 activates protein kinase C (PKC), a serine/threonine kinase, which is able to modulate insulin signaling by phosphorylation of a serine residue of IRS1 (*74, 75*).

Together with son of sevenless (SOS) and SH2 containing protein (Shc), the activation of Ras and Raf is mediated through the binding of growth factor receptor binding protein 2 (Grb2) to IRS (*76, 77*). Finally, this cascade leads to estrogen receptor kinase (ERK) and thus to mitogen-activated protein kinase signaling (*78, 79*) influencing the proliferative state of the cell.

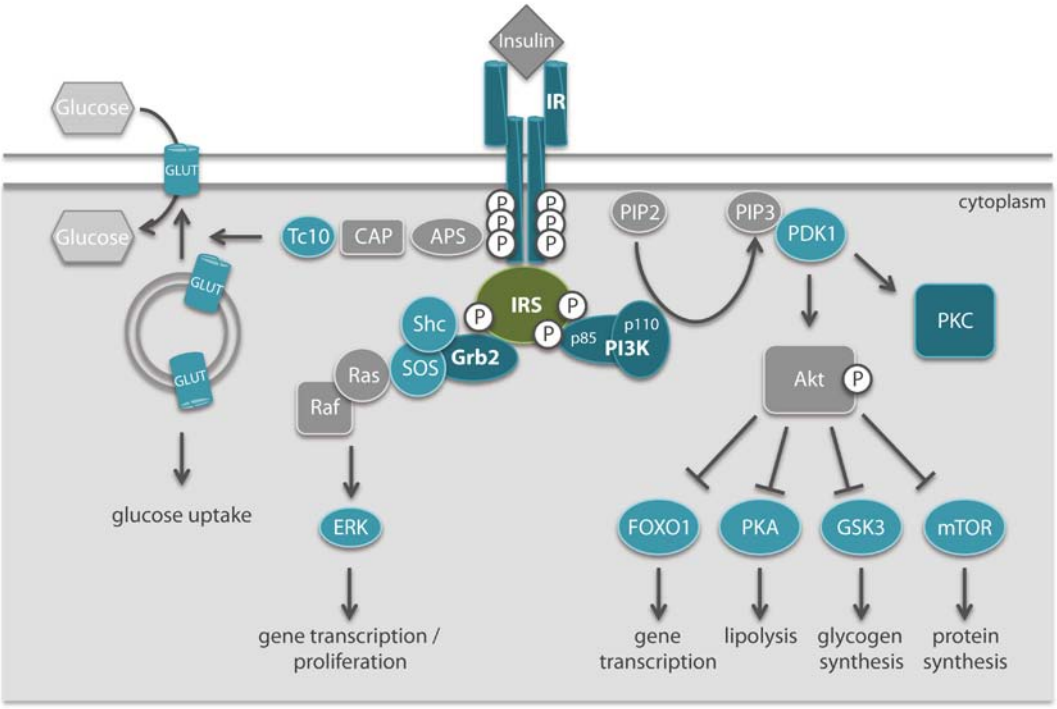

Figure 2: The insulin signal transduction pathway. Insulin binds to the insulin receptor on the cell surface, facilitating conformational change and thus autophosphorylation on intracellular domains. Further downstream signaling is directed by the insulin receptor substrates finally leading to insulin's effects like gene transcription, proliferation, lipolysis, glycogen synthesis and protein synthesis. Proteins interacting with IRS1 are in bold print. IR: insulin receptor, APS: adapter protein with a PH and SH2 domain, CAP: cbl-associated protein, Tc10: Ras-like protein Tc10, GLUT: glucose transporter, IRS1: insulin receptor substrate 1, Grb2: growth factor receptor binding protein 2, Shc: SH2 containing protein, SOS: son of sevenless, Ras: rat sarcoma, Raf: v-raf-leukemia viral oncogene, ERK: extracellular signal-regulated kinase, PI3K: phosphatidylinositol-3 kinase (subunits p85 and p110), PIP2: phosphatidylinositol-4,5-bisphosphate, PIP3: phosphatidylinositol-3,4,5-trisphosphate, PDK1: phosphoinositide dependent kinase 1, Akt: protein kinase B, FOXO1: forkhead transcription factor 1, PKA: protein kinase A, GSK3: glycogen synthase kinase 3, mTOR: mammalian target of rapamycin, PKC: protein kinase C.

Another pathway, bypassing the IRS proteins, leads to insulin-dependent translocation of GLUT4 to the plasma membrane facilitating glucose uptake into the cell (*80, 81*). Via insulin receptor activation of a signaling cascade including adapter protein with a PH and SH2 domain (APS), casitas B-lineage lymphoma (Cbl) and Ras-like protein Tc10, initial fusion of GLUT4 containing vesicles with the plasma membrane is initiated (*42, 81*).
In addition to the IRS proteins and APS, there are further proteins known to interact with the insulin receptor, like Grb2-associated binding protein 1 (Gab-1), $p60^{dok}$, and Cbl all of which exert distinct functions in downstream signaling (*42*).

1.3.3 Role of insulin receptor substrates in insulin signaling

The family of insulin receptor substrates consists of four known members and two putative new members, which were recently identified (*82-84*). So far, IRS1 and IRS2 have been most extensively studied. However, also research on IRS3 and IRS4 is more and more adding to the overall understanding of the differential signaling capabilities of insulin receptor substrates. In contrast, the function of IRS5 (DOK4) and IRS6 (DOK5) is still vague (*82*).
Detailed structural data are available, comparing the properties of protein domains and phosphorylation sites of insulin receptor substrates 1-4 (Figure 3) (*85*).
The phosphotyrosine binding domains facilitating interaction with the insulin receptor and pleckstrin homology domains facilitating localization to the plasma membrane are conserved between IRS1-4, suggesting similar insulin receptor binding characteristics of the different isoforms. Moreover, on a structural level, about 20 tyrosine residues are conserved between IRS1 and IRS2 concerning their approximate location and surrounding binding motif, while the overall comparison suggests a rather distinct C-terminus, and a 75% conserved N-terminus (*85*). Furthermore, IRS2 binds to the insulin receptor not only via the PTB domain but has an additional binding loop (Figure 3), providing a possible explanation for the different binding kinetics (*86*).

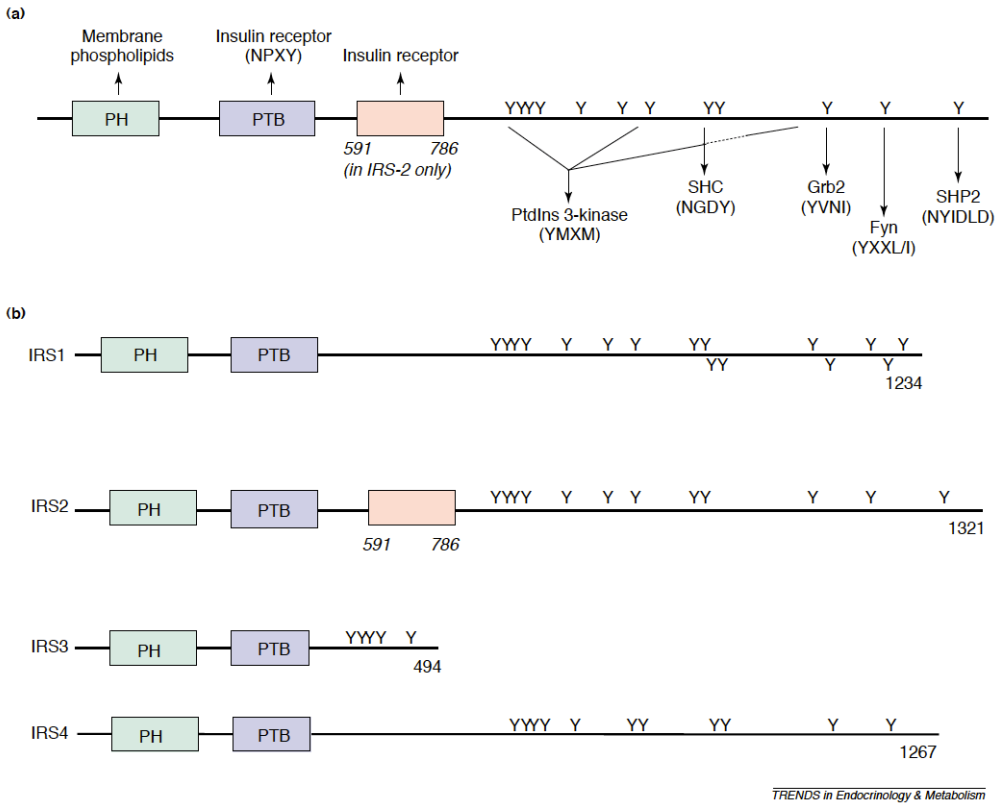

Figure 3: Comparison of protein structures of mouse insulin receptor substrates; from (*85*). PH domain of IRS proteins located at the N-terminus, PTB domain and tyrosine phosphorylation sites; known interacting proteins with the respective interaction motif indicated by arrows (a). Different structural features of isoforms 1-4 (b). PH: pleckstrin homology domain, PTB: phosphotyrosine-binding domain, Y: tyrosine phosphorylation sites. Numbers display amino acid count.

Functional characterization of the different insulin receptor substrate proteins was achieved by the analysis of knockout mice. IRS1 knockout studies revealed that integrity of insulin signaling is largely depending on functional IRS1, as IRS1 knockout mice are insulin resistant with increased insulin serum levels, glucose intolerant and further exhibit growth retardation (*87, 88*). However, these mice failed to develop diabetes and thus, an alternative substrate compensating for IRS1 was identified and named IRS2 (*88*). In comparison, a knockout of IRS2 also led to insulin resistance, but additionally mice developed type 2 diabetes and had impaired β-cell function (*89, 90*).

Furthermore, differential dephosphorylation kinetics were observed for IRS1 and 2, where total IRS1 tyrosine phosphorylation was detected up to 60 minutes after stimulation with insulin, while total IRS2 tyrosine phosphorylation lasted for only 3-10 minutes (*91*). In parallel, PI3K activation times correlated with the duration of tyrosine phosphorylations. Taken together, these findings suggest differential roles for IRS1 and IRS2. Yet, this plays an even more important role in tissues with parallel expression of both proteins, like the

liver (*85*). In liver of whole-body IRS1 knockout mice, IRS2 is able to compensate for IRS1-mediated activation of PI3K and thus ameliorates the loss of regulation of blood glucose levels (*87*). In addition, knockout of IRS2 leads to a declined suppression of hepatic glucose production and reduces glycogen synthesis in the liver. Furthermore, these mice show a dysregulated lipid metabolism (*92*).

Knockdown of IRS1 specifically in liver, performed by adenoviral RNA interference, increases gluconeogenesis and reduces glucokinase expression, whereas knockdown of IRS2 in liver increases the expression of lipogenic enzymes like fatty acid synthase and hepatic lipid accumulation (*93*).

Overall, these findings suggest that in liver IRS1 and IRS2 have overlapping roles in the control of metabolism, while IRS1 seems to regulate glucose homeostasis and IRS2 seems to play a role in lipid metabolism (*92, 93*).

It is known for tissues where glucose uptake is insulin-dependent and facilitated via GLUT4, that primarily IRS1 and IRS3 are expressed, and only little amounts of IRS2 (*94*). Thus, in muscle tissue of IRS1 knockout mice, PI3K activation is decreased and not compensated for by IRS2. Moreover, muscle and adipose tissues of these mice exhibit reduced insulin-induced glucose transport (*87*).

In summary, IRS1 and IRS2 regulate a variety of insulin's major effects in the tissues involved in glucose and lipid metabolism, whereas IRS3 expression so far has only been shown in rodents and might not play an important role in humans (*95*). Also IRS4 seems to have only a limited influence on the metabolic effects of insulin, although it is expressed in brain, liver, kidney and muscle (*96*).

The insulin receptor substrates are also involved in insulin-like growth factor (IGF) 1 signaling and it is known that they interact with the IGF-1 receptor via their PTB domain upon activation of the receptor by IGF-1 (*97*). The liver, when stimulated by growth hormone, produces IGF-1, but also numerous other tissues are a source of IGF-1. Circulating IGF-1 then stimulates growth by its anabolic effects on almost every cell-type (*98*).

1.3.4 Molecular basis of insulin resistance

Since the insulin signaling pathway is comprised of a complex network of several interlinked downstream cascades, it is prone to disturbances when one or more of the components are dysregulated. Such dysregulation, which may originate from a certain genetic or environmental background, can lead to insulin resistance.

Over the last decades, research dedicated to the elucidation of mechanisms involved in insulin resistance has accumulated a variety of involved pathways and regulation machineries. Insulin resistance thus was found to have multifaceted molecular causes and is possibly further complicated by combinations of different resistance mechanisms.

On the one hand numerous kinases convey the modulation of insulin signaling on protein level, providing a well-balanced signaling network, which may easily be disturbed.

Because of their central role in insulin signaling, IRS proteins are of major research interest and as the insulin signal branches off into the different pathways at this level, these proteins form a level of extensive regulation. Numerous kinases and phosphatases are known, which modulate IRS activity by the addition or removal of phosphate residues (*99-101*). Further, phosphorylations involving different functional domains of IRS proteins indicate interference on different levels of IRS function, like impaired association with the insulin receptor, or with downstream signaling components (*100, 101*).

Generally, tyrosine phosphorylations are considered to have an activating effect on IRS proteins, whereas serine phosphorylations are considered to be inhibitory. While this assumption holds true for tyrosine phosphorylations, phosphorylation of some serine residues can as well amplify the insulin signal (Figure 4). In the physiological state, activating serine phosphorylations by Akt (PKB) or PKCζ appear first, allowing for correct tyrosine phosphorylations and protect from inhibitory serine phosphorylations (*102, 103*), and later in a time-controlled manner, inhibitory serine phosphorylations are added by PKCζ or mTOR decreasing tyrosine phosphorylations and presumably turning off the signaling (*99, 104*). In pathophysiology, kinases known to be activated by several inflammatory stimuli can cause inhibitory phosphorylation of serine residues in an uncontrolled manner. Kinases contributing to these inhibitory phosphorylations and thereby leading to insulin resistance are IκB kinase β (IKKβ), c-jun N-terminal kinase (JNK), extracellular signal-regulated kinase (ERK) or protein kinase S6K (*99*).

Indeed, a link between metabolism and the immune system was established, laying grounds for the finding that obesity corresponds to a state of low-level inflammation (*105*). This condition is especially true for the adipose tissue, where in lean individuals insulin reduces the secretion of free fatty acids (*106*). It is known that in obesity and type 2 diabetes, serum levels of free fatty acids are elevated, imposing inhibitory effects on insulin sensitivity *in vitro* and *in vivo (106, 107)*. Interestingly, these effects could in part be reversed, when soluble tumor necrosis factor-α (TNF-α) receptor was administered to rats (*105*).

TNF-α signals through the formation of TNF-α receptor complex and TRAF2, ultimately resulting in the activation of downstream serine/threonine kinases JNK and IKK (*108-110*). In response to TNF-α signaling, these serine/threonine kinases are able to disrupt insulin signaling through the phosphorylation of murine IRS1 on Ser307 close to the PTB domain (corresponding to Ser312 in humans) (*111, 112*). Furthermore, the mutation of Ser307 to alanine in case of JNK (*111*), and alternatively the deletion of IKK resulted in a partial rescue of the insulin resistant phenotype (*112*).

Direct phosphorylation of IRS proteins by JNK and IKK certainly is one of the central mechanisms by which insulin signaling may be disturbed, however, also secondary effects on the phosphorylation state of insulin receptor and IRS1 have been described (*113*). Driven by IKKβ, the protein-tyrosine phosphatase 1B facilitates the removal of tyrosine phosphorylations on both the insulin receptor (*114, 115*) and IRS1 (*116, 117*), thereby leading to reduced insulin sensitivity.

According to the observations regarding TNF-α, an increase of several other inflammation-associated markers, for example interleukin (IL)-6 (*118-120*), IL-1 receptor antagonist (IL-1Ra) (*121*), IL-8 (*120, 122*), C-reactive protein (*119*), and MCP-1 (*119, 123*), is known for adipose tissue or plasma levels of obese mice and humans, suggesting similar outcomes for the disturbance of insulin signaling through the activation of JNK and IKK.

In addition, the phosphorylation state of the IRS proteins has been studied extensively during the last years and a variety of other kinases involved in the modulation of insulin signaling has been identified. Among those, mammalian target of rapamycin (mTOR) is capable of phosphorylating Ser307 on IRS1 upon insulin signaling (*124*). Studies on mTOR and mitogen-activated protein (MAP) kinases have revealed additional phosphorylation target sites, like Ser612 and Ser632 (*125*). Also Ser24 in the PH domain of IRS1 seems to be the target for several serine/threonine kinases, as at least PKC and pelle-like kinase (PLK) a homolog of human IL-1 receptor-associated kinase (IRAK) have been shown to catalyze this phosphorylation reaction (*126, 127*).

For IRS2 considerably less interventions by serine/threonine kinases have been detected so far, but JNK and GSK3 phosphorylate IRS2 and thus negatively regulate insulin signaling by disruption of the association with the insulin receptor or constraining tyrosine phosphorylations (Figure 4) (*99, 128, 129*).

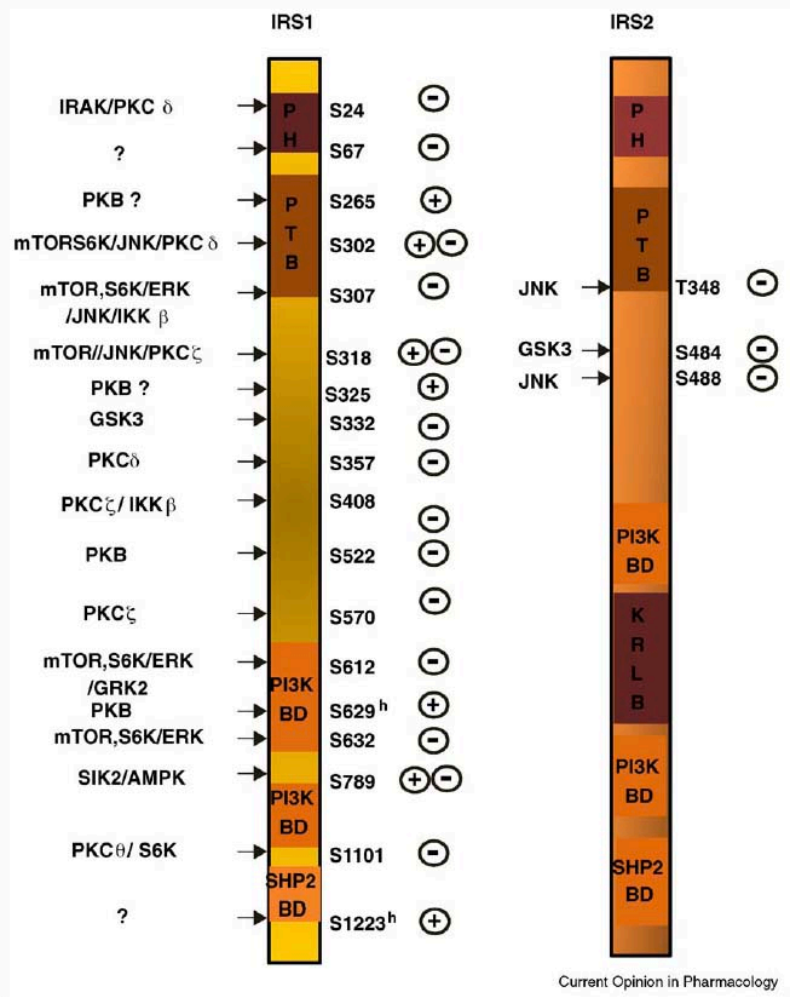

Figure 4: Known serine phosphorylation sites on IRS1 and IRS2 and the respective kinases inducing the phosphorylation. PH: Pleckstrin homology domain, PTB: phosphotyrosine binding domain, KRLB: kinase regulatory-loop binding domain, BD: binding sites, h: numbering according to human IRS1 protein sequence; from (*99*).

Several groups recently concentrated on the mass spectrometric assessment of IRS interaction partners (*130*), IRS phosphopeptides (*131, 132*), and specifically of phosphopeptide-mediated interactions (*133*), aiming at a better understanding of the IRS binding network with the identification of novel interactions.

Although the main research interest concentrates on phosphorylations mediating insulin resistance, other posttranslational modifications of serine/threonine residues are known to interfere with proper signal transduction. For example, O-linked N-acetylglucosamine (O-GlcNAc) modifications close to phosphorylation sites may have a regulatory function on the respective protein (*134-136*). The production of O-GlcNAc from fructose-6-phosphate is regulated by the hexosamine biosynthesis pathway, which is

increased during hyperglycemia due to the abundance of glucose and was shown to induce insulin resistance as well (*137, 138*).

Also ubiquitinations have been studied in the relation to pathological consequences. The ATP-dependent ubiquitin-proteasome system primarily serves as cellular proteolytic machinery, degrading proteins in a regulated manner. Importantly, insulin is not only able to increase protein synthesis, but also inhibits the proteasomal degradation of proteins (*139, 140*). Indeed, prolonged exposure of cells to insulin leads to proteasomal degradation of IRS1 after ubiquitin modification of the N-terminus (*141, 142*) and thus to the development of insulin resistance (*143*).

Further research indicated that suppressor of cytokine signaling (SOCS) 1 and SOCS3 specifically serve as adapter proteins bringing together IRS1 or IRS2 with elongin BC ubiquitin ligase, thereby targeting the IRS proteins for proteasomal degradation and inhibiting insulin action for example in mouse liver (*144, 145*).

Also dysregulated transcriptional components may negatively influence insulin signaling. Expression of the insulin receptor, for example, is mediated by the forkhead family transcription factor FOXO1, acting as transcription factor in a feedback mechanism (*146*). FOXO1 activity is regulated by insulin signaling itself via phosphorylation through Akt, ultimately leading to its nuclear export (*147-149*). Nuclear export upon phosphorylation leads to the inhibition of gene expression of genes originally activated by FOXO1, but also to activation of gene expression of genes originally repressed by FOXO1 (*150, 151*). The nutritional state of cells, as shown for C2C12 cells, mediates phosphorylation of FOXO1 and thereby FOXO1 serves as an insulin sensor. When cells are starved, FOXO1 is unphosphorylated and thus resides in the nucleus, where it induces expression of the insulin receptor gene upon binding to the promoter. When insulin is added to the cells, insulin signaling promotes FOXO1 phosphorylation through Akt, which ultimately reduces insulin receptor expression (*152*). This mechanism allows for rapid transmission of the insulin signal when nutrient levels are high. As in the pathophysiology of obesity, insulin levels are constantly increased, also FOXO1 phosphorylation is elevated, in turn reducing the amount of transcribed insulin receptor mRNA and thus also reducing the amount of insulin receptor (*152*).

Posttranscriptional gene silencing mediated by miRNA species has been identified to be a potent regulator in the control of protein expression. miRNA-143 is overexpressed in the liver of obese mice and was identified to cause a reduction of Akt activation, thus leading to impaired insulin signaling (*153*). Furthermore, in mice overexpressing miRNA-143,

glucose homeostasis was compromised, whereas in mice with miRNA-143 deletion, protection from obesity-induced insulin resistance was detected (*153*).

On the other hand, insulin resistance may already start with mutations at the genomic level, disturbing functional expression of signaling components. Almost two decades ago, a missense mutation in the insulin receptor gene was detected in individuals suffering from hereditary insulin resistance, exchanging the amino acid alanine (Ala1134) to threonine and thereby affecting the tyrosine kinase domain of the receptor (*154*). Thus, in spite of regular binding of insulin to the receptor, impaired induction of autophosphorylation of the intracellular domains prevented functional downstream signaling. In line with these findings, insulin receptor knockout mice display hyperglycemia and hyperinsulinemia, however also leading to fatal ketoacidosis shortly after birth (*155, 156*).

Further downstream, a polymorphism is known featuring a glycine to arginine (G972R) mutation of IRS1, which is associated twice as often with type 2 diabetes mellitus patients than healthy individuals (*157*). The polymorphism is located close to two tyrosine phosphorylation sites in the p85-binding domain of IRS1 and leads both to reduced tyrosine phosphorylation and increased IRS1 binding to the insulin receptor inhibiting its autophosphorylation, ultimately reducing systemic insulin sensitivity (*158*).

IRS1 deletion accordingly revealed a similar outcome with mild insulin resistance in mice (*87, 88*) and even simultaneous heterozygous deletion of insulin receptor and IRS1 causes severe insulin resistance with the development of diabetes, more closely resembling the situation seen in human patients (*159*).

Downstream of insulin receptor and the IRS proteins, function of protein kinase B β (Akt2), a mediator in the insulin signaling pathway, can be disturbed by a polymorphism in the human Akt2 gene (*160*). As expected, expression of mutant Akt2 carrying the polymorphism leads to disruption of insulin sensitivity in cell culture. Further also co-expressed wildtype Akt2 function is inhibited (*160*). In mice, the deletion of Akt2 impairs the regulation of blood glucose and leads to a diabetes-like syndrome (*161*).

Glucokinase is a key enzyme in homeostasis of blood glucose, and its genetic alteration can cause early onset type 2 diabetes mellitus (*162*), by a variety of different mutations (*163*).

Although these single gene mutations served as an explanation for the basis of insulin resistance in the respective patients, overall monogenic alterations only rarely account for the metabolic disorder, while more often the combination of several inherited traits may affect the fine-tuned machinery of the insulin signaling network (*164*).

1.4 Proteomic studies in the context of insulin signaling

As the development of type 2 diabetes is inextricably connected with obesity and insulin resistance, numerous studies have been conducted trying to elucidate the development of insulin resistance and to find the underlying mechanisms causing the disease (*87, 88, 92, 165*). In the course of time, various mediators of insulin resistance have been identified, like the serine/threonine kinases JNK and IKK (*111, 112*). However, so far the known mechanisms only give an incomplete view on the insulin resistant state. Moreover, research specifically defining key mediators involved in insulin resistance mechanisms was further complicated by the lack of suitable methods to tackle this complex protein network.

In recent years however, holistic and quantitative proteomic studies were made possible by the development of high-performance mass spectrometry with high sensitivity suited for the analysis of complex protein networks.

Originally, mass spectrometry evolved from the studies of Eugen Goldstein and Wilhelm Wien in the late 19th century, before in 1918 the first mass spectrometer was developed. Further improvements led to increasing mass accuracies and adaptations were made for the use with amino acids and peptides in 1958 (*166*). The principle of mass spectrometry is based on the analysis of mass-to-charge ratios of ionized and thus charged compounds or their fragments. In 2002 the Nobel Prize in chemistry was awarded to John B. Fenn and Koichi Tanaka for the development of electrospray ionization and soft laser desorption, which made biological macromolecules a more feasible source for mass spectrometry. Matrix-assisted laser desorption/ionization time-of-flight (MALDI/TOF) tandem mass spectrometry and liquid chromatography-coupled electrospray ionization (LC-ESI) mass spectrometry as standard tools for protein identification have been established for peptide mass fingerprinting and peptide sequencing (*167, 168*).

Based on those powerful tools to examine the components of protein networks, recently several proteomic studies have emanated dealing with the insulin signaling pathway.

Via peptide immunoprecipitation with an antibody directed against phospho-tyrosine residues, tyrosine phosphorylation sites of components of the insulin signaling cascade were characterized in a time-dependent setting in 3T3-L1 adipocytes. In a total of 89 different proteins changing their phosphorylation state, the study found 122 tyrosine phosphorylation sites, of which again 89 increased at least 1.3 fold upon insulin

treatment. A total of 69 novel phosphorylation sites were identified in the adipocyte proteome (*169*).

Another study that combined a similar immunoprecipitation approach with high-resolution mass spectrometry and stable isotope labeling of amino acids in cell culture (SILAC) in differentiated brown adipocytes found 40 insulin-induced tyrosine phosphorylations on proteins involved in insulin signaling. Among those, 7 were described for the first time, for example SDR, PKCδ binding protein, LRP-6 and PISP/PDZK11 (*132*).

Further research has led to the identification of IRS1-specific phosphorylations and based upon these, also protein interactions. In myotubes derived from C2C12 cells, 52 interacting proteins were identified specifically interacting with 109 phosphorylation sites in the insulin receptor, the IGF-1 receptor and IRS1 and IRS2 (*133*). A SILAC approach was combined with pulldowns of synthetic peptides, which were either phosphorylated or unphosphorylated. Although this procedure is based on an artificial approach, several proteins were found in pulldowns of IRS1 specific peptides, which have been previously described, like Grb2 or the p85 subunit of PI3K (*133*).

A new mass spectrometry-related method has been used in a study, dealing with insulin-stimulated IRS1 interactions. To this end, endogenous IRS1 was co-immunoprecipitated with interacting proteins and subsequently these protein complexes were subjected to mass spectrometry analysis. The results were quantified with a label-free method relating the site-specific abundance of phosphorylations to the respective precursor ions, finally leading to the identification of 11 novel insulin-stimulated IRS1 interactions in L6 myotubes (*130*). An earlier related study of the same group concentrated on the quantification of serine phosphorylations in human IRS1 after insulin treatment *in vitro* using a similar technique *(131)*.

In addition to the classical approach using co-immunoprecipitations as a means of characterizing protein interactions, a method combining affinity purifications with mass spectrometry-based interactomics was developed, with the aim to analyze protein interactions and their implications on a larger scale. Direct assessment of protein interactions was made practicable by the development of numerous protein tagging strategies, which have added to the understanding of protein interactions, like myc-tag, His-tag or FLAG-tag (*170*).

Further, using the affinity of streptavidin to biotin produces considerable advantages over antibody-driven purifications due to high affinity with a dissociation constant of 10^{-15} M (*171*). Additionally, the streptavidin-binding peptide (SBP) can be used for pulldown

experiments with superior purities compared to the His-tag or maltose-binding protein-tag (*172*).

From these one-step purifications using single tags, a number of tandem affinity purification (TAP) techniques evolved, driven by the need to further reduce the possibility of false-positive identifications originating from unspecific binding.

The first tag of this kind, composed of calmodulin binding peptide (CBP), a TEV cleavage site, and protein A, was used in yeast (*173*). Subsequently, the same tag was also adapted for mammalian cell culture (*174*) and interestingly, even used with IRS1 as bait protein (*175*). The study identified 35 interacting proteins specifically induced upon IGF-1 signaling, of which 5 were verified by co-immunoprecipitations (*175*).

Later, also a different TAP tag, the Strep II-FLAG-tag was developed (*176*). Recently, even a triple tag combining the streptavidin and calmodulin binding peptide tags with a His-tag was developed and successfully used on Bruton's tyrosine kinase in HEK-293 cells (*177*).

One disadvantage of the so far developed tandem affinity purification methods is insufficient yield. In all tags, which require a time-consuming TEV cleavage step, low yield is mostly due to insufficient cleavage, so most of the material is lost after the first purification step. For higher efficiency, therefore SBP and CBP tags were combined in order to facilitate a purification of the bait protein in native buffer conditions with the possibility for specific elution.

1.5 Objectives

As described in literature, obesity and insulin resistance, as well as type 2 diabetes as a result of different risk factors, are becoming a progressing problem in society. However, the exact molecular changes that occur during development of the disease have yet to be determined completely.

Among all major insulin-responsive organs, the liver plays an important role in glucose, protein, and lipid homeostasis. But still, the basis of the molecular derailment in the development of hepatic insulin resistance and type 2 diabetes mellitus is not fully understood. Thus, the influence of inhibitory pathways impinging on insulin signaling has been one of the most intensively studied topics related to insulin resistance. IRS proteins have been identified as a central target in the modulation of insulin signaling by various kinases, but a complete picture of the cooperation of different kinase pathways was so far out of reach.

In this study, in order to facilitate purification of IRS1-associated protein complexes, a novel mouse model was established, featuring an affinity tagged IRS1 protein, which can be expressed specifically in liver.

Further, proteomic state-of-the-art techniques were applied, enabling the extensive quantitative analysis of *in vivo* protein interactions in the liver. To assess IRS1 interactions related to diet-induced obesity and insulin resistance, IRS1 interaction profiles in different nutritional conditions were examined as well as in basal and insulin-stimulated states.

2 Materials and methods

2.1 Molecular biology techniques

2.1.1 General considerations

All molecular biology techniques were performed according to standard protocols by Sambrook et al. (*178*) unless otherwise mentioned. For the display of DNA sequences of vectors and genes, the Gene Construction Kit Software was used (Textco Biosoftware, version 2.5).

2.1.2 Cloning PCR

Polymerase chain reaction (PCR) was employed for the amplification of specific DNA fragments for cloning purposes like the creation of insert DNA or the generation of Southern blot probes. Primers used to this end were custom made by Eurogentec (Table 1).

Table 1: Primers used for cloning PCRs. Sequences in 5'-3' direction.

Primer name	Primer Sequence
IRS1pCTAP1	TAA GCA ACT ATG CCA GCA TCA GCT TCC AGA AGC AGC CAG AGG ATC GTC AAG ACG AGA AG ACC ACC GGC TGG
IRS1pCTAP2	TCT TCT GAC TTT GCC ACC ATA AAA ACG CAC CTG CTG TGA TGT CCA GTT ACG CGA TCG CCT AGG GGT AAC C
IRS1TTori1	CCA TTT TGA TAA GAT TCT TGC TAC AGG CTC TGC TTG TTG AAG TAA ATT TGG TCT TAG ACG TCA GGT GGC ACT
IRS1TTori2	TGG GGG CGC TGG GGC GGA GGG GAC GCG GGT GAC CTG CTA GCT CTC ACC CAA ACC GGT GCG TCA GCA GAA TAT
IRS1TTAcsI1	GGC GCG CCA CCA TGG CGA GCC CTC CGG
IRS1TTAscI2	GGC GCG CCT CTA AAG TGC CCC GGA GGA
Neoprobe1	GCC GCC AAG CTC TTC AGC AAT AT
Neoprobe2	TGA ATG AAC TGC AGG ACG AGG CA
IRSprobe1	GGC GCG CCA CCA TGG CGA GCC CTC CGG ATA CC
IRSprobe2	GTC TGG CAG GTT ATC CTG AAA

For general cloning PCRs, a total volume of 25 µL per reaction was used, consisting of 25 pmol of the respective primers, 25 µmol dNTP mixture (Genaxxon, #M3015.4100), 0.5U DreamTaq Green DNA Polymerase (Fermentas, #EP0714) and DreamTaq Green Buffer. PCR reactions were performed in a DNA Engine Dyad Peltier Thermal Cycler (bio-rad) and standard cycling protocols were used.

For the generation of insert DNA for BAC cloning or TOPO TA cloning, High Fidelity PCR Master (Roche, #12 140 314 001) with proofreading function was used. Reactions of a total volume of 50 µL were set up as suggested by the manufacturer and 50 pmol of the primers (IRS1pCTAP1 and 2, IRS1TTori1 and 2, or IRS1TTAcsI1 and 2, Table 1) were added. The cycling program was adapted from the user instructions.

PCR reactions were analyzed on 1% (w/v) agarose gels substituted with 0.5 mg/mL ethidium bromide run in TAE buffer (40 mM Tris base, 1 mM EDTA, 20 mM glacial acetic acid).

2.1.3 DNA sequencing

Big Dye terminator v3.1 cycle sequencing kit (Applied Biosystems, #4337455) was used for DNA Sequencing based on the sequencing method developed by Sanger et al. (*179*). Concerning DNA amounts and reaction conditions the manufacturer's instructions were followed. Analysis of the sequencing reaction was done at the Cologne Center for Genomics at the University of Cologne. Verification of the final insert IRS1-TapTag sequence was performed with the primers listed below (Table 2).

Table 2: Sequencing primers used for verification of insert IRS1-TapTag DNA.

Primer name	Primer Sequence
Seq1	TTT CAG GAT AAC CTG CCA GAC
Seq2	TGA TGC TGG ACG GGA CAT GGT
Seq3	CTT TCG AAA CCG GTT ATC CAG
Seq4	ACT ACC ACT GGG TGA CAT CAT
Seq5	TGT GAG GCT TGA CTC TGG CCT
Seq6	CAT GTA GTC ACC ACG GCT ATT
Seq7	ACA CAC TGG AGC CGA CTC CTT
Seq8	AAGGAGTCGGCTCCAGTGTGT
Seq9	TACATAGACCTGGATTTGGC

2.1.4 Gel extraction

DNA fragments were excised manually from agarose gels under UV light and purified using E.Z.N.A. gel extraction kit (Omega Bio-Tek, # D2501-01) as described in the manufacturer's instructions.

2.1.5 Red E/T Recombination

The IRS1 BAC (bacterial artificial chromosome, BACPAC Resources Center, Children's Hospital Oakland Research Institute, #RP23-430H22) was modified by Red E/T Recombination (*180, 181*) as outlined in the technical protocol for the Counter-Selection BAC Modification Kit (Gene Bridges, #K002). In brief, an overnight culture of the BAC containing bacteria was transformed with the red E/T recombination vector by electroporation. Then, the transformed bacteria were grown at 30°C until an OD600 of 0.3, when 50 µL of 10% L-Arabinose (Sigma, #A-3256) were added to a total amount of 1.4 mL of BAC culture. After 60 minutes at 30°C and another 60 minutes at 37°C transformation by electroporation was carried out with 600 ng of pCTAPneokana insert DNA containing homology arms produced with IRS1pCTAP1 and 2 primers (Table 1). Cultures were incubated another 70 minutes at 37°C to allow for recombination and finally spread on agar plates.

Another BAC recombination step was performed on the resulting IRS1-TapTag BAC with the origin of replication of the pACYC177 plasmid (NEB, #E4151S) (*182*). For the amplification of the origin of replication with homology arms, primers IRS1TTori1 and 2 (Table 1) were used in a proofreading PCR.

2.1.6 Transformation of competent bacteria

Plasmids containing DNA constructs of interest were transformed into chemically competent TOP10 bacterial cells (Invitrogen, part of #K4500-01) by exposure to 42°C for 45 seconds, followed by 2 minutes on ice. Subsequently, cultures were grown in LB-medium for 1 hour at 37°C and spread on agar plates.

2.1.7 Purification of plasmid DNA

Bacteria containing plasmids of interest were grown overnight at 37°C in LB medium (AppliChem, AppliChem, #A0954) with 100 µg/mL Ampicillin (AppliChem, #A0839). Depending on further use of purified vector DNA either a miniprep or maxiprep was performed with QIAGEN Plasmid Mini or Maxi Kit (QIAGEN) following the manufacturer's

instructions. Minipreps of BAC DNA were prepared omitting the usage of supplied columns.

2.1.8 TOPO TA cloning

TOPO TA cloning (Invitrogen, #K4500-01) was used to insert the construct into the pCR2.1-TOPO vector according to the instructions manual. Next, the final vector was transformed into chemically competent TOP10 bacterial cells and the fusion construct was cut from the pCR2.1-TOPO vector by AscI restriction digest (Fermentas, #ER1892) following the product instructions.

2.1.9 Ligation

Ligation of vector and insert was performed overnight at 16°C with T4 DNA Ligase (NEB, #M0202S).

2.1.10 Linearization

For further ligation DNA vectors were linearized by digestion with AscI (Fermentas, #ER1892) and overhangs were dephosphorylated by shrimp alkaline phosphatase (Fermentas, #EF0511) for one hour at 37°C. The vector was then purified by sodium acetate precipitation.
An amount of 50 µg of the gene targeting vector was linearized with 30 units of the restriction enzyme AsiSI (Fermentas, #ER2091) and in buffer conditions recommended by the manufacturer overnight at 37°C.

2.1.11 Phenol chloroform extraction

DNA for transfection was purified by phenol chloroform extraction. One volume of phenol : chloroform : isoamyl alcohol 25:24:1 (AppliChem, # A0944) was vigorously mixed with the DNA solution and spun down at 17,000 x *g* for 15 minutes. Subsequently the upper phase was vigorously mixed with one volume chloroform. Another centrifugation step of 10 minutes followed and the upper phase was subjected to isopropanol precipitation with an equal volume. DNA was pelleted and washed with 70% ethanol. Finally, the DNA pellet was dried for ES cell transfection or stored at -20°C in 70% ethanol.

2.1.12 Preparation of ES cell DNA

In order to detect homologous integration of transfected ES cell clones, genomic DNA was extracted from separately grown DNA plates in a 96-well format. To this end, cell culture medium was removed from the cells and wells were washed with PBS. The cells were then lysed in cell lysis buffer (10 mM Tris/HCl pH7.5, 10 mM EDTA, 10 mM NaCl, 0.5% (w/v) N-Lauroylsarcosine, 4% Proteinase K; Roche, #03115844001) overnight at 55°C in a high humidity chamber. Then, equal volumes of chilled pure ethanol were added and incubated at room temperature for 4 hours. The ethanol was removed and after drying the DNA pellets were reconstituted in 20 µL of TE/RNAse A buffer (10 mM Tris/HCl pH8.5, 1 mM EDTA, 0.1% (v/v) RNAase A (Fermentas, #EN0531)).
For expanded ES cell clones, lysis was performed overnight at 55°C in cell lysis buffer and DNA was precipitated by an equal volume of isopropanol. The sample was centrifuged at 17,000 x *g* for 15 minutes to precipitate DNA. The DNA pellet was subsequently washed with an equal volume of 70% ethanol and dried, before being reconstituted in TE/RNAse A buffer.

2.1.13 Restriction digest of genomic DNA

Genomic DNA was digested with 100 U EcoRI (Fermentas, #ER0273), 3 mM DTT, 3 mM spermidine, 0.14 µg/µL RNAse A (Fermentas, #EN0531) and 0.1 µg/µL BSA overnight at 37°C in high humidity conditions.

2.1.14 Southern blot

A large 0.8% (w/v) agarose (Invitrogen, #16500-500) gel substituted with 0.5 mg/mL ethidium bromide (AppliChem, #A1152) carrying all 96 ES cell clones was run overnight at 30 V in TAE buffer (see 2.1.2).
DNA was blotted overnight from the gel onto Hybond XL membrane (GE Healthcare, #RPN203S) by capillary force induced by several layers of Whatman paper (Whatman, #3030-861) and transfer buffer (0.4 M NaOH) (*183*). The membrane was then incubated at 80°C for 30 minutes.
A Southern blot probe (ROSA-probe) upstream of the 5'homology region of the ROSA26 locus was generated from the A-04 plasmid (*184*) by restriction with BamHI and EcoRI in 2x Tango Buffer (Fermentas, #ER0051, #ER0271) and the resulting fragment of 1.2 kb was purified by gel extraction.
A 532 bp fragment from the ROSA-CAGS-IRS1-TapTag vector was amplified with the primers Neoprobe1 and Neoprobe2 for the use as neo probe and a 502 bp fragment

from the IRS1 gene was created with the primers IRS1probe1 and IRS1probe2 for use as IRS1 specific probe (Table 1).

Prehybridization solution (1 M NaCl, 50 mM Tris/HCl pH7.5, 10% (w/v) dextran sulfate, 1% (w/v) SDS, 250 µg/mL sonicated salmon sperm DNA (Biomol, #54653.5)) was applied to the pre-wet membrane and the radioactively labeled probe was added to the solution after 2 hours. Radiolabeling of 100 ng DNA probe (*185*) with 2.5 µCi α^{32}P desoxytriphosphate (α^{32}P dCTP) was performed with the Ladderman labeling kit (Takara, #6046) as described in the user's manual. Hybridization of the radioactive probe with the corresponding DNA fragments on the membrane was performed overnight at 65°C in a rotating oven. On the next day, excessive material was washed with 2xSSC (300mM NaCl, 30 mM tri-sodium citrate dihydrate, pH7.0), 0.1% (w/v) SDS at 65°C. The membrane was sealed in a plastic envelope and a phosphoimager screen (Fuji, BasIIIS) was exposed to the membrane overnight. The Typhoon 9400 (GE Healthcare) was used in storage phosphor mode with a resolution of 50 µm to visualize the signal on the phosphoimager screen.

2.1.15 Isolation of genomic mammalian DNA

Tail tip biopsies were taken from mice at the age of three weeks and incubated overnight on a shaker at 55°C in proteinase K buffer (100 mM Tris/HCl pH8.5, 5 mM EDTA, 0.2% SDS, 200 mM NaCl, 1% (v/v) proteinase K). Hair and cell debris were spun down and DNA was precipitated from the solution using isopropanol. Ethanol was used to wash the DNA pellet and after drying the DNA was reconstituted in TE/RNAse A buffer.

2.1.16 Genotyping PCR

Polymerase chain reaction (PCR) was used to amplify transgene specific and wildtype specific DNA fragments in order to detect transgenic alleles and thus determine the genotype of experimental cells or animals. For this purpose, primers were custom made by Eurogentec (Table 3) and standard cycling protocols were used. PCR reactions were analyzed on 1% (w/v) agarose gels substituted with 0.5 mg/mL ethidium bromide run in TAE buffer (see 2.1.2).

Table 3: Primers used for genotyping PCRs.

Primer name	Primer Sequence
CAGS1	AAA GTC GCT CTG AGT TGT TAT C
CAGS2	GAT ATG AAG TAC TGG GCT CTT
CAGS3	TGT CGC AAA TTA ACT GTG AAT C
Cre1	ACG AGT GAT GAG GTT CGC A
Cre2	ATG TTT AGC TGG CCC AAA TGT

2.2 Cell Culture Techniques

2.2.1 ES cell culture

v6.5 murine embryonic stem cells (ES cells), which originated from a hybrid mouse strain of C57BL/6 and 129/sv background, were used for ES cell culture. ES cells were grown in ES medium (DMEM with L-glutamine (PAA, #E15-810), 15% (v/v) fetal bovine serum (Biochrom AG, #S0115), 1 mM sodium pyruvate (Invitrogen, #11360), 1% (v/v) non essential amino acids (Invitrogen, #11140), 2 mM L-Glutamine (Invitrogen, #25030), 0.1% (v/v) leukemia inhibitory factor (LIF) (recovered from supernatant of ebna-h LIF-producing cells induced with puromycin), additional 0.1 mM β-mercaptoethanol (Invitrogen, #31350)). As underlying cell layer, mitotically inactivated embryonic fibroblasts (EF cells) were grown on cell culture plates coated with 0.1% (v/v) gelatin solution (Invitrogen, #G1393) in EF medium (DMEM with stable glutamine (PAA, #E15-883), 10% (v/v) fetal bovine serum, 1 mM sodium pyruvate). To this end, after three passages, EF cells were exposed to 10 µg/ml mitomycin C (Sigma, #M0503) for two hours. Both, ES and EF cells were maintained in incubators at 37°C, 10% CO_2 and 95% relative humidity.
Medium was replaced every day for ES cell culture and every other day for EF cell culture. Medium was washed off with PBS and cells were treated with 0.05% trypsin (PAA, #L11-003) when cells were needed in solution for passaging or freezing.
When necessary, cells were frozen in fetal bovine serum containing 10% (v/v) DMSO and stored at -80°C for up to four weeks or in liquid nitrogen for longer periods.

2.2.2 ES cell transfection

Fresh ES medium was applied to ES cells designated for DNA transfection four hours before the procedure was started. ES cells were then treated with Trypsin and the cell pellet was entered into 400 µL RPMI 1640 (Invitrogen, #11835063). Linearized and purified DNA was dissolved in 400 µL RPMI as well. Both solutions were mixed and

transferred to a chilled electroporation cuvette (bio-rad, #1652088) for electroporation in a GenePulser device (bio-rad) at 500 µF and 240 V while a time constant of 7-11 ms had to be achieved. Cells were kept in the cuvette for five minutes at room temperature and subsequently divided onto four 10 cm cell culture plates, which were precoated with gelatin and inactivated EF cells. After 48h, selection with G418 was started (0.5% v/v G418 (Invitrogen, #10131-027) in regular ES medium) and continued until no further cells died.

Nine days after transfection, surviving individual ES cell clones were picked from PBS filled cell culture dishes into round-bottom 96-well plates prefilled with 25 µL Trypsin and transferred to fresh flat-bottom 96-well plates in triplicates. Two of those plates were kept as backup plates while cells on the third plate were split onto three new 96-well plates coated only with gelatin. These plates were used to isolate genomic DNA from the ES cell clones and were stored at -20°C after washing with PBS.

2.2.3 Microinjection into blastocysts

Confirmed ES cell clones were expanded onto 10 cm dishes and prepared for microinjection into blastocysts as previously described (*186*). Essentially, the cells were trypsinized, pelleted and resuspended. The cell suspension was incubated on a gelatinized 10 cm plate for 30 minutes and the supernatant containing most of the ES cells was pelleted again. The plate was washed with ES medium removing all loosely attached cells, which were also pelleted. Both pellets were resuspended in 0.5 mL injection medium (DMEM without L-Glutamine (PAA, #E15-009), 15% (v/v) fetal bovine serum (Biochrom AG, #S0115), 1mM sodium pyruvate (Invitrogen, #11360), 1% (v/v) non essential amino acids (Invitrogen, #11140), 2 mM L-Glutamine (Invitrogen, #25030), 1x penicillin/streptomycin (PAA, #P11-010), 25 mM HEPES (Invitrogen, #15630-049), 0.015 % (w/v) DNAse (Sigma)). 50 blastocysts isolated from CB20 mice were injected with around 10 transfected v6.5 ES cells each by Sonja Becker and Tanja Tropartz at the Center for Mouse Genetics at the University of Cologne. Then, injected blastocysts were implanted into the uterus of pseudopregnant mice from the F1 generation of crossings between C57BL/6 and BALB/c mice.

2.2.4 In-vitro cre recombination

For treatment with cre, ES cells were incubated with cre recombinase medium (50% (v/v) EF or ES fasting medium (EF or ES medium lacking fetal bovine serum), 50% (v/v) PBS,

4 µM cre, sterile filtered through 0.22 µm PVDF filters) overnight. Fresh EF or ES medium was applied for another 24 hours before the cells were further analyzed.

2.2.5 Fluorescence Microscopy

Integration and expression of eGFP in targeted ES cells shown by green fluorescence was analyzed in cre-transfected cells with an Axioskop 40 (Carl Zeiss). ES cells were washed with PBS, all fluid was removed and plates were sealed with parafilm. During microscopy, cells were handled without medium for a maximum of 30 minutes.

2.2.6 siRNA transfection

Hepa 1-6 mouse hepatoma cells (*187, 188*) were grown in Hepa medium (DMEM with stable glutamine, 10% (v/v) fetal bovine serum, 1mM sodium pyruvate, 1% (v/v) non essential amino acids) at 37°C, 5% CO_2 and 95% relative humidity. Transient transfection of small interfering RNA (siRNA) into Hepa 1-6 mouse hepatoma cells was performed at 50% confluency with either 14-3-3ε siRNA (Invitrogen, Oligo ID MSS213024) or respective Stealth RNAi siRNA Negative Control (Invitrogen, #12935-100) in Opti-MEM medium (Invitrogen, #51985-026) with Lipofectamine 2000 Transfection Reagent (Invitrogen, #11668019). Transfections were performed according to Invitrogen's instructions in Hepa fasting medium (Hepa medium lacking fetal bovine serum). After transfection, cells were maintained in Hepa medium for 48 hours before insulin stimulation.

2.2.7 In-vitro insulin signaling

Cells were starved in fasting medium for 16 hours overnight. For insulin stimulation, the medium was removed from the cells and replaced by fresh fasting medium either containing 10 nM insulin (Sigma, #I9278) or equal volumes of PBS (PAA, #H15-002). The cells were placed in the incubator for 10 minutes, subsequently washed by PBS and finally harvested in fresh PBS from cell culture plates with cell scrapers (Sarstedt). Cell culture plates and samples were kept on ice from this step onwards. PBS was taken off the cells after centrifugation at 1,200 x *g* for two minutes and lysis was performed in IP lysis buffer, followed by a 20 minute centrifugation at 17,000 x *g* at 4°C. The supernatant was transferred to a fresh tube and protein concentration was assessed using the NanoDrop Spectrophotometer ND-1000 (Thermo Scientific). Samples were immediately prepared for Western blot analysis.

2.3 Animal Experiments

2.3.1 Animal care

All handling of experimental animals and all procedures conducted with experimental animals were in accordance with the animal care committee of the University of Cologne and approved by the Bezirksregierung Köln.
Mice were kept in small groups of less than six animals in a virus-free facility at 22-24°C. A light-dark cycle was maintained with 12 hours light from 7 a.m. to 7 p.m. and 12 hours darkness from 7 p.m. to 7 a.m. and changes during daylight savings time were avoided. Animals were either fed a normal chow diet (NCD; Harlan, Teklad Global Rodent #T.2018.R12) consisting of 53.5% carbohydrates, 18.5% proteins and 5.5% fat (12% calories from fat) or a high fat diet (HFD; Altromin, #C1057) consisting of 31.4% carbohydrates, 21% proteins and 35.3% fat (55.2% calories from fat). Access to food and water was ad libitum during regular maintenance and food was withdrawn overnight if needed for an experiment.

2.3.2 Mouse models

In addition to the transgenic ROSA-CAGS-IRS1-TapTag mouse established in this study, the Alfpcre-mouse line (*189*) expressing the cre recombinase in hepatocytes was used to direct hepatocyte specific expression of IRS1-TapTag.

2.3.3 Measurement of body weight and liver weight

Body weight of mice was measured on a weekly basis on a regular precision balance (Sartorius).

2.3.4 Analysis of body composition

Body fat content and lean mass of live mice were measured relative to total body weight using nuclear magnetic resonance with a minispec mq7.5 (Bruker Optik) for mice at the age of 20 weeks.

2.3.5 Collection of blood samples

Blood samples of a few drops were taken through a cut in the tail tip and blood glucose levels were examined in whole blood using a Glucomen PC (A. Menarini Diagnostics).

2.3.6 Glucose tolerance test

For assessment of glucose tolerance, mice were fasted for 16 hours overnight. The next morning, basal fasting blood glucose levels were measured with a Glucomen PC in blood collected from the tail tip capillaries and sterile glucose (Baxter) was intraperitoneally injected at a dose of 2 g glucose/kg body weight. Glucose concentration was measured at 15, 30, 60 and 120 minutes after injection.

2.3.7 Insulin tolerance test

Insulin tolerance was assessed on random-fed mice and the procedure was carried out in analogy to glucose tolerance. Sterile insulin (Insuman Rapid, Sanofi Aventis) was diluted in 0.9% sterile saline (Berlin-Chemie AG, #HCA001431) and injected intraperitoneally at a dose of 0.75 U/kg body weight and blood glucose levels were measured at 15, 30 and 60 minutes after injection.

2.3.8 Extraction of sample material

At the end of the experimental period, mice were sacrificed by overdosing CO_2 and body length was measured on dead mice from the tip of the nose to the proximal end of the tail. Different organs were dissected, weighed in case of epigonadal fat pad and immediately processed for affinity purifications or shock frozen in liquid nitrogen and stored at -80°C for further analysis.

2.3.9 In-vivo insulin signaling

Mice were fasted for 16 hours overnight and experiments were performed the following morning. The anesthetic Avertin (2,2,2-Tribromoethanol, Sigma-Aldrich) was injected intraperitoneally at a dose of 10 µL per g body weight. The abdomen of anesthetized mice was opened and 125 µL sterile human insulin (equivalent to 5U; Insuman Rapid, Sanofi Aventis) was injected into the *vena cava inferior*. Accordingly, 125 µL of 0.9% sterile saline (Berlin-Chemie AG) was injected as control. The whole liver was harvested 5 minutes after injection and immediately subjected to organ lysis. If needed, samples of skeletal muscle, white adipose tissue of the epigonadal fat pad and brain were taken 6, 7 and 10 minutes after injection, respectively, shock frozen in liquid nitrogen and stored at -80°C for further analysis.

2.4 Protein Analysis

2.4.1 Organ lysis

All steps of organ lysis and sample preparation were carried out on ice. For affinity purifications, whole liver was homogenized in chilled 15 mL IRS lysis buffer (25 mM Tris/HCl pH8.0, 10 mM MgCl2, 100 mM NaCl, 0.5% Triton X-100, 10% glycerol, complete protease inhibitor cocktail (Roche, #11697498001), 10 mM β-mercaptoethanol; adapted from (*175*)) using a Dounce Tissue Grinder (Wheaton, #357544). The lysate was centrifuged for 20 minutes at 290 x *g* at 4°C in 50 mL Falcon tubes. The concentration of the supernatant was measured using the NanoDrop Spectrophotometer and protein lysates were immediately used for TAP experiments.

2.4.2 Streptavidin affinity purification

The complete purification was carried out on ice and incubation as well as centrifugation steps were performed at 4°C.

An amount of 400 mg protein was adjusted to a total volume of 15 mL with IRS lysis buffer, 15 mL dilution buffer (100 mM KCl, 50 mM Tris/HCl pH7.5, 2 mM PMSF) was added and the mixture was completed by the addition of 2 mM EDTA and 10 mM β-mercaptoethanol.

Equilibration of UltraLink immobilized streptavidin beads (Thermo Scientific, #53114) was achieved by washing the beads with wash buffer (150 mM KCl, 40 mM Tris/HCl pH7.5, 0.5% Triton X-100, 1 mM PMSF, 10 mM β-mercaptoethanol, complete protease inhibitors) three times. Centrifugation steps were performed at 1,500 x *g* for 5 minutes and finally the streptavidin beads were reconstituted as 50% gel slurry.

500 µL of 50% streptavidin beads gel slurry were added to prepared protein samples each with a total volume of 30 mL and the mixture was rotated gently for 30 minutes. To collect the beads, the sample was centrifuged at 290 x *g* for 5 minutes and the supernatant was discarded or an aliquot was kept for further analysis of unbound proteins. The beads were washed twice with 15 mL IRS lysis buffer, rotated for 5 minutes and centrifuged. The supernatant was thoroughly removed and if necessary an aliquot was kept for analysis. In order to elute the bound proteins, the beads were rotated with 500 µL of biotin elution buffer (150 mM NaCl, 40 mM Tris/HCl pH7.5, 0.1% Triton X-100, 1 mM PMSF, 10 mM β-mercaptoethanol, 2 mM Biotin, complete protease inhibitors) for 30 minutes in Spin Columns (Thermo Scientific, #69725). The biotin eluate was collected by centrifugation at 1,500 x *g* for 1 minute.

Biotin eluates were concentrated using NanoSep Columns (Pall Corporation, #OD003C33) with a molecular weight cutoff of 3 kDa. To this end, eluates were loaded onto columns and concentrated by centrifugation at 17,000 x *g* at 4°C until a volume of 100 µL was reached.

2.4.3 Protein gel electrophoresis

In order to pre-separate samples for subsequent mass spectrometry, samples diluted with Reducing Agent and LDS sample buffer (Invitrogen, #NP0004 and #NP0007), NuPAGE® Novex 4-12% Bis-Tris Gels (Invitrogen, #NP0335) were run with MOPS SDS Running Buffer (Invitrogen, #NP0001). Antioxidant (Invitrogen, #NP0005) was added to the running buffer in the inner gel chamber. PageRuler Prestained Protein Ladder (Fermentas, #SM0671) was loaded as a size marker and the gels were run at constant 200 V according to Invitrogen's technical guide.

Following electrophoresis, the gels were Coomassie stained with Colloidal Blue Stain Kit (Invitrogen, #LC6025) as instructions in the user manual suggest.

For Western blot analysis, samples were either processed for NuPAGE® Novex 4-12% Bis-Tris Gels or diluted with 4x SDS sample buffer (250 mM Tris-HCl pH 6.8, 8% (w/v) SDS, 40% (v/v) glycerol, 40 mM DTT, 0.004% Bromophenolblue; adapted from (*190*)) and run on 10% tris-glycine mini gels (*190*) in electrophoresis buffer (190 mM glycine, 25 mM Tris base, 3.5 mM SDS) at 100 V. PageRuler Prestained Protein Ladder was used as a size marker. Tris-glycine gels were immediately subjected to Western Blot analysis.

2.4.4 Western Blot

Western Blot transfer of proteins from NuPAGE® Novex 4-12% Bis-Tris Gels was performed with mini trans blot cells (bio-rad, # 170-3930) onto Hybond ECL nitrocellulose membranes (GE Healthcare, # RPN2020D). Blotting chambers were cooled on ice while blotting was carried out at 2 mA/cm^2 for 3 hours.

In contrast, Western Blot transfer of proteins from Laemmli gels onto Immun-Blot PVDF Membranes (bio-rad, #162-0177) was performed in Trans-Blot SD Semi-Dry Transfer Cells (bio-rad, #170-3940) at 2 mA/cm^2 for 1 hour. Following the blotting procedure, the membranes were blocked in 1x Western Blocking Reagent (Roche, #11 921 673 001) in TBS buffer (2 mM Tris base, 13,7 mM NaCl, pH7.4) for 1 hour at room temperature. Antibodies (Table 4) were diluted in 0.5x Western Blocking Reagent and applied to the membranes overnight.

Table 4: Antibodies used for immunodetection of proteins, with dilution applied and the ordering information.

Antibody	Dilution	source	Distributor
IRS1	1:1000	mouse	BD Bioscience, #611394
PI3K p85	1:5000	rabbit	Millipore, #06-195
PI3K p85α	1:1000	mouse	Abcam, #ab22653
PI3K p85β	1: 500	mouse	Abcam, #ab28356
PI3K p110α	1: 250	rabbit	Santa Cruz Biotechnology, #sc-7174
PI3K p110β	1: 250	rabbit	Santa Cruz Biotechnology, #sc-602
pIR (Tyr972)	1: 250	rabbit	Abcam, #ab5678
IRβ	1: 500	rabbit	Santa Cruz Biotechnology, #sc-711
pAkt (Ser473)	1:1000	rabbit	Cell Signaling Technology, #4058
Akt	1:1000	rabbit	Cell Signaling Technology, #4685
β-Actin	1:5000	mouse	Sigma, #A5441
pGSK3β (Ser9)	1:1000	rabbit	Cell Signaling Technology, #9323
GSK3β	1:1000	rabbit	Cell Signaling Technology, #9315
14-3-3ε	1:1000	mouse	Santa Cruz Biotechnology, #sc-130547
14-3-3ζ/δ	1:1000	rabbit	Cell Signaling, #9639
Lyn	1: 100	rabbit	Santa Cruz Biotechnology, #sc-15
Lyn	1: 100	mouse	Santa Cruz Biotechnology, #sc-7274
PKC	1: 100	mouse	Santa Cruz Biotechnology, #sc-17804
QSK (SIK3)	1: 250	rabbit	Abcam, #ab88495
pTyr	1: 500	mouse	Millipore, #05-321
pIRS1 (Ser307)	1: 250	rabbit	Cell Signaling Technology, #2381
anti-mouse IgG HRP	1:1000	goat	Sigma, #A4416
anti-rabbit IgG HRP	1:1000	goat	Sigma, #A6154

Excessive antibody was removed in two washing steps with TBS-T buffer (TBS buffer supplied with 0.1% (v/v) Tween 20 (AppliChem, #A1974)) and subsequently the respective horseradish peroxidase (HRP)-coupled secondary antibody was applied for 1 hour at room temperature. Another washing step was included before ECL Western Blotting Substrate (Thermo Scientific, #32106) was used for chemiluminescence detection of protein bands with Hyperfilm ECL (GE Healthcare, #28-9068-37).

2.4.5 In-gel trypsin digest

All steps of gel preparation and trypsin digest were carried out in a sterile workbench at room temperature unless otherwise noted. Eppendorf Protein LoBind tubes were used for all peptide solutions. Each lane of the stained bis-tris gradient gel containing a protein sample was cut into ten small gel slices beginning with the smallest molecular weight. The gel slices were further minced and destained in 100 µL destaining solution (50% 10 mM NH_4HCO_3 / 50% ACN (acetonitrile)) for 30 minutes at 55°C. Supernatant was discarded before dehydrating the gel pieces in 500 µL 100% ACN for 20 minutes with occasional vortexing. Supernatant was again discarded and 30-50 µL of trypsin mixture (12.5 ng/µL sequencing grade trypsin (Promega, #V5111) in 10 mM NH_4HCO_3) depending on the size of the gel pieces. The dried gel pieces were incubated for 90 minutes on ice to allow complete absorption of the trypsin mixture. After incubation the remaining trypsin mixture was removed and replaced by 20 µL 10 mM NH_4HCO_3 and digestion was carried out at 37°C overnight. The digest was stopped by the addition of 5 µL 5% TFA, spun down and the supernatant was collected in a fresh tube. For extraction, 20 µL 1% TFA were added to the gel pieces and incubated on a shaker at 700 rpm for 30 minutes. The supernatant was collected and the extraction step was repeated once more. The third extraction step was carried out with 20 µL 60% ACN / 40% H_2O / 0.1% TFA and otherwise repeated. After the extraction 30 µL 100 % ACN were added to the gel pieces and incubated on a shaker at 700 rpm for 15 minutes. The supernatant was collected and the step was repeated. During the protocol all supernatants of one gel slice were collected in the same tube. After final collection of the supernatant the combined supernatant containing the tryptic peptides was concentrated in a vacuum concentrator (Christ, RVC 2-25) at 55°C until they reached a volume of less than 65 µL.

2.4.6 Desalting

Desalting of the peptide samples was achieved using Stage Tips (Thermo Scientific, #SP201) and centrifuge adaptors. All centrifugation steps were carried out at 500 x *g* for 30 seconds. The protocol was adapted from Rappsilber et al. (*191*) in two instances: conditioning with buffer A (0.5% acetic acid) was performed twice and elution with buffer B (80% ACN / 0.5% acetic acid) was carried out three times.

The desalted peptide solution was concentrated in a vacuum concentrator at 55°C to approximately 10 µL to remove ACN. The sample volume was then adjusted to 20 µL with 0.5% acetic acid and subjected to nano-LC-ESI-MS/MS.

2.4.7 Nano-LC-ESI-MS/MS mass spectrometry

Experiments were performed on a Thermo LTQ Orbitrap Discovery mass spectrometer which was coupled to a split-less Eksigent nano-LC system. Intact peptides were detected in the Orbitrap at 30,000 resolution in the mass-to-charge (m/z) range 400-2000. Internal calibration was performed using the ion signal of $(Si(CH_3)_2O)_6H$ at m/z 445.120025 as a lock mass. For LC-MS/MS analysis, up to five CID spectra were acquired following each full scan. Aliquots of the samples were separated on a 10 cm, 75 µm reversed phase column (Thermo Fisher/Proxeon). Gradient elution was performed from 2 to 30% ACN within 80 minutes at a flow rate of 200 nL/min. All mass spectrometry equipment used was available through the CECAD Proteomics Facility at the University of Cologne.

2.5 Data Analysis

2.5.1 Label-free quantitative analysis

Mass spectrometry data sets were processed using MaxQuant quantitative proteomics software (v 1.1.1.36) allowing for label-free normalization and quantification of identified proteins (*192-194*).

2.5.2 General calculations and analysis

Data from all experiments were gathered in Microsoft Excel and prepared for the comparison of average values, standard error of the mean (SEM), student's t test and graphical displays.

2.5.3 Statistical methods

Statistical significance was analyzed with the unpaired two-tailed student's t test, while all probability (p) values below 0.05 were considered significant and were indicated by an asterisk: * $p < 0.05$, ** $p < 0.01$, *** $p < 0.001$ stating the significance level versus controls.

For average values standard errors are expressed and depicted as standard error of the mean (SEM).

3 Results

3.1 Generation of the targeting vector

The pCTAPneokana construct (Figure 5) containing the TapTag sequence (Table 5) was amplified by primers IRS1pCTAP1 and 2 (Table 1) and inserted into the IRS1 BAC by Red E/T recombination, thereby placing the TapTag sequence in frame behind the IRS1 open reading frame and creating the IRS1-TapTag fusion construct. In this step, the endogenous stop codons were removed in order to prevent premature termination of transcription after the IRS1 and in front of the TapTag sequence.

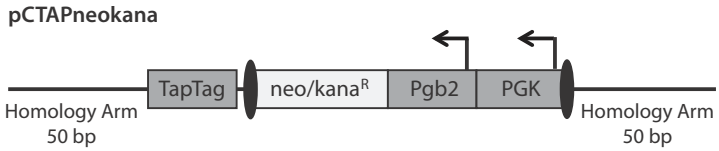

Figure 5: Scheme of the pCTAPneokana construct, containing the TapTag sequence and a FRT (ellipses) flanked resistance cassette under the control of prokaryotic Pgb2 and eukaryotic PGK promoters.

Table 5: Amino acid sequence of the components of the TapTag, streptavidin binding peptide (SBP) (*172*) and calmodulin binding peptide (CBP) (*173*).

Tag	Sequence
SBP	MDEKTTGWRGGHVVEGLAGELEQLRARLEHHPQGQREPSGGCKLG
CBP	KRRWKKNFIAVSAANRFKKISSSGAL

Another BAC recombination step was performed on the resulting IRS1-TapTag BAC with the origin of replication of the pACYC177 plasmid (*182*), thereby reducing the BAC size by 180kb and shaping the IRS1-TapTag-neokana vector. For the amplification of the origin of replication with homology arms, primers IRS1TTori1 and 2 (Table 1) were used in a proofreading PCR.

Finally, primers containing AscI restriction sites (IRS1TTAscI1 and 2, Table 1) were used to amplify the IRS1-TapTag sequence from the IRS1-TapTag-neokana vector. TA overhangs produced by the polymerase were subsequently used for TOPO TA cloning into the pCR2.1-TOPO vector.

From this source, the IRS1-TapTag insert was sequenced and afterwards excised by AscI restriction through the restriction sites introduced earlier and ligated into the ROSA-CAGS vector (*195*), which was also linearized by AscI restriction.

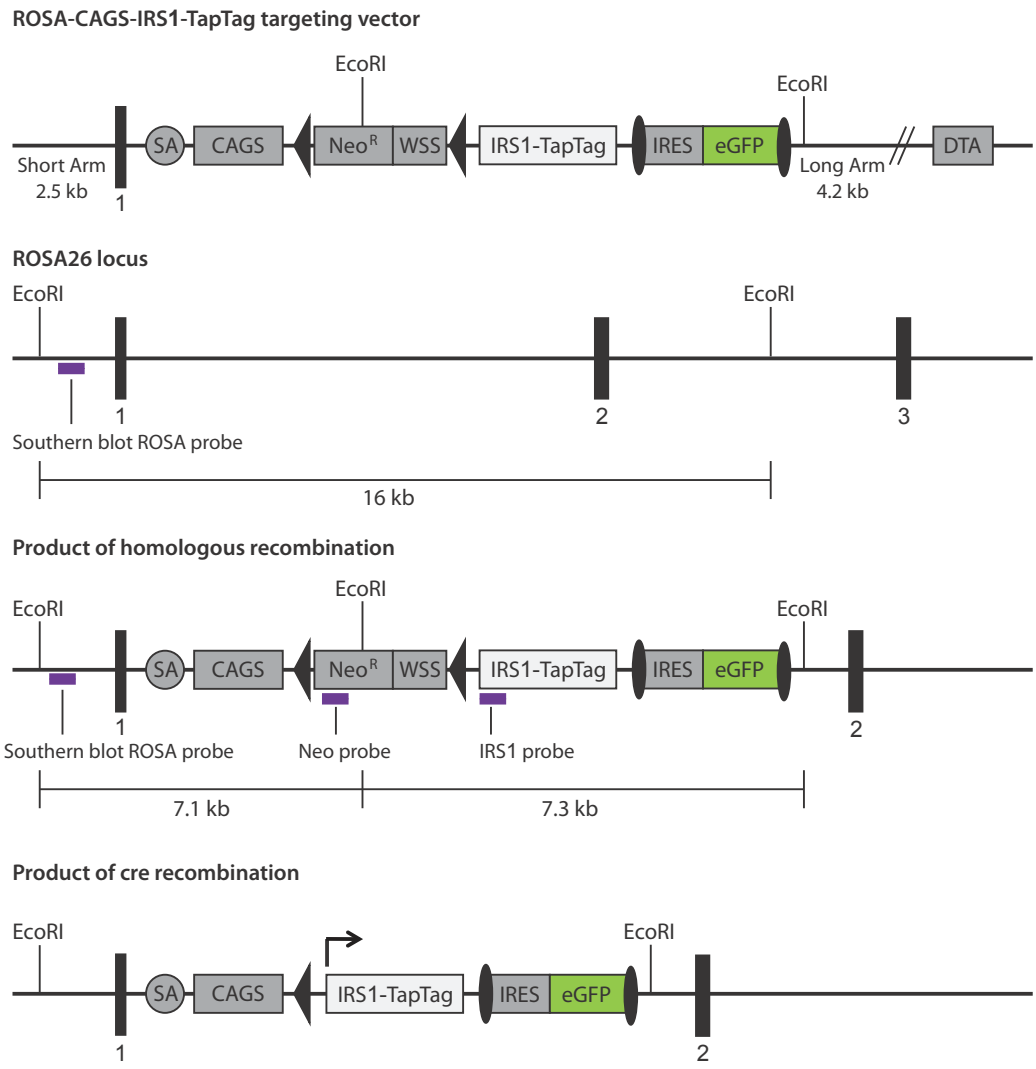

Figure 6: Gene Targeting strategy for the homologous recombination of the ROSA-CAGS-IRS1-TapTag targeting vector into the ROSA26 locus and the modified locus after cre-mediated excision of the loxP flanked stop signal. SA: splice acceptor, CAGS: chicken β-actin promoter, WSS: Westphal stop signal, IRES: internal ribosome entry site, eGFP: enhanced GFP, vertical black bars: exons, triangles: loxP (locus of X-over P1) sites, ellipses: frt sites, arrow: start of transcription.

The ROSA-CAGS-IRS1-TapTag targeting vector (Figure 6), including the fusion construct, was generated to enable overexpression of the IRS1-TapTag fusion protein driven by the ubiquitously expressed chicken β-actin (CAGS) promoter, while the expression was initially inhibited by a loxP flanked stop signal. Upon cre recombination, the stop signal along with a neomycin resistance cassette was excised, enabling expression of

IRS1-TapTag. In addition, the vector contained an IRES-eGFP sequence allowing for fluorescence detection of the integration of the construct in cells.

3.2 Generation of ROSA-CAGS-IRS1-TapTag mice

3.2.1 ES cell targeting

The linearized gene targeting vector ROSA-CAGS-IRS1-TapTag was purified and transfected into v6.5 ES cells. After the selection period individual cell clones were isolated and screened by Southern blot. Clones 2 and 3 showed the correct integration pattern for the ROSA and neo probes as well as the IRS1 specific probe detecting both, the ROSA-CAGS-IRS1-TapTag construct at 7.3 kb and the endogenous IRS1 locus at 4.3 kb (Figure 7).

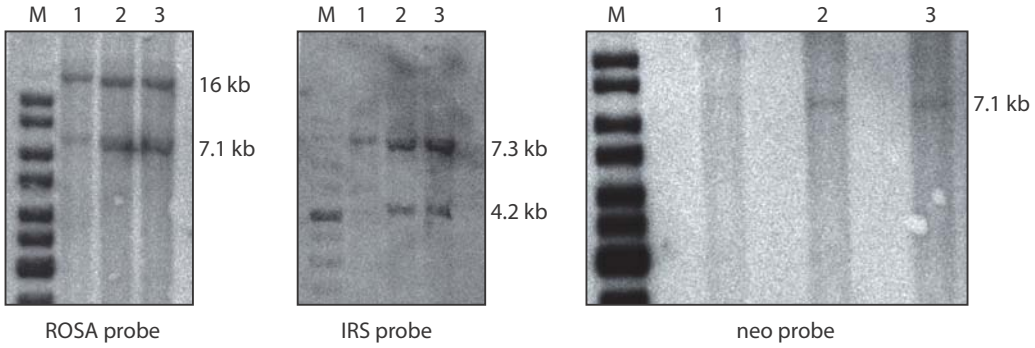

Figure 7: Southern Blot results for three individual ES cell clones. Clones 2 and 3 show the correct band pattern resulting from homologous recombination into the ROSA26 locus.

Those clones were further expanded for injection into blastocysts. In parallel, green fluorescent light emission was detected in targeted ES cells treated with recombinant cre recombinase (Figure 8), further validating the integration of the ROSA-CAGS-IRS1-TapTag construct.

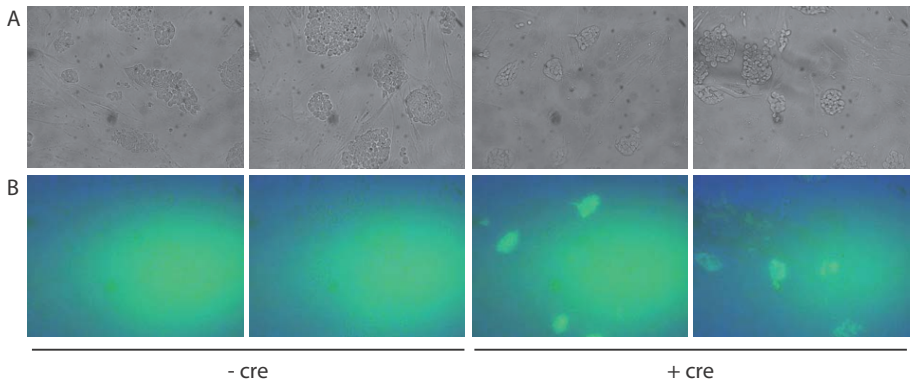

Figure 8: Verification of functional integration of the ROSA-CAGS-IRS1-TapTag construct in transfected ES cells. Cells were either treated with cre or left untreated. Light microscopy (A) and eGFP expression in cells shown by the emission of green fluorescent light (B).

3.2.2 Transgenic mice

Chimeric transgenic ROSA-CAGS-IRS1-TapTag mice were created by the injection of transfected v6.5 ES cells into blastocysts of CB20 mice, which were implanted into the uterus of pseudopregnant mice (F1 generation of C57BL/6 x BALB/c). The chimeric offspring (Figure 9) of those mice with the highest chimerism was crossed to C57BL/6 mice and offspring of the next generation was scanned for the transgene with the CAGS genotyping PCR (Table 3).

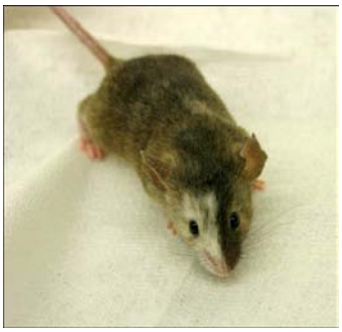

Figure 9: Chimeric mouse with an estimated 95% chimerism. White coat color represents cells derived from the CB20 blastocyst, while brown or black coat color represents cells derived from v6.5 ES cells.

Once germline transmission of the transgene was established, the ROSA-CAGS-IRS1-TapTag mice were backcrossed to C57BL/6 mice. In the next step, ROSA-CAGS-IRS1-TapTag mice were crossed with Alfp-cre mice to trigger hepatocyte specific cre-mediated excision of the loxP flanked stop signal and thereby enabling liver restricted expression of IRS1-TapTag. Mice were bred to homozygosity for the TapTag

allele, whereas the Alfp-cre allele was kept at heterozygosity. Homozygous IRS1-TapTag mice carrying the Alfp-cre allele were analyzed as IRS1-TapTag mice (further abbreviated as TapTag mice), while Alfp-cre negative littermates served as control (further mentioned as wildtypes, WT).

3.2.3 Physiological verification

Functionality of the IRS1-TapTag construct in mice was verified by Western blot analysis. Livers and other selected organs were dissected from control and TapTag mice and protein samples were obtained. On Western blots of liver proteins, both the endogenous IRS1 and IRS1-TapTag were detected and the levels of expression of the heterozygous transgene was comparable to the endogenous expression (Figure 10).

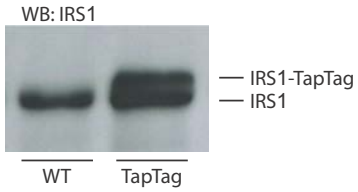

Figure 10: Western blot of hepatic endogenous IRS1 and the elongated IRS1-TapTag in a mouse heterozygous for IRS1-TapTag.

Other organs were examined in order to rule out aberrant expression of IRS1-TapTag. All organs and tissues examined, like white adipose tissue, brain, kidney, heart and skeletal muscle were tested negative for IRS1-TapTag and showed a band for endogenous IRS1 only (Figure 11).

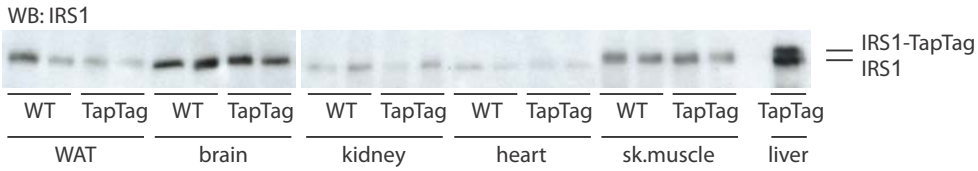

Figure 11: Western blot of IRS1 expression in selected tissues. IRS1-TapTag protein was only detected in liver. WAT: white adipose tissue, sk.muscle: skeletal muscle.

3.3 Phenotypic analysis of ROSA-CAGS-IRS1-TapTag mice

The metabolic phenotype of transgenic IRS1-TapTag mice was assessed in order to examine the influence of additional IRS1 expression on parameters like body weight, body composition and blood glucose levels. Furthermore, insulin and glucose tolerance were assessed to study the systemic response of the transgenic mice to these stimuli. One of two different diets, normal chow diet (NCD) or high fat diet (HFD), was fed from the day of weaning at the age of three weeks and maintained throughout the course of the study.

3.3.1 Body weight

Body weight of transgenic mice and littermate controls was assessed in mice either fed a normal chow diet or a high fat diet. Measurements of body weight of both female and male mice were performed from the time of weaning until the age of 16 weeks on a weekly basis.

The average body weight was unchanged between IRS1-TapTag animals and controls, for both NCD and HFD (Figure 12, Figure 13). However, both female and male mice fed a HFD were significantly heavier approaching week 16.

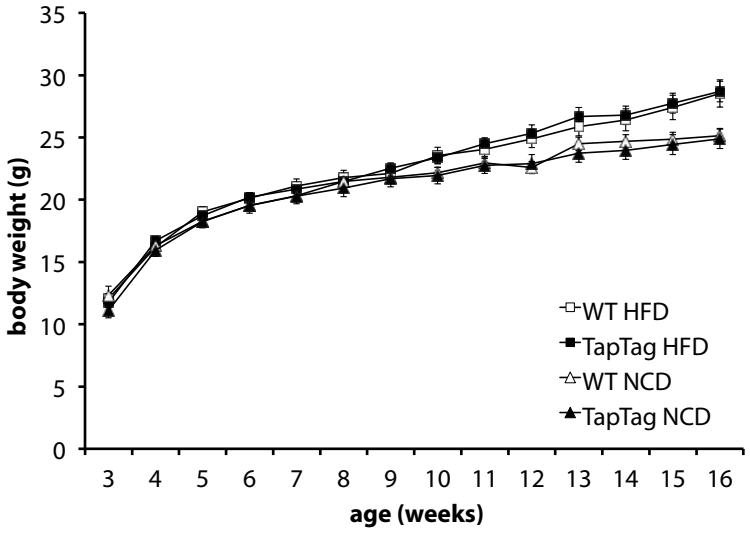

Figure 12: Average body weight of female IRS1-TapTag mice and controls over the course of 13 weeks. Error bars depict SEM values; n=17-25.

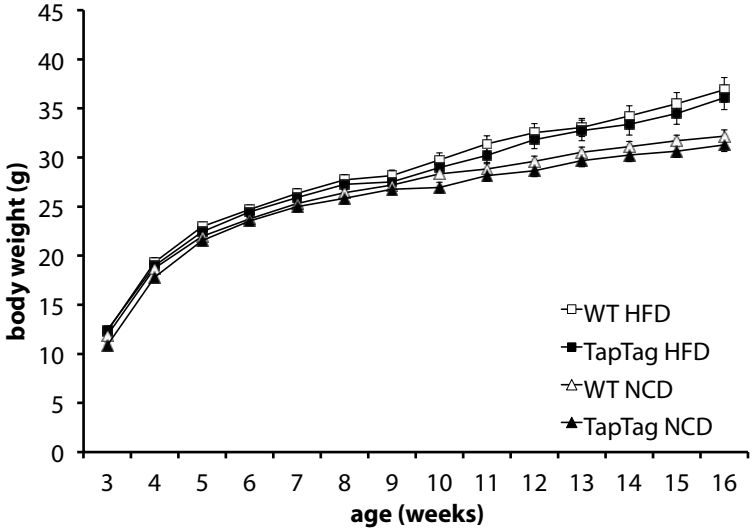

Figure 13: Average body weight of male IRS1-TapTag mice and controls over the course of 13 weeks. Error bars depict SEM values; n=20-26.

3.3.2 Body composition

Body fat content was assessed at the age of 20 weeks relative to total body weight for female and male mice and for mice on NCD as well as on HFD. For both, controls and TapTag mice regardless of gender, the percentage of body fat increased significantly on HFD, whereas on NCD mice remained lean throughout adulthood (Figure 14).

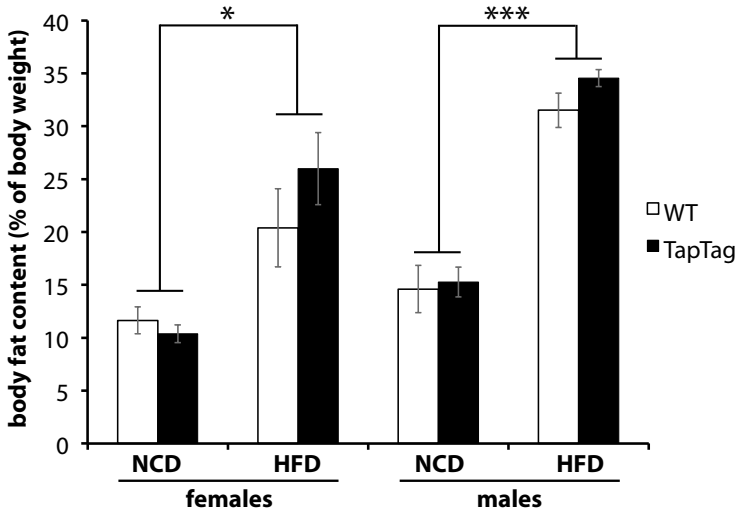

Figure 14: Average body fat content of IRS1-TapTag mice and controls at the age of 20 weeks. Error bars depict SEM values; n=7.

3.3.3 Epigonadal fat pad weight

The complete epigonadal fat pad was weighed after dissection and its weight was unchanged between IRS1-TapTag animals and wildtypes, for both NCD and HFD

(Figure 15). Comparing mice fed NCD with those fed HFD, a significant increase in fat pad weight was observed.

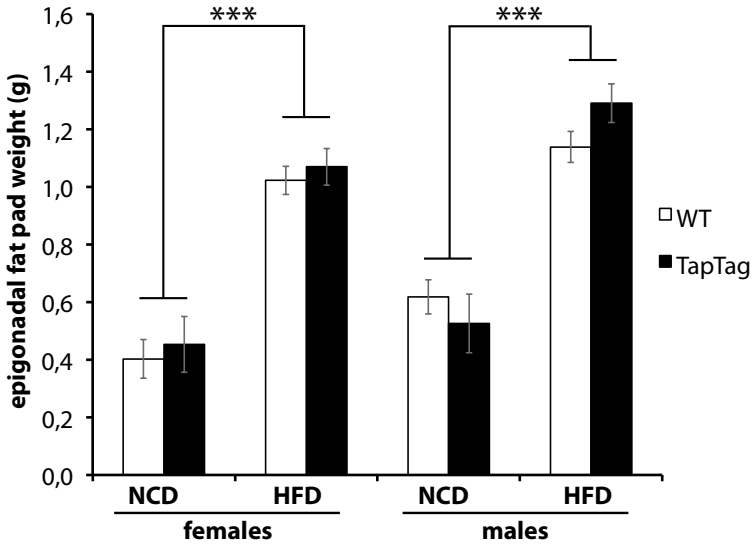

Figure 15: Average epigonadal fat pad weight of IRS1-TapTag mice and controls at the age of 16 weeks. Error bars depict SEM values; n=8-12.

3.3.4 Blood glucose levels

Blood glucose was measured in mice at the age of 8 and 16 weeks and was found to be unchanged between female IRS1-TapTag mice and controls (Figure 16).

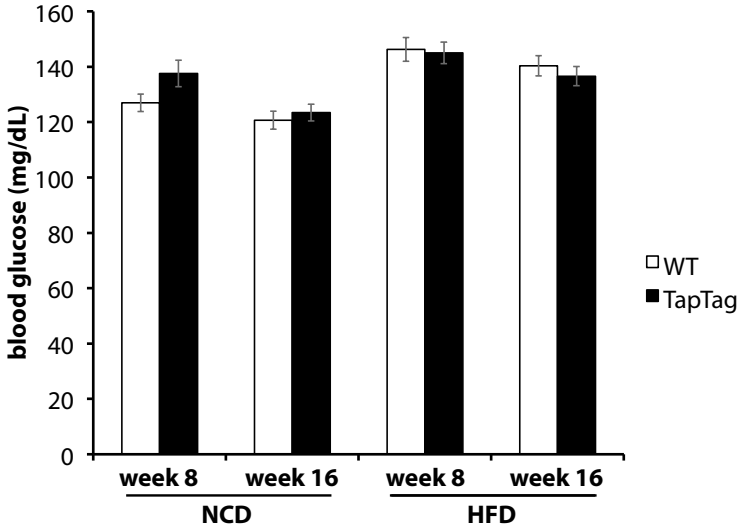

Figure 16: Average blood glucose of female mice with ad libitum access to the respective diet. Error bars depict SEM values; n=14-19.

Accordingly, blood glucose levels were similar for male IRS1-TapTag mice and controls of different age and when fed different diets (Figure 17).

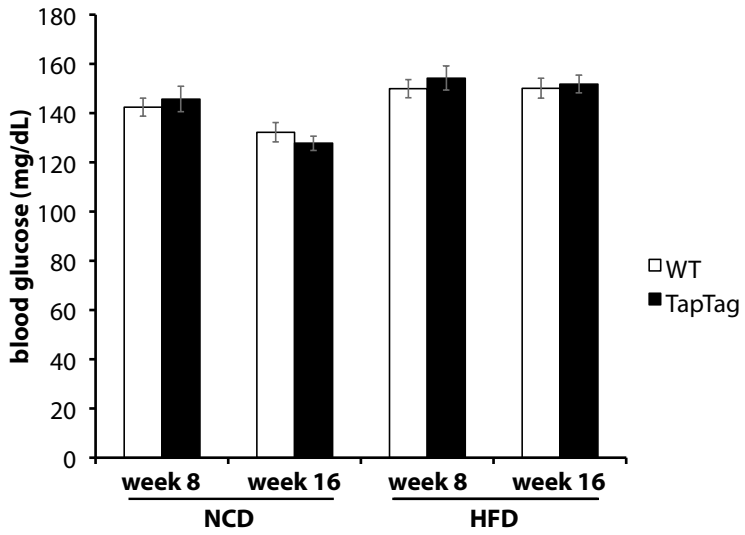

Figure 17: Average blood glucose of male mice with ad libitum access to the respective diet. Error bars depict SEM values; n=16-24.

In addition, fasting blood glucose levels were measured at the age of 12 weeks while preparing fasted mice for glucose tolerance test. In fasted mice, blood glucose levels were comparable for IRS1-TapTag mice and controls, both on NCD and on HFD (Figure 18).

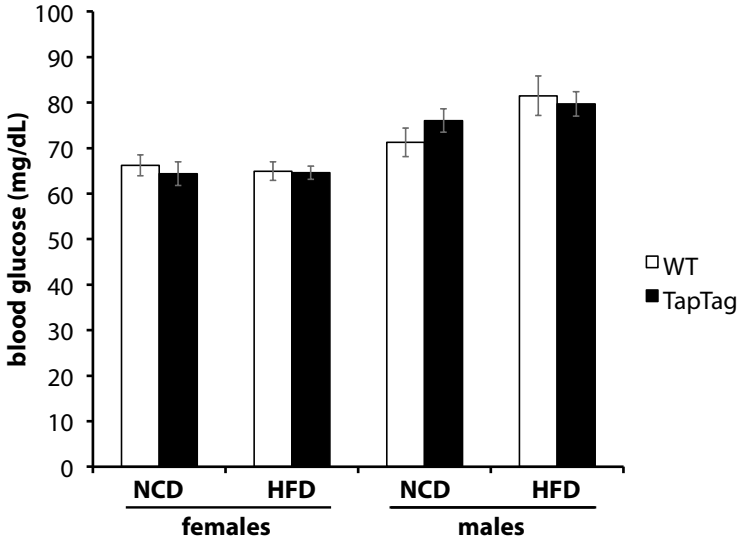

Figure 18: Average blood glucose of fasted mice at the age of 12 weeks. Error bars depict SEM values; females: n=13-19; males: n=19.

3.3.5 Glucose tolerance

In order to assess systemic glucose tolerance of IRS1-TapTag mice, the animals were fasted overnight at the age of 12 weeks and a bolus of glucose was intraperitoneally injected. Reaction to a glucose stimulus was mirrored in the blood glucose level, which reflects the responsiveness of peripheral organs to clear glucose from the blood (Figure 19, Figure 20). Glucose tolerance was unchanged between female IRS1-TapTag mice and controls, but a significant decrease in glucose sensitivity was observed in HFD fed female mice (Figure 19).

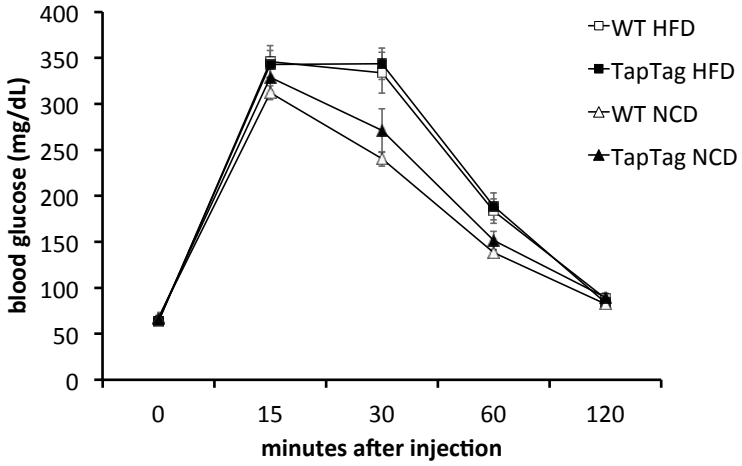

Figure 19: Blood glucose levels of female mice in response to a bolus injection of glucose in a glucose tolerance test. Error bars depict SEM values; n=17-24.

For male IRS1-TapTag mice, higher blood glucose values and thus a decreased peripheral glucose response was measured for HFD-fed IRS1-TapTag mice and controls compared to IRS1-TapTag mice on NCD (Figure 20). However, control mice on NCD responded similar to mice on HFD, which indicates that these mice reacted with a reduced peripheral response to the glucose stimulus.

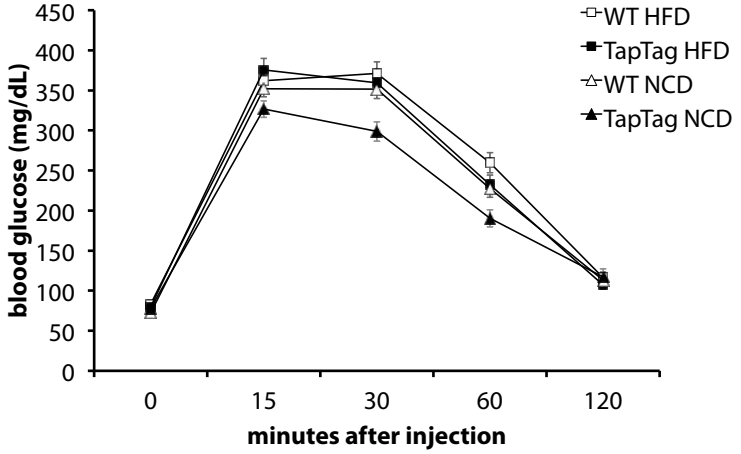

Figure 20: Blood glucose levels of male mice in response to a bolus injection of glucose in a glucose tolerance test. Error bars depict SEM values; n=20-27.

3.3.6 Insulin tolerance

Insulin tolerance of peripheral organs of IRS1-TapTag mice was evaluated for random-fed mice by the intraperitoneal injection of an insulin bolus. Values of blood glucose after the injection reflect the response of the peripheral organs to the insulin stimulus.

Female IRS1-TapTag mice and controls on HFD responded to the same extent to the insulin stimulus (Figure 21). In addition, female IRS1-TapTag mice on NCD showed a tendency to increased insulin sensitivity when compared to controls on NCD and female mice on HFD. However, the statistical analysis did not reveal a significant difference.

For male mice, insulin sensitivity was comparable between IRS1-TapTag mice and controls. Furthermore, the initial response to insulin was decreased in HFD-fed animals for the first time point measured 15 minutes after the injection (Figure 22).

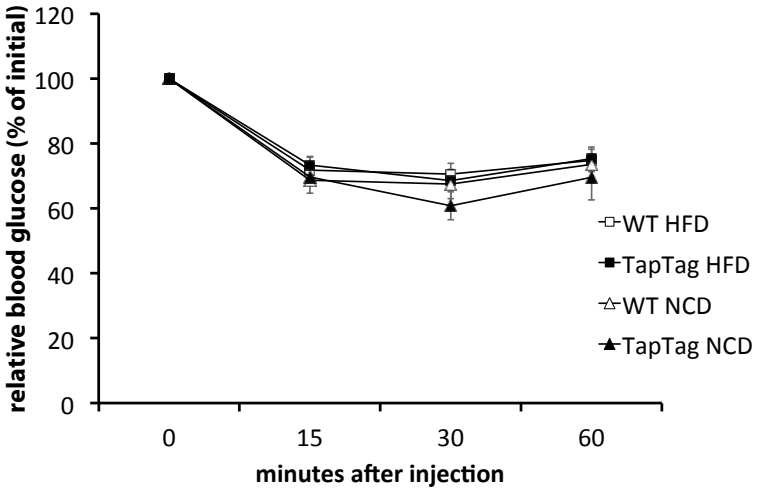

Figure 21: Blood glucose levels of female mice in response to a bolus injection of insulin in an insulin tolerance test. Error bars depict SEM values; n=15-23.

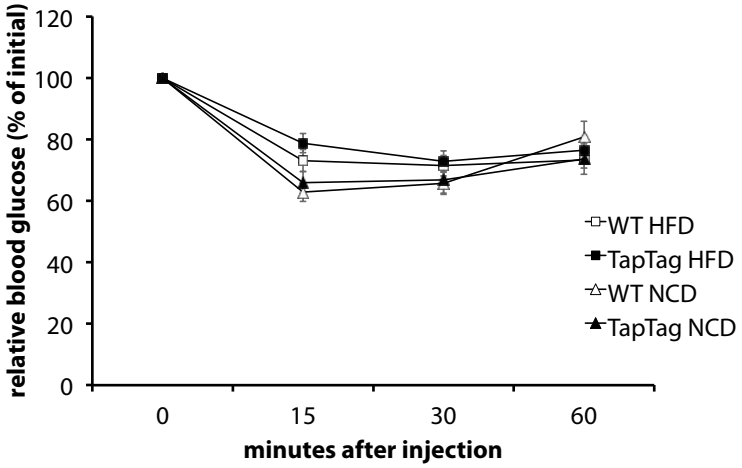

Figure 22: Blood glucose levels of male mice in response to a bolus injection of insulin in an insulin tolerance test. Error bars depict SEM values; n=23-27.

3.3.7 Influence of IRS1 on metabolic phenotype

As added expression of IRS1-TapTag from the transgenic allele increases the overall amount of available IRS1 (Figure 10), an increased response to the insulin signal mediated by additional IRS1 was a substantial concern. However, the phenotyping data indicate that additional expression of IRS1 from the ROSA-CAGS-IRS1-TapTag allele has no effect on the measured metabolic characteristics (Figure 12-Figure 22).

3.4 Proteomic analysis of IRS1 interactions

3.4.1 Sample generation

Proteomic analysis of the IRS1 interactome was performed on mouse liver protein lysates. Both, control wildtype mice and IRS1-TapTag mice were used for the analysis. Groups were split into mice receiving normal chow diet or high fat diet. And furthermore, mice of each group were either treated with sodium chloride or insulin on the day of the experiment.

To this end, a set of 24 hepatic protein extracts was collected originating from 24 mice. The set included 12 controls and 12 IRS1-TapTag mice of which 6 were fed NCD diet and 6 were fed HFD (Figure 23). Animals were fasted overnight, and three animals of each group were stimulated either by sodium chloride or insulin injection into the *vena cava inferior* of anesthetized mice.

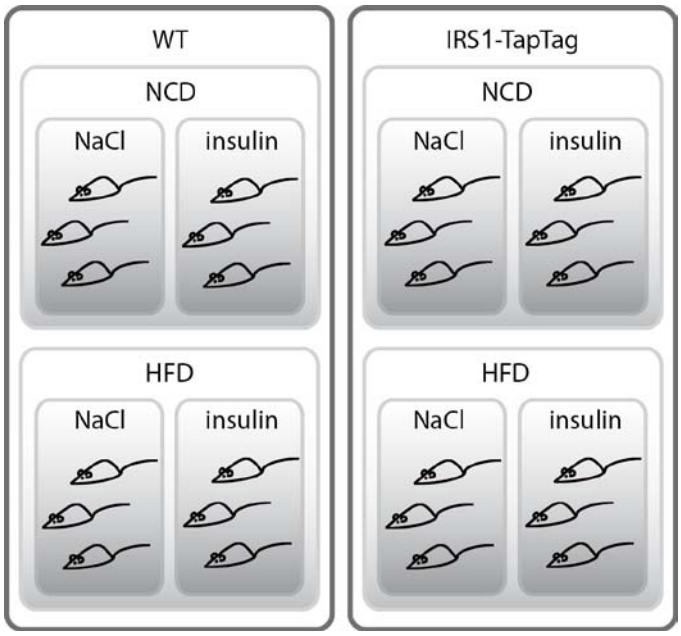

Figure 23: Scheme of different conditions applied for a set of 24 mice.

3.4.2 Verification of insulin signaling

For Western blot confirmation, protein lysates of all 24 samples were compared regarding their protein content (Figure 24). In TapTag animals, extra bands are detected for IRS1-TapTag. While p85 and total Akt content remains unchanged, the appearance of pAkt in insulin stimulated samples indicates functional insulin signaling downstream of IRS1 as a verification of *vena cava* injection of insulin. Additionally, β-Actin levels reflect equal total protein content of all 24 samples.

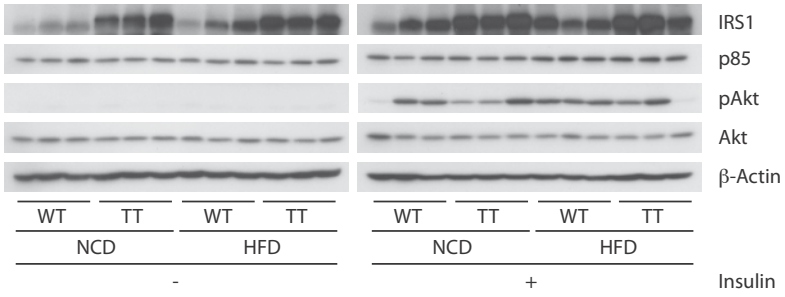

Figure 24: Western blot analysis of protein lysates used for affinity purifications and subsequent mass spectrometry analysis. Western blot was probed with IRS1 antibody, revealing endogenous IRS1 and IRS1-TapTag, p85 antibody and pAkt antibody as a marker for activated insulin signaling downstream of IRS1. Additionally, Akt and β-Actin serve as loading control.

3.4.3 Streptavidin affinity purification

One-step affinity purifications were carried out using the streptavidin binding peptide of the TapTag. Performance of the experiment was routinely checked by Western blot analysis of various fractions of the purifications (Figure 25). In the initial protein input both, endogenous IRS1 and p85 are detected, while in the TapTag sample an additional band for IRS1-TapTag appears. As expression levels were similar in heterozygous IRS1-TapTag mice (Figure 10), in livers of homozygous IRS1-TapTag mice expression of IRS1-TapTag exceeds the expression of endogenous IRS1 (Figure 25). After the binding step, IRS1-TapTag has bound to the beads. However, residual IRS1-TapTag is detected in the unbound protein fraction due to limited capacity of the beads. Moreover, both endogenous IRS1 and unbound p85, or p85 initially bound to endogenous IRS1, are removed from the mixture. After two washing steps, no further IRS1 or p85 are removed from the beads, and finally, elution with biotin displaces IRS1-TapTag with bound proteins from the streptavidin beads.

Whether the biotin elution was effectively removing all bound bait protein was not conclusive from the biotin eluate only, and thus, after biotin elution, beads were boiled in

SDS sample buffer. Proteins recovered from this last fraction show the amount of protein not included in the analysis of interacting proteins.

Figure 25: Representative Western blot of input, unbound protein fraction, wash fractions and biotin eluate of a streptavidin affinity purification. Additionally, beads were boiled with SDS sample buffer after elution. Blots were probed with primary antibodies IRS1 and p85.

In addition, biotin eluates of all 24 purifications were analyzed on Western blots for the assessment of successful purification of IRS1 and co-purification of p85 (Figure 26). Both, IRS1 and p85 were detected in all 12 TapTag samples but not in wildtypes, indicating a TapTag-specific elution.

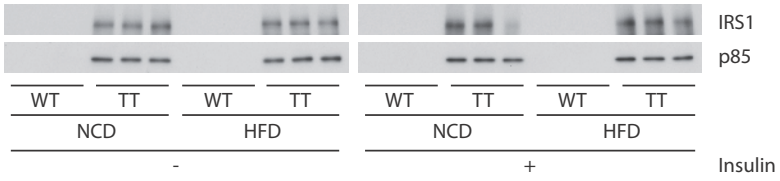

Figure 26: Western blot analysis of biotin eluates of affinity purification. IRS1 was specifically purified in TapTag samples only; p85 was co-purified with IRS1-TapTag.

For the proteomic analysis of IRS1 interaction profiles under conditions of diet-induced obesity, biotin eluates were separated on gradient gels and lanes of the Coomassie stained gel were cut in 10 slices each (Figure 27). From Coomassie stained gels, differences in band patterns between experimental conditions were not apparent, however, the overall protein content in wildtype samples seemed reduced.

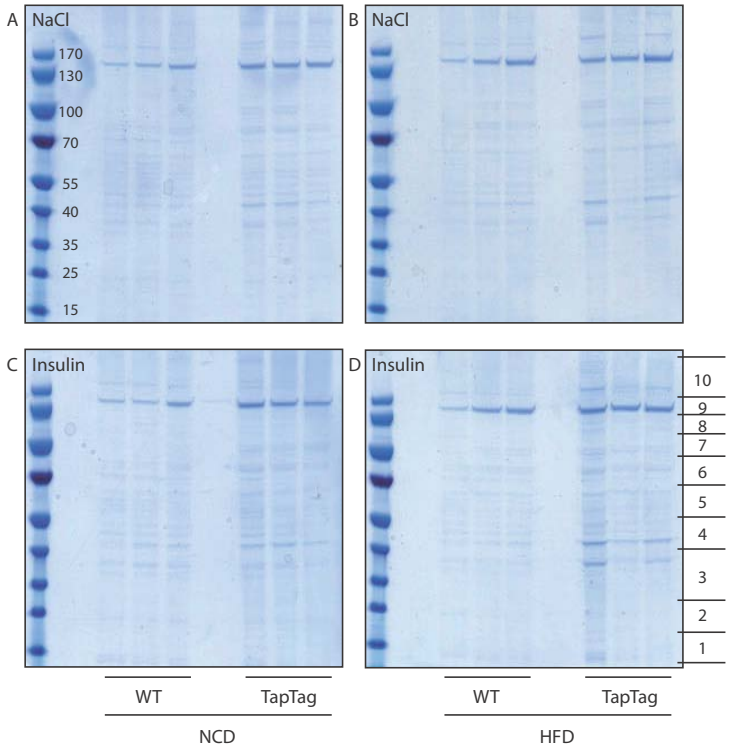

Figure 27: Coomassie gradient gels with all 24 biotin eluates prepared for subsequent mass spectrometry analysis. On the left, numbers reflect molecular weight (kDa) in protein marker (A). On the right, horizontal lines indicate the gel slices cut for in-gel trypsin digest (D).

3.4.4 Mass spectrometry and label-free quantification

A total of 809 different proteins were identified in nano-LC-ESI-MS/MS experiments, while three proteins were listed as “putative uncharacterized protein” and remained unidentified (Table 8-S). Skin-derived keratins were considered contaminants and thus were excluded manually from the list. Proteins identified in wildtype samples with an average intensity above $5x10^6$ were considered unspecific and also excluded from the analysis.

Lower and upper limits for intensity ratios were defined to eliminate mathematically misleading ratios from the list and to narrow the distribution of the results. This was necessary to display ratios for protein interactions with IRS1 that were not detectable in one of the conditions and were therefore assigned values of zero. A maximum of 50 was defined to replace all conditions in which the respective protein was not detected in HFD or insulin samples. In analogy, a minimum of 0.02 was set for conditions in which proteins were not detected in NCD or sodium chloride samples.

Average intensities, calculated as average between NCD and HFD and NCD/HFD ratios for identified interacting proteins in samples from either NaCl- or insulin-treated mice were displayed as scatter plots on logarithmic scale (Figure 28). Respective values for IRS1

were marked individually. Proteins found at a ratio of 1 were unchanged between NCD and HFD biotin eluates. Higher ratios represent a decrease of interaction on HFD, while lower ratios indicate an increased interaction on HFD. In biotin eluates from NaCl-treated mice, 697 potentially interacting proteins were identified, while in the biotin eluates from insulin-treated mice, 646 proteins were identified.

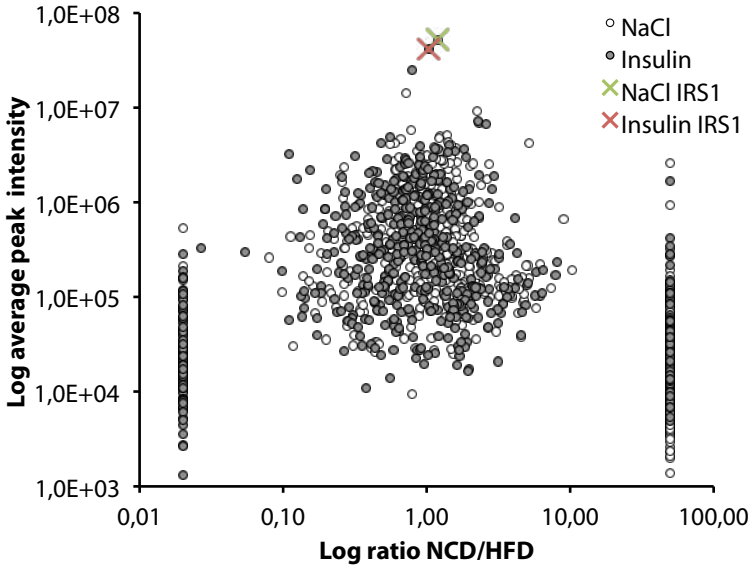

Figure 28: Scatter plot of identified interacting proteins after NaCl and insulin treatment. Proteins with a log ratio of 1 were found to be associated to IRS1 in comparable amounts on both, NCD and HFD. Below a log ratio of 1, protein interaction with IRS1 was increased on HFD compared to NCD and above 1 the interaction was decreased on HFD.

Additionally, ratios comparing NaCl and insulin samples were summarized in a scatter plot showing individual values for samples from NCD and HFD mice (Figure 29). Again, respective values for IRS1 were marked individually. In biotin eluates from NCD-fed mice, 717 potentially interacting proteins were identified, while in the biotin eluates from HFD-fed mice, 595 proteins were identified.

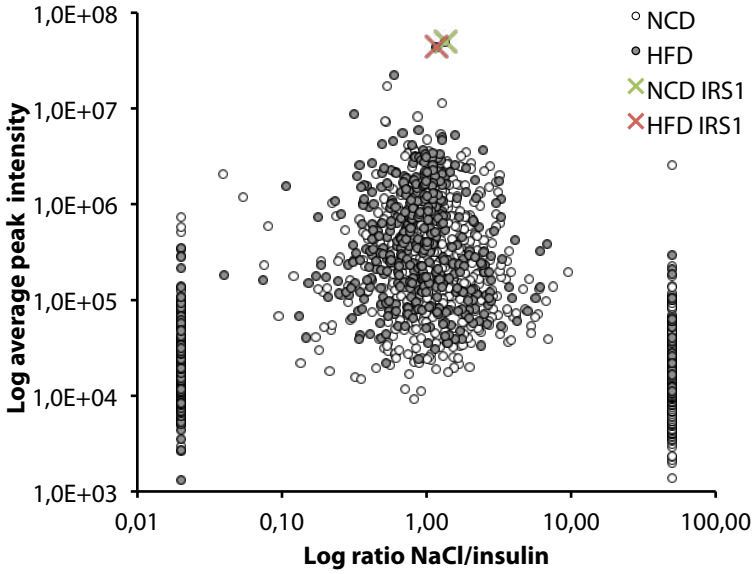

Figure 29: Scatter plot of identified interacting proteins for NCD- and HFD-fed mice.

Intensity and ratio for significant changes in IRS1 interactions were extracted and plotted separately (Figure 30, Figure 31).

Overall, comparing NCD and HFD mice, IRS1 interaction with 106 proteins was significantly altered between the conditions. For the set of NaCl treated TapTag mice, 13 proteins interacting with IRS1 were significantly increased upon HFD feeding as analyzed by Student's t test, while 53 proteins were significantly decreased. On the other hand, in insulin-treated TapTag mice, administration of HFD led to a significantly increased interaction of 25 proteins with IRS1 and also a significantly decreased IRS1 interaction of 15 proteins was detected in HFD-fed mice treated with insulin (Figure 30, Table 6).

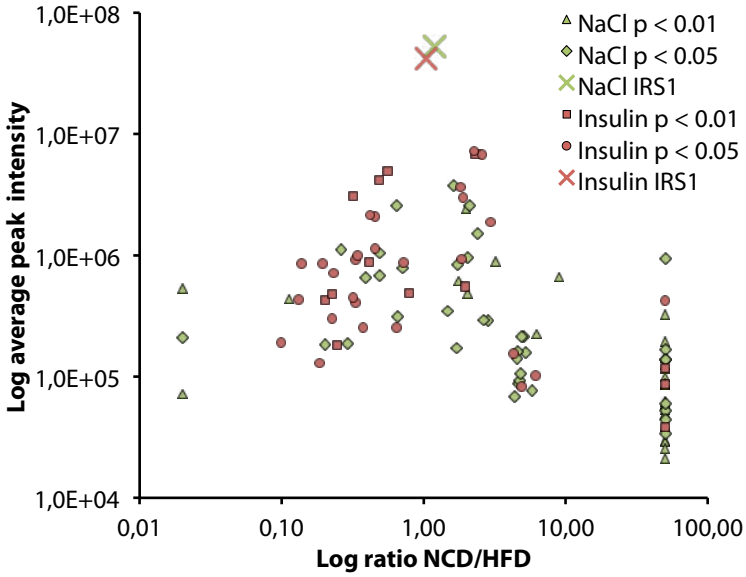

Figure 30: Scatter plot of IRS1 interacting proteins, significantly changed between NCD and HFD.

Table 6: IRS1 interacting proteins identified in biotin eluates of affinity purifications, which significantly varied between NCD controls and mice fed HFD. Ratio NCD/HFD: ratio of average intensities, average intensity: arithmetic mean of NCD and HFD intensities, significance assessed by Student's t test.

protein	ratio NCD/HFD	average intensity	significance (p-value)
NaCl: increased by HFD			
Ribonuclease UK114	0,02	536552	0,00082428
5-hydroxyisourate hydrolase	0,02	71863	0,00652843
D-dopachrome decarboxylase	0,02	211857	0,03657367
Igh protein	0,11	436829	0,00713017
ATP-dependent RNA helicase A	0,20	184493	0,03500638
Heterogeneous nuclear ribonucleoprotein A3	0,26	1113210	0,03767205
Regulator of chromosome condensation 1	0,29	188720	0,03577194
14-3-3 protein beta/alpha	0,39	659837	0,01100881
Beta III spectrin	0,49	1045487	0,01664590
Aldehyde dehydrogenase family 3, subfamily A2	0,49	680903	0,02175244
60S ribosomal protein L23	0,65	2580067	0,01319390
Formimidoyltransferase-cyclodeaminase	0,65	315258	0,04814504
Radixin	0,71	788105	0,01281583
NaCl: decreased by HFD			
Probable urocanate hydratase	1,47	346642	0,03367752
Tubulin beta-2C chain	1,61	3754567	0,01960744
Glyoxylate reductase/hydroxypyruvate reductase	1,71	172293	0,01450478
Sarcosine dehydrogenase, mitochondrial	1,72	833153	0,03480824
Cytochrome P450 2F2	1,75	616523	0,00499669

protein	ratio NCD/HFD	average intensity	significance (p-value)
NaCl: decreased by HFD (continued)			
10-formyltetrahydrofolate dehydrogenase	1,99	2442150	0,00805952
Endoplasmin	2,03	957012	0,03475376
Succinate dehydrogenase subunit A	2,03	484232	0,00394639
ATP synthase subunit b, mitochondrial	2,10	2563650	0,03137530
ATP synthase subunit delta, mitochondrial	2,38	1521188	0,02684807
Cytochrome P450 2C29	2,64	291608	0,04791424
Aspartate aminotransferase	2,85	291290	0,03536053
ATP synthase subunit gamma, mitochondrial	3,20	891683	0,00910801
Cytochrome P450 2D9	4,34	68001	0,03134083
3-alpha-hydroxysteroid dehydrogenase type 1	4,54	141862	0,03804481
60S ribosomal protein L10a	4,61	162235	0,02671896
Estradiol 17-beta-dehydrogenase 8	4,67	87320	0,02472089
Cathepsin Z	4,75	93385	0,03147981
Cytochrome P450 2C50	4,77	107135	0,03699983
C-1-tetrahydrofolate synthase, cytoplasmic	4,92	215268	0,03326627
Mannosyl-oligosaccharide glucosidase	5,06	216000	0,01588389
Rab GDP dissociation inhibitor beta	5,20	157467	0,01465577
Voltage-dependent anion-selective channel protein 2	5,80	76237	0,02383055
Cytochrome P450 2D10	6,19	224823	0,00989160
Receptor of activated protein kinase C 1	8,98	661152	0,00936571
Mitochondrial import TIM50	50,00	58462	0,00000925
Ribophorin-1	50,00	143137	0,00002744
Fatty acid synthase	50,00	99465	0,00005099
Aldo-keto reductase family 1 member C13	50,00	53139	0,00007597
Neutral alpha-glucosidase AB	50,00	38922	0,00020581
Cytochrome P450 4A14	50,00	86130	0,00029406
UDP-glucose 6-dehydrogenase	50,00	117535	0,00030213
Cytochrome P450 1A2	50,00	88078	0,00058619
Ceruloplasmin	50,00	29511	0,00167798
Probable D-lactate dehydrogenase, mitochondrial	50,00	85035	0,00194381
Cystathionine gamma-lyase	50,00	125282	0,00328819
1,4-alpha-glucan-branching enzyme	50,00	59565	0,00346123
Cytochrome P450 3A11	50,00	323120	0,00346364
Transaldolase	50,00	48045	0,00371966
Apolipoprotein A-IV	50,00	28885	0,00401632
Proliferation-associated protein 2G4	50,00	21110	0,00405390
Diaphorase-1	50,00	194152	0,00442902
Peroxisomal acyl-coenzyme A oxidase 2	50,00	25748	0,00476434
T-complex protein 1 subunit gamma	50,00	62426	0,00704655
Flotillin-1	50,00	49505	0,00778784
Eukaryotic peptide chain release factor subunit 1	50,00	33596	0,01006718
Ces5 protein	50,00	53039	0,01049759
Cytochrome P450 2J5	50,00	44197	0,01125364
Heat shock 70 kDa protein 4	50,00	137115	0,01284088
Serine-threonine kinase receptor-associated protein	50,00	167488	0,01532933
Plasma kallikrein	50,00	59956	0,02047452
ATP synthase subunit alpha, mitochondrial	50,00	941383	0,03414592
Histone H2A type 3	50,00	139057	0,04478532

protein	ratio NCD/HFD	average intensity	significance (p-value)
insulin: increased by HFD			
Heterogenous nuclear ribonucleoprotein U	0,10	190359	0,01780266
Polypyrimidine tract binding protein 1	0,13	433432	0,02945082
Cofilin-2	0,14	848842	0,01857239
ATP-dependent RNA helicase A	0,18	129375	0,03170103
Splicing factor, arginine/serine-rich 7	0,19	848945	0,01184797
Heterogeneous nuclear ribonucleoprotein A/B	0,20	425652	0,00487370
Catalase	0,23	301057	0,03385420
Heterogeneous nuclear ribonucleoprotein D0	0,23	479819	0,00590583
Heterogeneous nuclear ribonucleoprotein K	0,23	718155	0,02461895
TAR DNA-binding protein 43	0,25	181852	0,00556680
Formimidoyltransferase-cyclodeaminase	0,32	447148	0,03739451
Heterogeneous nuclear ribonucleoproteins A2/B1	0,32	3074333	0,00065202
Splicing factor, arginine/serine-rich 1	0,33	409842	0,02454686
Heterogeneous nuclear ribonucleoprotein A3	0,33	924378	0,02537710
Actin-related protein 2	0,34	995370	0,02778201
AP-2 complex subunit alpha-1	0,37	254440	0,02100234
Talin-1	0,41	884063	0,00224929
AP-2 complex subunit beta-1	0,42	2150425	0,03392636
AP-2 complex subunit alpha-2	0,45	1133193	0,02312266
Beta III spectrin	0,45	2075550	0,02376896
Spectrin beta chain, brain 1	0,48	4195183	0,00173724
Myosin-9	0,56	4928417	0,00365483
Heat shock 70 kDa protein 1B	0,65	253175	0,02075014
Serotransferrin	0,72	869552	0,01998260
Actin-related protein 2/3 complex subunit 2	0,79	489270	0,00550855
insulin: decreased by HFD			
Protein transport protein Sec24A	1,83	3649233	0,01199740
Desmoplakin	1,85	933275	0,04816860
Protein transport protein Sec23A	1,89	3008500	0,01276602
Protein transport protein Sec23B	1,95	553625	0,00801024
Acetyl-CoA carboxylase 2	2,27	7258083	0,02726718
14-3-3 protein epsilon	2,32	6826100	0,00055545
14-3-3 protein gamma	2,58	6778733	0,02570782
14-3-3 protein zeta/delta	2,97	1888058	0,02156504
Voltage-dependent anion-selective channel protein 1	4,32	154882	0,03573597
2-oxoglutarate dehydrogenase E1 component	4,87	82876	0,02780820
Cathepsin Z	6,16	101753	0,01375986
Annexin A2	50,00	86342	0,00051851
Mitochondrial 2-oxodicarboxylate carrier	50,00	38359	0,00248245
Leucine-rich repeat-containing protein 59	50,00	118288	0,00486852
Receptor of activated protein kinase C 1	50,00	424322	0,03037874

A total of 91 protein interactions were significantly regulated comparing NaCl and insulin-treated samples. For NCD-fed TapTag mice, 31 protein interactions with IRS1 were significantly increased after insulin injection as analyzed by Student's t test, while 34 proteins were significantly decreased. Further, in HFD-fed TapTag mice, injection of insulin led to a significantly increased interaction of 18 proteins with IRS1, however also

significantly decreased interaction of 8 proteins with IRS1 was detected in insulin-treated mice (Figure 31, Table 7).

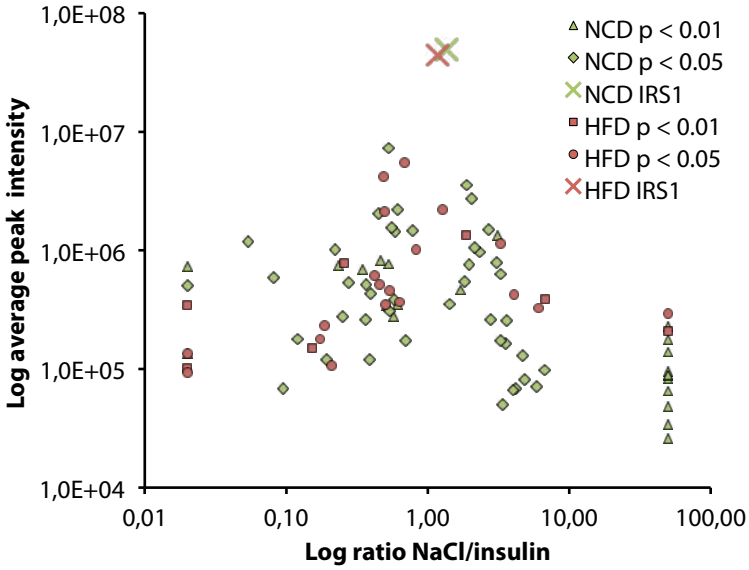

Figure 31: Scatter plot of IRS1 interacting proteins, significantly changed between NaCl and insulin treatment.

Table 7: IRS1 interacting proteins identified in biotin eluates of affinity purifications, which significantly varied between NaCl controls and insulin-treated mice. Ratio NaCl/insulin: ratio of average intensities, average intensity: arithmetic mean of NaCl and Insulin intensities, significance assessed by Student's t test.

protein	ratio NaCl/insulin	average intensity	significance (p-value)
NCD: increased upon insulin			
Thioredoxin	0,02	134450	0,00117861
Ribonuclease UK114	0,02	729133	0,00150522
ATP synthase e	0,02	506705	0,02575948
Clathrin light chain B	0,05	1188298	0,01353605
Igh protein	0,08	592723	0,04380832
Moesin	0,09	68282	0,02383953
Cingulin	0,12	178828	0,01418280
Splicing factor, arginine/serine-rich 1	0,19	121125	0,04766261
14-3-3 beta/alpha	0,22	1019550	0,02160806
Desmoplakin	0,24	748713	0,00620093
Glyoxalase II	0,25	277580	0,02453758
CytC somatic	0,27	533935	0,01858194
Junction plakoglobin	0,34	693903	0,00094079
Lamin-B2	0,36	262415	0,01630094
Transcription factor A	0,37	516398	0,04842617
Annexin A2	0,39	119748	0,04951861
Lamin-B1	0,39	434458	0,01348655
14-3-3 zeta/delta	0,45	2046417	0,04125169

protein	ratio NaCl/insulin	average intensity	significance (p-value)
NCD: increased upon insulin (continued)			
Aldh4a1	0,46	820965	0,00439232
Beta-filamin	0,51	343368	0,00170217
14-3-3 epsilon	0,53	7291867	0,01519247
Clathrin light polypeptide (Lca)	0,53	767798	0,00773365
GTPase Ran	0,54	307320	0,01961267
Vinculin	0,55	1567727	0,04312590
Bile acid-CoA ligase	0,57	276495	0,00855864
DEAD box protein 5	0,58	384830	0,02513798
Carboxylesterase 3	0,59	1441168	0,01973892
Beta-II-Spectrin	0,61	2196650	0,01256377
Arp2/3 complex subunit 2	0,61	347507	0,00485367
H2-Ke6	0,70	174613	0,01405080
Peroxisomal multifunctional enzyme type 2	0,78	1467667	0,01481826
NCD: decreased upon insulin			
Probable urocanate hydratase	1,42	352187	0,03489161
Aconitate hydratase	1,71	462282	0,00362565
Decr1	1,81	546998	0,02424911
Tubulin beta-2C chain	1,88	3548650	0,04251287
Acyl-CoA oxidase 1	1,96	762773	0,02534985
Fructose-1,6-bisphosphatase 1	2,03	2725317	0,03207546
Thiosulfate sulfurtransferase	2,13	1051077	0,03354674
ATP synthase subunit gamma	2,34	969185	0,01736927
Peptidyl-prolyl cis-trans isomerase B	2,70	1498473	0,04731116
Cytochrome P450 2D10	2,78	263298	0,04470201
Arp2/3 complex subunit 4	3,05	794627	0,04775045
MCG5400	3,13	1331005	0,00705186
Peroxiredoxin-5	3,24	633710	0,03179279
60S ribosomal protein L10a	3,29	173823	0,01542303
Glucosidase II alpha	3,41	50339	0,01670608
Hydroxysteroid (17-beta) dehydrogenase 13	3,56	165548	0,01330282
Glycine N-acyltransferase	3,60	257347	0,01274160
Aldo-keto reductase a	4,00	66415	0,04325229
Cytochrome P450 2D9	4,17	68514	0,03644352
CapZ alpha-1	4,67	129782	0,02933035
Acetyl-CoA acyltransferase A	4,80	80799	0,02367134
Nitrilase homolog 2	5,87	70833	0,01004585
Probable D-lactate dehydrogenase	6,67	97791	0,01408472
Perioredoxin-3	50,00	139170	0,00000064
Succinate dehydrogenase FeS	50,00	229163	0,00000122
UMP-CMP kinase	50,00	65172	0,00005065
Mn SOD	50,00	177383	0,00008827
CytP450 C27/25	50,00	82700	0,00016248
Annexin A6	50,00	34053	0,00103924
Sepiapterin reductase	50,00	95337	0,00313611
Transaldolase	50,00	48045	0,00371966
Abhydrolase domain-containing protein 14B	50,00	87375	0,00462482
Acox2	50,00	25748	0,00476434
GTP-binding protein SAR1b	50,00	89283	0,00700857

protein	ratio NaCl/insulin	average intensity	significance (p-value)
HFD: increased upon insulin			
ATP synthase alpha	0,02	342428	0,00002851
Ribophorin-1	0,02	102067	0,00299000
Plasma kallikrein	0,02	93538	0,01266945
HSP70	0,02	135557	0,04134671
T-complex protein 1 zeta	0,15	151233	0,00731748
Bile acid-CoA ligase	0,17	178997	0,01361373
Heterogeneous nuclear ribonucleoprotein F	0,19	231673	0,03756442
Cytochrome P450 2C50	0,21	106967	0,02523418
Talin-1	0,26	785628	0,00637427
Cytochrome c, somatic	0,42	615958	0,03179426
Glutaryl-CoA dehydrogenase	0,46	519525	0,03782171
Beta-II-Spectrin	0,49	4220650	0,02219327
Beta-III-Spectrin	0,49	2131183	0,02502917
UDP-glucose pyrophosphorylase	0,50	347185	0,01916395
Succinate dehydrogenase subunit A	0,54	458298	0,01067276
Hepatic flavin-containing monooxygenase 5	0,63	368117	0,03375016
Peroxiredoxin-1	0,68	5515283	0,04616739
Radixin	0,83	1021058	0,04275227
HFD: decreased upon insulin			
Fructose-1,6-bisphosphatase 1	1,28	2195333	0,04220511
Elongation factor 2	1,87	1340607	0,00738175
Peptidyl-prolyl cis-trans isomerase A	3,27	1138043	0,03239641
Succinyl-CoA ligase alpha	4,07	423333	0,03921015
Succinate dehydrogenase FeS	6,06	326865	0,03193280
Peroxiredoxin-5	6,78	387477	0,00806316
Glycine N-acyltransferase	50,00	210707	0,00411546
Major urinary protein 24	50,00	292803	0,01081099

Individual analysis of average intensities for proteins detected in all four different conditions was conducted for wildtype and IRS1-TapTag mice in bar charts, which represent average interaction with IRS1.

For IRS1 itself, no difference was detected between NaCl and insulin samples or between NCD and HFD samples (Figure 32, A). As expected, peptides derived from the IRS1 protein were only found in mass spectrometry analysis of IRS1-TapTag mice and were absent in wildtypes.

A known high affinity interaction between IRS1 and PI3K (Phosphatidylinositol 3-kinase) (*70*) was used for verification in this study. Different isoforms of the subunits of the PI3K complex, p85α and β (Figure 32, B and C), as well as p110α and β (Figure 32, D and E) were detected in TapTag samples but not in wildtypes. IRS1 interaction with the regulatory subunit p85, also used as verification in Western blots of affinity purifications (Figure 25), was increased for p85α after insulin treatment as compared to

NaCl treatment (Figure 32, B), although the difference was not statistically significant. IRS1-p85β interaction showed a tendency towards increased association after insulin treatment (Figure 32, C). Moreover, interaction of IRS1 with the catalytic subunit p110 seemed to be largely depending on the insulin signal, as only low levels of basal IRS1-p110α interaction were detected in NaCl samples (Figure 32, D) and p110β only associated with IRS1 after insulin treatment (Figure 32, E).

Remarkably, five members of the 14-3-3 family interact with IRS1 in TapTag livers in all four conditions, while 14-3-3 proteins were absent in wildtype biotin eluates (Figure 33, B and D) or detected only at low levels (Figure 33, A, C and E). Overall, interaction of 14-3-3 proteins and IRS1 was increased after insulin stimulation on NCD. Basal interaction in NaCl samples was comparable between NCD and HFD. However, HFD feeding blunted insulin-stimulated interaction of IRS1 and 14-3-3 proteins.

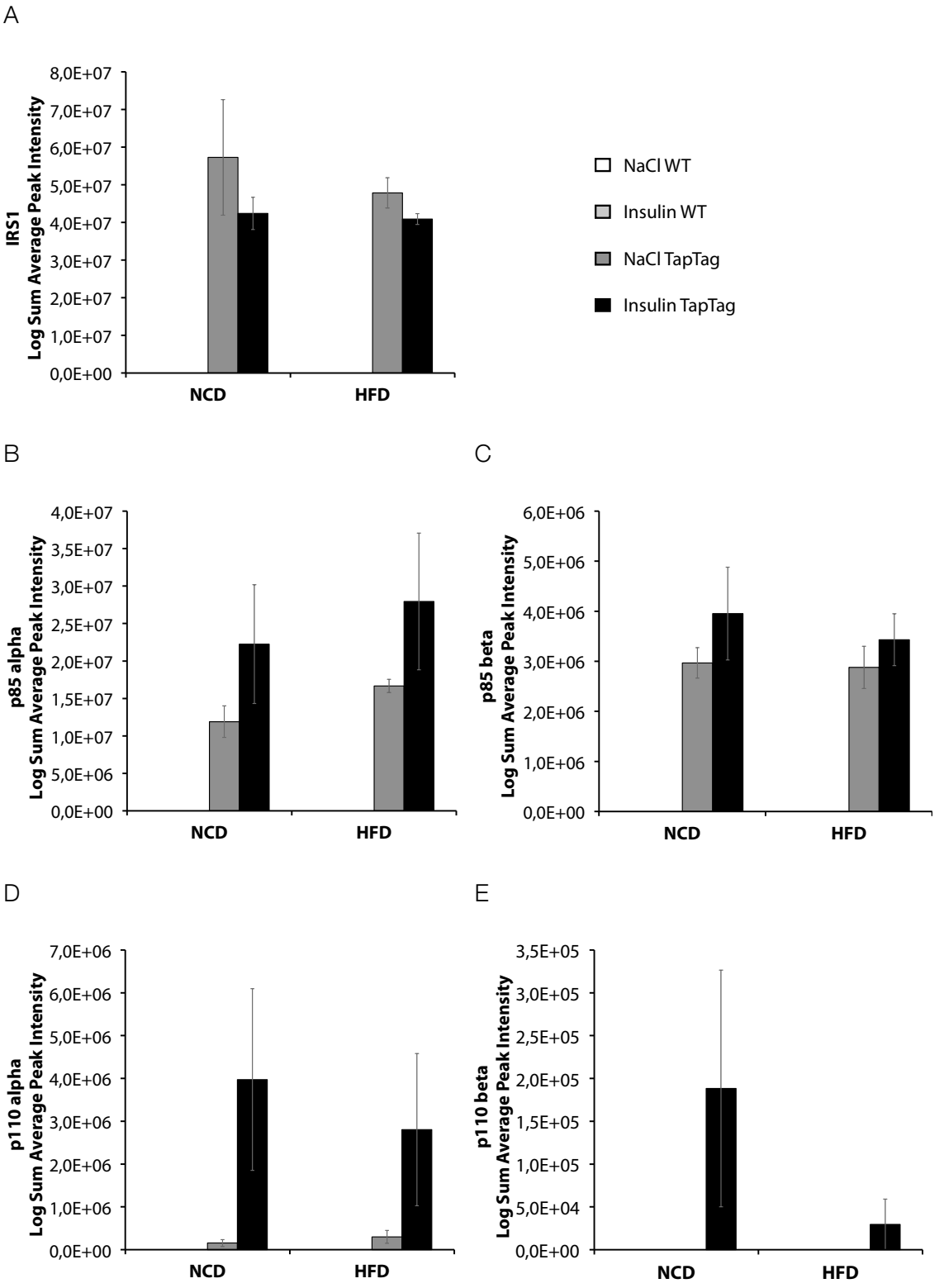

Figure 32: Label-free quantification of bait protein IRS1 (A) and identified subunits of the known interacting protein phosphatidylinositol 3-kinase. Interactions with α (B) and β isoforms (C) of regulatory subunit p85 were detected as well as interactions with the catalytic subunits p110 α (D) and β (E).

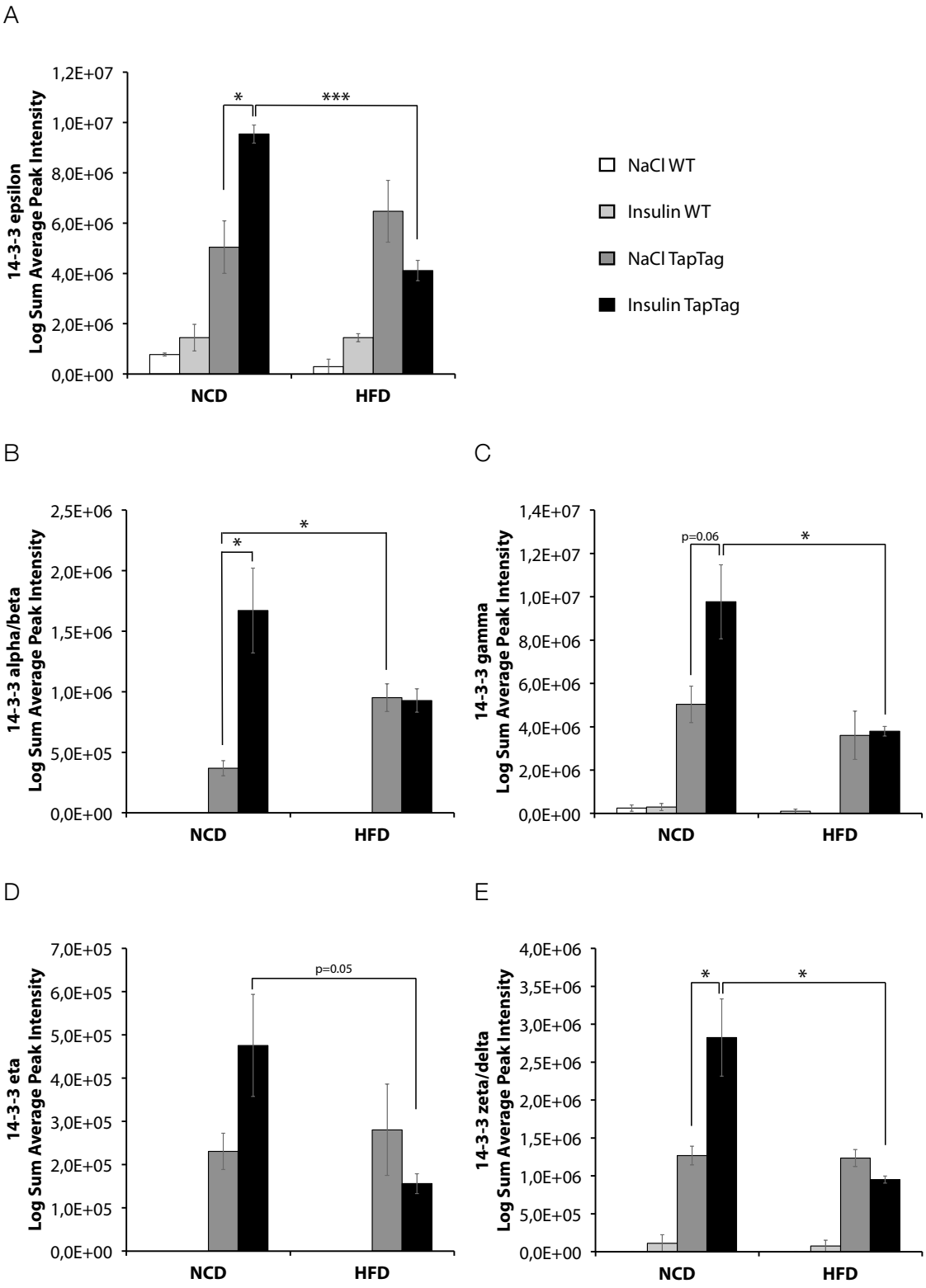

Figure 33: Label-free quantification of members of the 14-3-3 protein family. 14-3-3ε (A), 14-3-3α/β (B), 14-3-3γ (C), 14-3-3η (D) and 14-3-3ζ/δ (E) were found in biotin eluates of TapTag samples.

In contrast, IRS1 interaction with tyrosine-protein kinase Lyn was increased after insulin treatment in HFD-fed mice (Figure 34). In NCD samples, both after NaCl and insulin treatment, interaction was similar. However, despite the fact that no peptides corresponding to Lyn protein were detected in wildtype biotin eluates, comparing Lyn average intensities among TapTag samples, the detected difference was not statistically significant.

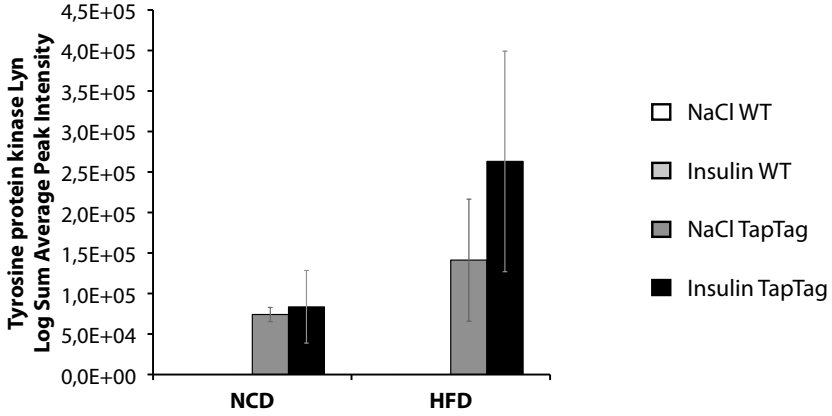

Figure 34: Label-free quantification of tyrosine-protein kinase Lyn.

Taken together, a number of protein associations with IRS1 seem to be increased upon insulin treatment, however this effect was more pronounced on NCD than on HFD. Furthermore, the proteins more closely examined, like subunits of PI3K and the 14-3-3 protein family, show an association pattern that suggests an increased association with IRS1 upon insulin signaling, which was blunted on HFD.

3.4.5 Immunodetection of putative IRS1 interaction partners

As confirmation of the mass spectrometry results, selected putative IRS1 interaction partners were verified on Western blots in lysates and eluates of the streptavidin purifications of IRS1-TapTag mice (Figure 35). In lysates similar amounts of p85β, p110α, p110β, 14-3-3ε and 14-3-3ζ/δ were detected in all groups. In contrast, p85α, QSK, PKC, and Lyn were mildly increased in HFD lysates (Figure 35, A). In biotin eluates obtained after streptavidin purification of IRS1-associated complexes, all of those proteins were verified by Western blot analysis (Figure 35, B).

As seen in mass spectrometry quantifications of putative interacting subunits of the PI3K (Figure 32, B, C, D and E), Western blots reproduced the tendency towards an elevated association of hepatic IRS1-TapTag and p85α after insulin treatment for NCD- and HFD-fed mice. Also p85β association with IRS1 was slightly increased upon insulin

signaling both in NCD and HFD conditions. This effect was even more pronounced for p110α and p110β, which both showed low association with IRS1-TapTag in unstimulated conditions, i.e. in livers of mice treated with sodium chloride, on NCD and HFD, whereas interaction of IRS1-TapTag with p110α and p110β drastically increased upon insulin signaling in NCD samples. Interestingly, this effect was blunted in livers of insulin-treated HFD-fed mice.

Further, 14-3-3ε was found to interact with IRS1-TapTag, however, while the association of these proteins was elevated in NCD compared to HFD, association after sodium chloride and insulin treatment was similar on HFD. These findings were in contrast to the results suggested by label-free quantifications of mass spectrometry measurements, where the highest interaction between IRS1 and 14-3-3ε was found in livers of insulin-treated NCD-fed mice (Figure 33, A).

14-3-3ζ/δ was found in both mass spectrometry and Western blot analyses in lower amounts than 14-3-3ε. Furthermore, mass spectrometry results suggest that 14-3-3ζ/δ associates with IRS1 in a similar pattern as 14-3-3ε across all experimental groups (Figure 33, E). But, as for 14-3-3ε in Western blots of biotin eluates this was not confirmed (Figure 35, B).

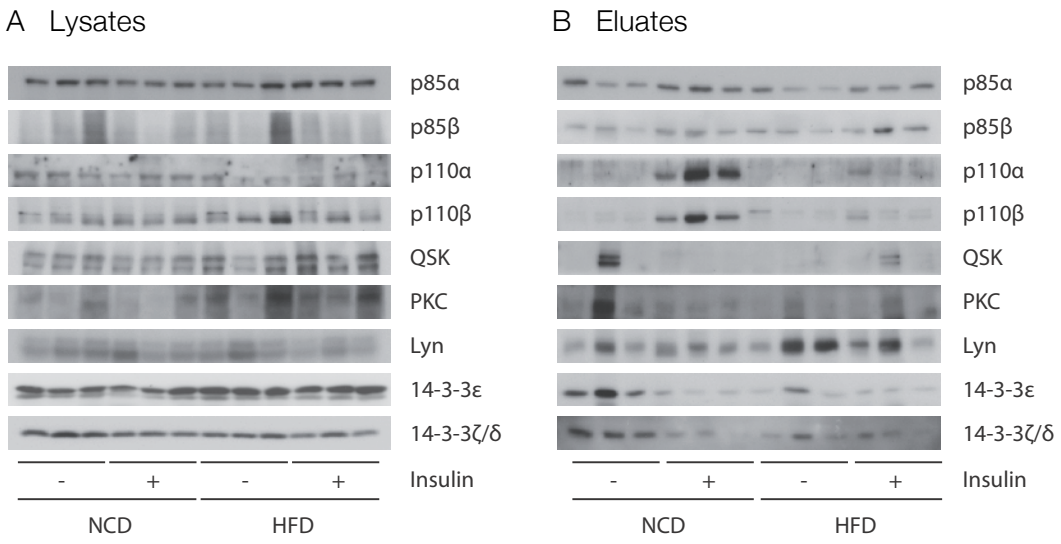

Figure 35: Western blot analysis of putative IRS1 interaction partners in IRS1-TapTag liver lysates and eluates after streptavidin purification; lysates from NCD- and HFD-fed mice were tested in NaCl- and insulin-stimulated conditions.

Lyn was found associated with IRS1-TapTag in mass spectrometry experiments. Also in Western blot analysis the interaction was verified. Here, association seemed to be

increased in HFD conditions, while label-free quantifications suggested levels, which were not significantly altered (Figure 34).

Interaction of PKC and IRS1-TapTag was shown previously (*75*) and was verified in this study by Western blots of biotin eluates of streptavidin purifications. No obvious differences were detected comparing the different experimental groups, but overall levels of PKC were low in all biotin eluates.

In addition, serine/threonine-protein kinase QSK (salt-inducible kinase 3, SIK3) was identified by mass spectrometry among the putative interacting proteins of IRS1 in all samples obtained from IRS1-TapTag mice. In lysates of livers of IRS1-TapTag mice QSK was identified with a mild increase in HFD-fed mice, while differences between sodium chloride and insulin treatments were not detected. In eluates of streptavidin purifications QSK was clearly identified in only one NCD-fed mouse treated with sodium chloride and only one HFD-fed mouse treated with insulin.

In summary, p85α, p85β, p110α, p110β, QSK, PKC, Lyn, 14-3-3ε and 14-3-3ζ/δ, initially identified in mass spectrometry, were verified by Western blot analysis.

3.5 Role of 14-3-3ε interaction with IRS1

14-3-3ε knockdown experiments were performed in order to further characterize the role of 14-3-3ε in insulin signaling. Hepa 1-6 cells treated with control siRNA or 14-3-3ε siRNA were compared with untreated cells (Figure 36). In cells with reduced 14-3-3ε content, IRS1 protein content was decreased, however, this had no detectable influence on IRS1 phosphorylation, as indicated by unchanged tyrosine (pTyr) and serine phosphorylation (pSer307 IRS1). Moreover, insulin receptor tyrosine phosphorylation (pIR) was unchanged, i.e. pIR was efficiently increased after the treatment of the cells with insulin. Also downstream signaling was unaffected, as the phosphorylation states of pAkt and pGSK3β, after insulin treatment of the cells, were comparable to the control cells.

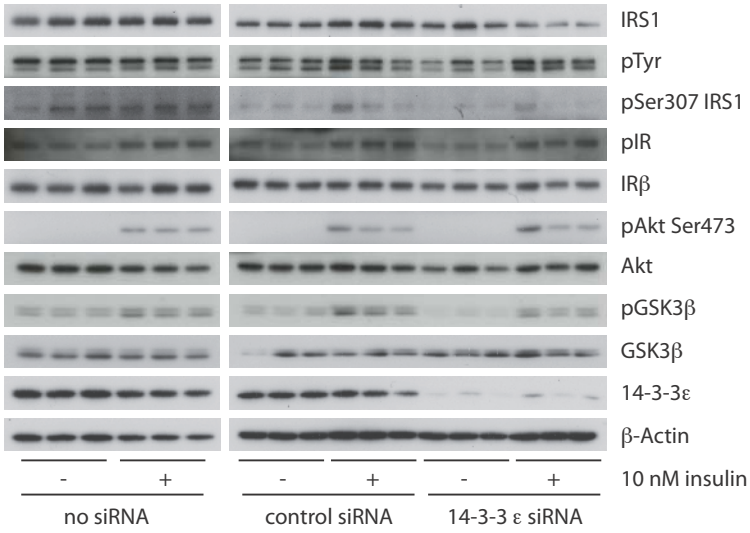

Figure 36: Western blot analysis of Hepa 1-6 cells. Content of the indicated proteins in control cells and after 14-3-3ε siRNA knockdown.

In summary, these results indicate a possible role of 14-3-3ε in the regulation of IRS1 stability, but not in the functional regulation of downstream signaling.

4 Discussion

Obesity, insulin resistance and type 2 diabetes are closely associated pathologies. In the pursuit of the underlying mechanisms leading to the development of insulin resistance upon overweight or obesity, numerous mouse models have been used to study loss-of-function scenarios. Not only whole body knockouts of the insulin receptor, (*155*) as well as IRS1 (*87, 88*) and IRS2 (*89*) have been studied. But also the respective conditional knockouts in an organ-specific setup contributed to the understanding of the distinct roles of those central signaling components (*45, 90, 196, 197*). While knockout studies concentrated on the role of single proteins, new methods have been explored to characterize the IRS proteins. In recent years the advantages brought about by the vast improvements made in mass spectrometry-based proteomic methods, have been utilized to examine IRS1 interactions and phosphorylations.

In this study, a combination of a streptavidin-specific affinity purification of IRS1, mass spectrometric identification and subsequent label-free quantification analysis of interacting proteins was applied in order to detect regulatory differences between normal body weight conditions and diet-induced obesity in basal and insulin-stimulated states. To this end, a construct expressing IRS1-TapTag was stably integrated in the ROSA26 locus. Expression was controlled by the CAGS promoter and only enabled after cre-mediated recombination. As the liver is one of the main organs in the development of insulin resistance, in order to examine liver-specific interactions of IRS1, the Alfpcre mouse line was used to enable liver-restricted expression of IRS1-TapTag.

4.1 Implications of transgenic expression of IRS1-TapTag on the metabolic phenotype

The additional expression of a protein primarily mediating major metabolic and proliferative effects of insulin signaling, like IRS1, implies potential alterations in the overall physiological state. Thus, the phenotype related to insulin and glucose metabolism was analyzed for mice expressing IRS1-TapTag in hepatocytes in comparison to control mice.

As intended, additional expression of IRS1-TapTag was restricted to livers of IRS1-TapTag mice. Altogether, the overall amount of available IRS1 is increased in liver of IRS1-TapTag mice in comparison to the physiological situation observed in the liver of wildtype mice, bearing the potential to possibly alter the physiology of insulin signaling.

As expected, female and male mice gained more weight on HFD compared to NCD, had larger epigonadal fat pads and exhibited an overall increase in body fat content. However, no differences were observed between wildtype and IRS1-TapTag mice. These findings suggest that the transgenic expression of IRS1-TapTag in the liver neither affects physical parameters of body composition, nor changes body weight.

Further, the finding that regulation of blood glucose remains unchanged, rules out that additional hepatic expression of IRS1-TapTag had any aberrant effect on hepatic glucose production. As also, the clearance of glucose from the blood, as seen in the glucose tolerance test was unaltered between the genotypes, hepatic IRS1-TapTag overexpression seems not to affect general glucose metabolism. In line with this, IRS1-TapTag mice responded similar to an insulin challenge, indicating that these mice also exhibit unaltered insulin sensitivity.

Previous studies indicate a role for increased levels of IRS1 in the regulation of neoplastic transformation (*198*), tumorigenesis and metastasis (*199*) in various organs. However, this was not observed in the hepatic IRS1-TapTag mouse model. An explanation for this can be the amount of IRS1 overexpression used in the latter study, which produced increases of IRS1 of up to 9 fold (*200*), whereas amounts of IRS1-TapTag in livers of transgenic IRS1-TapTag mice only increased mildly.

Taken together, these findings indicate that in the IRS1-TapTag mouse model, due to the additional transgenic expression of IRS1-TapTag, total IRS1 levels were increased, but an effect on physiological parameters was not observed, thereby suggesting that all further results can be attributed to the performed treatments, i.e. feeding with NCD or HFD and injection of sodium chloride or insulin and are not likely caused by artifacts of any component of the transgene.

4.2 IRS1 interactions

Numerous studies have shown the complex regulation of insulin signaling on the level of the IRS proteins. Altogether, from the 809 proteins identified, 30 IRS1 interacting proteins of the previous studies (*130, 133, 175*) were confirmed by the affinity purification and mass spectrometry approach used in this study. In 54 additional cases the identified proteins were closely related to previously known interactions, i.e. they belonged to the same protein family or were different isoforms. This accounts for a total of 3.7% (6.7% for similar isoforms) of previously known IRS1 interactions identified in previous proteomic studies.

4.2.1 Phosphatidylinositol-3 kinase interaction

In the past, the interaction of IRS1 with the p85 subunit of the PI3K has been studied extensively. PI3K regulatory subunits associate with IRS1 upon insulin signaling (*66*). In this study, the IRS1-p85 interaction occurred with high variance within the different experimental groups and thus, only a tendency for increased association upon insulin signaling was observed. Overall, the association of IRS1 and p85 subunits was unchanged between NCD and HFD. However, HFD blunted the insulin-stimulated association of p110α and β. So far, p110 association with IRS1 was described to be secondary through p85 (*66*).

Total regulatory p85 exists in two different forms, p85α, which makes up about 70-80% of total p85 content of the cell and p85β, which accounts for the rest (*201*). Therefore, low levels of p85β detected in Western blots were expected in liver lysates. In contrast, upon purification with IRS1, p85β was clearly detected.

In accordance with previous findings reported in the literature, in this study p85α levels in livers of HFD-fed animals were increased as compared to levels on NCD (*201, 202*).

Within the cell, an equilibrium of p85 monomers and p85-p110 complexes exists. While p110 levels remain similar, an increase of p85 induced by HFD may disturb the equilibrium and shift the balance towards an increased amount of p85 monomers (*201*). Since p85 and p85-p110 complexes compete for the same binding site on IRS1, ultimately this will reduce PI3K signaling. Supporting this fact, in mice with heterozygous deletion of p85α, improved insulin sensitivity is observed (*203*). Similar findings were reported for mice lacking p85β (*204*).

Since increases in the predominant subunit p85α have been reported previously (*201, 202*) and in this study p110 levels remained unchanged in liver lysates across the different experimental groups, the lack of p110 association to IRS1 upon insulin treatment in HFD-fed IRS1-TapTag mice may be attributed to a competitive hindrance of p85-p110 complexes by free p85 monomers. However, the increase of p85α expression upon HFD-feeding is rather moderate in this study, whereas the repression of p110 association upon insulin signaling in HFD mice is highly pronounced. Therefore, other proteins may be involved in the regulation of the association of IRS1, p85 and p110 or even the differential phosphorylation state of IRS1 may influence p110 binding.

Taken together, after insulin stimulation of HFD-fed mice, the reduction of p110α and p110β associated to IRS1 and p85 may prevent further PI3K signaling and thereby may play a role in the development of insulin resistance.

On a methodological level, the appearance of PI3K components validates the adequate purification of IRS1-associated complexes.

4.2.2 14-3-3 protein interaction

Moore and Perez discovered the first members of the 14-3-3 protein family in 1967. The 14-3-3 proteins have since been found across mammalian species, with high amounts in brain and lower amounts in all other tissues examined so far. Moreover, the 14-3-3 proteins are conserved not only among mammals, but also among plants, insects, amphibians, and yeast. To date, 7 different isoforms have been identified (*205*).

14-3-3 proteins are involved in various cellular signaling processes like tryptophan and tyrosine hydroxylase activation, regulation of phospholipase A_2, inhibition of PKC, activation of Ca^{2+}-dependent kinases and various signaling outcomes like regulation of growth in yeast and neurotransmitter synthesis in mammals (*205*).

The ability of the 14-3-3 proteins to form homodimers and heterodimers consequently led to the proposal for a function of 14-3-3 dimers as adaptors bringing together distinct regulatory proteins (*206*).

Further, 14-3-3ε is a known interaction partner for IRS1 (*63*) and IGF-1R depending on the phosphorylation of serine residues as established by yeast-two-hybrid screens (*207*). The interaction of 14-3-3β with IRS1 was previously shown to increase upon insulin treatment in 3T3 L1 adipocytes, thereby reducing IRS1-PI3K association (*208*).

Eventually, binding of 14-3-3 proteins to IRS1 was attributed to phosphorylated serine residues in the PTB domain of IRS1 (*209*). Based upon this finding, an additional mechanism was proposed by which the IRS1-14-3-3 protein complex may also induce insulin resistance through hindrance of insulin receptor-IRS1 binding via the PTB domain of IRS1.

As a means of regulation, 14-3-3 association with IRS1 is able to regulate intracellular localization and trafficking of IRS1 (*210*), suggesting a close relationship with cytoskeletal proteins.

Recently, an epitope tagging strategy was applied for Chico, the IRS homologue in *Drosophila melanogaster*, identifying 14-3-3ε and ζ as well as insulin receptor to be increasingly associated with IRS1 upon insulin signaling (*211*). In the same study in two analyses another 64 and 75 proteins were identified as IRS1 interaction partners, 11 of which were also found after streptavidin affinity purifications of IRS1-TapTag in mouse livers, suggesting the existence of a protein complex consisting of IRS1, 14-3-3 and the respective proteins identified in both, mouse liver and fruit flies.

In label-free quantifications of mass spectrometry results in this study, a conserved pattern of IRS1 interaction in liver was found for five different 14-3-3 isoforms. Consistently, 14-3-3 interaction of the ε, α/β, γ, η and ζ/δ isoforms with IRS1 was notably increased upon insulin treatment in NCD conditions, an effect which was blunted in HFD conditions. However, Western blot analysis of 14-3-3ε and 14-3-3ζ/δ did not reproduce the pattern seen in mass spectrometry, maybe due to sample deterioration after storage.

Nevertheless, in this study for the first time, the IRS1-14-3-3 protein interaction in liver was verified by *in vivo* proteomics.

In siRNA knockdown experiments, lack of 14-3-3ε reduced the overall amount of IRS1 upon insulin treatment. However, this had no detectable consequences on insulin signaling, as reflected by pAkt and pGSK3β levels. For the experiment, Hepa 1-6 cells were used, which are a cell model resembling hepatocytes. Since in the liver IRS2 function is induced in parallel to IRS1 signaling, levels of activated downstream components like pAkt and pGSK3β may be kept at regular levels through IRS2 signaling.

4.2.3 Novel mechanism for the modulation of IRS1 serine phosphorylation

Recently, interaction between IRS1, protein kinase Cα (PKCα) and 14-3-3ε has been established in NIH-3T3 cells (*75*). As reflected by 14-3-3ε knockdown experiments in the same study, insulin action is diminished upon reduced 14-3-3ε through downregulation of tyrosine phosphorylation of insulin receptor and IRS1. The additional knockdown of PKCα reversed the effects of the 14-3-3ε knockdown. Interestingly, this interaction seems to be specific for the 14-3-3ε isoform.

Neither PKCα nor any PKC isoform were detected among the interacting proteins of IRS1 by mass spectrometry. However, association of total PKC and IRS1 was shown by Western blot analysis of biotin eluates. This inconsistency may be explained by considering the variety of different PKC isoforms. The abundance for each isoform may have been below the detection limits of the mass spectrometry procedure, while, in Western blot analysis the presumably higher total PKC content was assessed by the use of a pan-PKC antibody.

Another PKC isoform, PKCθ is known to phosphorylate IRS1 at Ser1101, thereby inhibiting insulin signaling (*74*). In a similar mechanism, the association of PKCα could lead to the modulation of insulin signaling on the level of IRS1 (Figure 37, A). Based on this assumption the role of 14-3-3ε in the complex would then be to serve as adaptor protein,

mediating the association of the two proteins maybe even regulating the relative localization within the cell.

Here, a similar but novel mechanism is proposed also for IRS1 association with 14-3-3ζ/δ and the serine/threonine kinase salt-inducible kinase 3 (SIK3 or QSK) (Figure 37, B). QSK, a member of the AMPK-activated protein kinase subfamily, is activated by serine/threonine kinase liver kinase B1 (LKB1), a kinase also targeted by Fyn (*212*). Furthermore, 14-3-3 and LKB1 together regulate the activity and localization of QSK and SIK (*213*). Moreover, salt inducible kinase 2 (SIK2 or QIK) phosphorylates IRS1 on Ser789 in adipocytes, on the same residue also phosphorylated by AMPK, an effect that was increased in diabetic animals (*214*).

Taken together, this study provides an explanation for the considerable involvement of 14-3-3 proteins in insulin signaling, namely through the interaction with IRS1 and further provides a hypothesis for a novel interaction of IRS1, 14-3-3ζ/δ and QSK. The resulting protein complex may serve to regulate insulin signaling by the modulation of serine phosphorylation on IRS1.

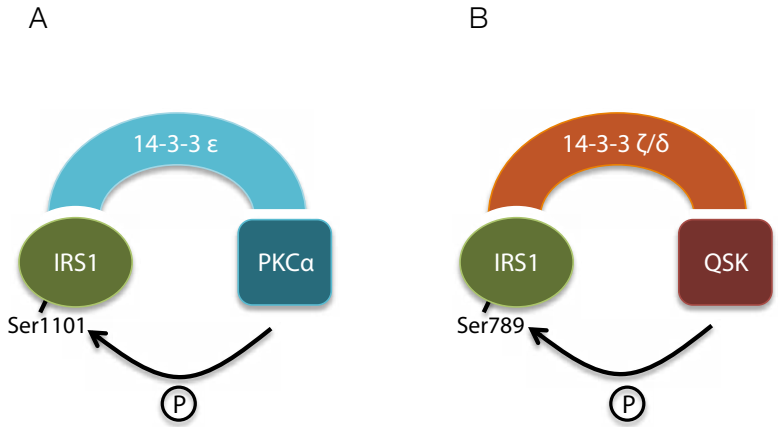

Figure 37: Role of 14-3-3ε and possible role of 14-3-3ζ/δ in the modulation of serine/threonine kinases PKC and QSK. IRS1 as a known target for serine phosphorylation in the IRS1–PKCα–14-3-3ε complex, possibly on Ser1101 (A). Proposed model for the hypothetical complex formation and novel proposed interaction of IRS1, QSK and 14-3-3ζ/δ with possible phosphorylation on Ser789 (B).

Maybe on a superordinate level, through the activation of LKB1 also Lyn plays a role in the activation of the 14-3-3-modulated regulation of kinases on IRS1, ultimately modulating insulin signaling.

4.2.4 Lyn protein interaction

Lyn, a member of the src family of non-receptor tyrosine kinases, is a putative interaction partner of IRS1. So far, a possible interaction of IRS1 and Lyn has not been described.

Label-free quantifications suggest an increased association of IRS1 and Lyn upon HFD-feeding. However, the difference was not significant. Nevertheless, Lyn is a promising candidate for further analysis, as it closely resembles Fyn on a structural level. Fyn is known to bind tyrosine-phosphorylated IRS proteins via its SH2 domain (*215*). Moreover, Fyn has recently been shown to regulate energy expenditure and fatty acid oxidation in skeletal muscle and adipose tissue via serine/threonine kinase LKB1 and subsequent AMP-activated protein kinase (AMPK) activation (*212*). As in Fyn knockout experiments higher energy expenditure and fatty acid oxidation rates were observed, the role of increased Lyn association with IRS1 upon HFD may likely lead to the reversed outcome, i.e. reduced energy expenditure and fatty acid oxidation, further aggravating overweight.

4.2.5 Nuclear protein interactions

Streptavidin affinity purifications were performed on whole-cell lysates. Nuclear proteins found in the streptavidin affinity purification analysis can be explained considering that upon IGF-1 signaling, IRS1 was recently found to localize to the nucleus (*216-218*).
This study identified several transcription factors associated with IRS1 and it is known that IRS1 triggers transcriptional processes in the nucleus. Upon translocation to the nucleus, IRS1 can bind upstream binding factor 1 (UBF1) a regulator of RNA polymerase I (*219*), thereby regulating the synthesis of ribosomal RNA (*217*) and ultimately cell size (*220*). Furthermore, IRS1 plays a role in cell cycle progression. Through a novel mechanism, IRS1 seems to bind directly to regulatory DNA elements to drive transcription of target genes involved in mitogenic and anti-apoptotic regulation (*221*). Additional binding proteins may be involved in different signaling outcomes for IRS1 in the nucleus, and further investigation of the nuclear proteins identified here will be needed to elucidate the possible role of nuclear IRS1 signaling in the development of insulin resistance.

4.2.6 Mitochondrial protein interactions

In addition, a considerable number of mitochondrial proteins was found to associate with IRS1 in mass spectrometry experiments and also previously, the insulin signaling pathway has been shown to influence mitochondrial physiology (*222, 223*). For example, peroxiredoxin isoforms 1, 2, 5, and 6 were identified as putative IRS1 interactors. The protein group of peroxiredoxins is involved in the reduction of hydroperoxides and its members are therefore considered antioxidant enzymes (*224*). Peroxiredoxin levels are

altered in obese diabetic patients, potentially affecting the state of oxidative stress in the cell (*225*), and could therefore contribute to insulin resistance (*226*).

On a more general level, mitochondrial dysfunction plays a role in the development of insulin resistance and diabetes (*227-229*). Further, a connection of IRS1 regulation with mitochondrial dysfunction, as seen in insulin resistance, was established (*230*). During mitochondrial dysfunction, kinases like JNK and p38 MAPK are increased, leading to decreased levels of tyrosine phosphorylation and increased levels of inhibitory serine phosphorylation on IRS1 (*230*). Ultimately, during mitochondrial dysfunction glucose utilization is disturbed as seen in insulin resistance and as expected, inhibitors of JNK and p38 MAPK are able to reverse this effect.

4.2.7 Metabolic protein interactions

In streptavidin purifications, an impressive number of metabolic enzymes like Acetyl-CoA carboxylase, pyruvate carboxylase and ATP synthase has been identified. These proteins are involved in fatty acid synthesis, citric acid cycle and electron transport chain, respectively. Some of these proteins were identified in previous proteomic studies as proteins interacting with IRS1. Further, acetyl-CoA carboxylase is a mediator of the metabolic syndrome and cancer, so research has focused on the inhibition of the respective proteins (*231, 232*).

However, the carboxylases found as putative interactors of IRS1, are likely co-purified as false-positives. Pyruvate carboxylase, the protein identified with the highest average intensity in mass spectrometry, uses biotin as cofactor to facilitate binding of CO_2 (*233*). The same is true for Acetyl-CoA carboxylase, propionyl-CoA carboxylase and methylcrotonyl-CoA carboxylase (*234*), all of which were identified with high average intensities in streptavidin purifications of IRS1-TapTag. Biotin as a component of the respective protein will bind to the resin-coupled streptavidin with high affinity and also elute pseudo-specifically with IRS1-complexes via competitive displacement from the beads.

Via the CBP tag also present in the IRS1-TapTag mouse model, calmodulin may have been purified as false-positive. Calmodulin is a widely expressed temporally and spatially regulated protein involved in various pathways (*235, 236*). Therefore a putative interaction with IRS1 is likely to occur, however it is rather improbable given the possibility of IRS1-independent purification. This fact is further supported as calmodulin was identified as putative interaction partner of 14-3-3ε in another tandem affinity purification study using a Flag-CBP tag (*237*).

4.2.8 Cytoskeletal protein interactions

IRS1 is likely transported within the cell along transportation routes established by the cytoskeletal network. Not only is IRS1 transported to the nucleus, but also concentrates at the plasma membrane. Therefore, a variety of cytoskeletal proteins identified in biotin eluates of streptavidin purifications like plectin, vimentin, radixin and spectrin may play a role in IRS1 trafficking.

However, there is a certain possibility that multi-purpose cytoskeletal proteins may interact with the streptavidin-binding peptide of the affinity tag, streptavidin, or the bead resin due to their generalized binding capabilities (*238*).

Further research will be needed to determine if disturbed IRS1 trafficking may contribute to the development of insulin resistance.

4.3 Affinity purifications and their limitations

Over the last decade, affinity purifications have been largely used to study protein interactions. When affinity purifications are combined with modern mass spectrometry instrumentation, highly precise characterization of protein networks may be achieved.

Initially, the SBP and CBP tags were introduced in the IRS1-TapTag mouse model for the use in tandem affinity purifications. While the tandem affinity purification was successfully performed by using both tag moieties sequentially, as assessed by Western blot analysis, the yield of the bait protein after the second purification step was very low. Therefore, nano-LC-ESI-MS/MS analysis was not feasible. Several improvements by the adjustment of buffer systems or the replacement of biotin with desthiobiotin for elution were endeavored. The refined buffer system helped to improve final yield, however, desthiobiotin was inefficient to improve the final yield. Thus, the purification was performed using only the SBP tag in combination with the adapted buffer conditions and biotin elution (2.4.2, page 45).

There are some limitations to the other affinity purification techniques. High yields of the respective affinity purification approach are a major interest and are frequently also a central concern, when designing an affinity purification method. When the yeast tandem affinity purification was adapted for mammalian cells, up to 10^9 cells were used for a single purification in order to elute as little as 0.2 µg of interacting protein (*174*). The use of triple SBP-CBP-His-tag even required eight 15-cm cell culture plates, adding up to approximately 2 g of cells (*177*). In comparison to purifications from cultured cells, for SBP affinity purifications of liver protein in this study, almost a whole mouse liver of a

mean weight of 1.1-1.5 g per purification was subjected to protein lysis in order to lead to successful purification of IRS1-TapTag complexes.

IRS1-TapTag was expressed from a transgenic allele in liver. Thus, endogenous IRS1 levels are unaffected and endogenous IRS retain the capability to bind a given fraction of respective interaction partners. Therefore, in this affinity purification approach only the amounts of proteins interacting with IRS1-TapTag and not endogenous IRS1 were analyzed, which are only assumed to correspond to total IRS1-associated amounts of the respective binding proteins.

Overall, affinity purifications benefit from moderate lysis conditions throughout the whole procedure (*172, 174*). Those moderate lysis conditions are however compromised to a certain extent by the low solubility of IRS1, probably due to its interaction with membrane-bound proteins and the plasma membrane itself via PTB and PH domains, respectively (*64*). Therefore up to 1% Triton X-100 had to be used to solubilize IRS1 in non-denaturing buffers, increasing the risk of higher detergent concentrations interfering with protein interactions. Other detergent conditions of 0.5% NP40, as previously described for lysis of cultured cells (*175*), were not efficient to solubilize IRS1 in liver samples.

In general, the study of endogenous proteins in their native form may be superior over affinity purifications, which require artificial protein tags. Especially for smaller proteins, the addition of relatively large protein tags may interfere with initial folding or regular protein physiology. However, the 8 kDa SBP-CBP TAP tag used in this study is smaller than the original 21 kDa TAP tag (*174, 176*) and in combination with a large protein like IRS1, risk of interference with protein structure and protein interactions is minimized.

In this study for the first time IRS1-associated protein complexes were affinity purified from liver facilitating *in vivo* proteomics of interactions involved in insulin signaling. Moreover, a unique feature of this study is the large-scale proteomic assessment of IRS1 protein interactions influenced by HFD-feeding, which are only possible in an animal model.

4.4 Implications for insulin resistance

For the first time, a mouse model was used in combination with affinity purification to extensively examine the IRS1 protein network in the liver with proteomic methods regarding alterations provoked by insulin and diet-induced obesity. In summary, the generated mouse model was successfully used to identify candidate interacting proteins of IRS1 in liver. Over 800 proteins were identified as putative interaction partners for IRS1 and comparison with known interactions nicely validated the novel combination of the

methods used. Label-free quantification of mass spectrometry results led to unique intensity profiles for basal and insulin-stimulated interactions, as well as for NCD and HFD conditions.

Not only protein interactions suggesting inhibitory regulatory mechanisms were detected, but also proteins possibly involved in stimulatory interactions were found associated with IRS1.

The examination of IRS1 interactions with p85 and p110 subunits of PI3K revealed an increased association of p110α and β with IRS1 upon insulin signaling, possibly secondary through p85. Unexpectedly, p110α and β interaction with IRS1-p85 was blunted on HFD, suggesting a mechanism by which downstream signaling of the insulin signal may be reduced in conditions of diet-induced obesity.

Most importantly, 14-3-3ε, α/β, γ, η and ζ/δ specifically interacted with IRS1, an interaction which was stimulated by insulin on NCD, but blunted on HFD. Generally, 14-3-3 proteins seem to serve as adaptor proteins, mediating and modulating the interaction of IRS1 with various binding proteins. Thereby, they are possibly involved in the development of insulin resistance.

Novel IRS1 protein interactions were implied for Lyn and QSK. For the Lyn-related kinase Fyn a role in the reduction of energy expenditure and fatty acid oxidation was identified. Interestingly, as Lyn seems to increasingly bind to IRS1 upon HFD-feeding, via a mechanism similar to Fyn, Lyn may be able to contribute to the development of obesity-related insulin resistance. For QSK, an interaction with 14-3-3ζ/δ has been described, while the interaction with IRS1 was so far unknown. SIK2, a related serine/threonine kinase, plays a role in the phosphorylation of Ser789, providing a possible comparable mechanism also for the kinase QSK in the development of insulin resistance.

Overall, these findings may help to advance the current knowledge of serine/threonine kinase-mediated regulation of insulin signaling at the level of IRS1.

5 Perspectives

Thorough verification and numerous further experiments are needed to characterize the respective role of the vast amount of putative IRS1 interactions identified by this study. Their relevance for the development of obesity as well as for insulin resistance will have to be determined by particular functional studies. Furthermore, for each experimental condition, interaction-related alterations of the phosphorylation state of IRS1 have to be examined in order to characterize the respective molecular function. Mainly, immunoprecipitations are feasible to verify interactions and determine phosphorylations of IRS1. Main focus will be on the p110 subunit of PI3K, 14-3-3 proteins, Lyn, PKC isoforms and the novel putative interaction partner QSK.

Finally, as follow-up of the 14-3-3ε knockdown experiments, influence of 14-3-3ε on IRS2 will be assessed. This will allow for a more complete interpretation of the effects of IRS1-14-3-3ε binding and the possibility of IRS2 compensating for IRS1 signaling. The findings for 14-3-3ε function will also be analyzed for other 14-3-3 isoforms to examine if there is evidence for a differential influence of the isoforms.

Mice containing the IRS1-TapTag fusion construct under endogenous control of gene expression providing for physiological levels of the fusion protein are currently produced in parallel to this study. This mouse model will closely resemble the physiological and possibly pathological regulation of expression of the IRS1 gene in conditions of diet-induced obesity and it will therefore be interesting to compare interaction profiles of IRS1 in livers of these mice with those found in this study, in order to establish a direct correlation of these results to a more physiological state.

Furthermore, the IRS2-TapTag fusion construct was generated and can be studied in mice expressing IRS2-TapTag under physiological control. Thereby, differences of interactions of the insulin receptor substrates can be examined and advance the understanding of possible redundancies between different IRS proteins.

Another aspect of the mouse model introduced in this study and those placing the IRS-TapTag proteins under physiological control is the possibility to study IRS interactions in different organs, as the former model can be crossed to different cre-mouse lines to induce organ-specific expression, while the latter models express IRS1- and IRS2-TapTag in exactly those tissues that also express the native IRS1 and IRS2.

6 Supplemental Data

Table 8-S: List of proteins potentially interacting with IRS1, which were identified in biotin eluates derived from TapTag liver lysates of affinity purifications. Proteins are sorted descending from highest average intensity detected in samples from NCD-fed, sodium chloride treated mice. Known interactions are in bold print, known similar interactions are in italic print.

		Average Intensities			
Protein ID	**Protein Name**	**NCD NaCl**	**HFD NaCl**	**NCD insulin**	**HFD insulin**
IPI00114710	Pyruvate carboxylase, mitochondrial	1,61E+09	1,26E+09	1,12E+09	1,21E+09
IPI00468481	ATP synthase subunit beta, mitochondrial	7,74E+07	3,40E+07	3,56E+07	2,68E+07
IPI00605223	Insulin receptor substrate 1	5,73E+07	4,78E+07	4,24E+07	4,09E+07
IPI00848443	Acetyl-CoA carboxylase 1	5,41E+07	2,77E+07	3,88E+07	2,19E+07
IPI00857439	Atp5a1 ATP synthase, H+ transporting, mitochondrial F1 complex alpha subunit 1	4,88E+07	1,89E+07	2,65E+07	2,02E+07
IPI00111908	Carbamoyl-phosphate synthase [ammonia], mitochondrial	4,72E+07	3,00E+07	3,95E+07	3,14E+07
IPI00880839	*Heat shock 70 kDa protein 9*	4,53E+07	3,52E+07	3,97E+07	3,30E+07
IPI00845802	Alpha-globin	2,90E+07	1,91E+07	1,58E+07	2,16E+07
IPI00223367	Uricase	2,80E+07	6,09E+07	2,65E+07	5,66E+07
IPI00323357	Heat shock cognate 71 kDa protein	2,63E+07	2,50E+07	2,15E+07	2,56E+07
IPI00555023	Glutathione S-transferase P 1	2,63E+07	1,92E+07	1,01E+07	1,33E+07
IPI00223092	Trifunctional enzyme subunit alpha, mitochondrial	2,60E+07	2,39E+07	2,32E+07	3,03E+07
IPI00330523	Propionyl-CoA carboxylase alpha chain, mitochondrial	2,07E+07	1,36E+07	1,44E+07	1,57E+07
IPI00648173	Clathrin, heavy polypeptide (Hc)	2,01E+07	5,14E+07	1,61E+07	3,58E+07
IPI00553333	Hemoglobin subunit beta-1	1,71E+07	1,54E+07	1,07E+07	1,26E+07
IPI00320850	**Methylcrotonoyl-CoA carboxylase subunit alpha, mitochondrial**	1,65E+07	1,38E+07	1,58E+07	1,34E+07
IPI00553717	**Methylcrotonoyl-CoA carboxylase beta chain, mitochondrial**	1,29E+07	1,41E+07	1,04E+07	1,35E+07
IPI00115607	Trifunctional enzyme subunit beta, mitochondrial	1,28E+07	1,62E+07	1,35E+07	1,59E+07
IPI00421241	Acetyl-CoA carboxylase 2	1,28E+07	5,68E+06	1,01E+07	4,44E+06
IPI00319992	78 kDa glucose-regulated protein	1,27E+07	8,58E+06	8,50E+06	8,33E+06
IPI00322466	**Phosphoinositide 3-kinase p85alpha**	1,19E+07	1,67E+07	2,22E+07	2,79E+07
IPI00226430	3-ketoacyl-CoA thiolase, mitochondrial	1,05E+07	7,00E+06	5,93E+06	5,90E+06
IPI00134746	Argininosuccinate synthase	1,01E+07	6,38E+06	9,51E+06	6,49E+06
IPI00131695	Serum albumin	9,88E+06	6,98E+06	5,25E+06	9,16E+06
IPI00420718	Hydroxymethylglutaryl-CoA synthase, mitochondrial	9,86E+06	1,00E+07	7,91E+06	9,89E+06
IPI00857142	Major urinary protein 5	9,85E+06	4,29E+06	1,76E+06	4,85E+06
IPI00118899	Alpha-actinin-4	9,63E+06	8,96E+06	1,06E+07	1,36E+07
IPI00127206	Fructose-bisphosphate aldolase B	9,59E+06	6,71E+06	7,70E+06	7,85E+06
IPI00918862	Pccb protein	9,54E+06	8,08E+06	8,43E+06	8,44E+06
IPI00308885	60 kDa heat shock protein, mitochondrial	9,18E+06	1,22E+07	9,34E+06	1,04E+07
IPI00222228	Putative uncharacterized protein	8,95E+06	1,69E+07	3,88E+06	5,34E+05
IPI00395100	Try10-like trypsinogen	8,85E+06	1,62E+07	8,77E+06	4,75E+06
IPI00307837	*Elongation factor 1-alpha 1*	8,28E+06	6,23E+06	6,22E+06	4,85E+06
IPI00130950	Betaine--homocysteine S-methyltransferase 1	8,17E+06	4,02E+06	6,67E+06	5,70E+06

Protein ID	Protein Name	Average Intensities			
		NCD NaCl	HFD NaCl	NCD insulin	HFD insulin
IPI00127841	ADP/ATP translocase 2	7,69E+06	6,76E+06	8,87E+06	6,26E+06
IPI00848801	Glyceraldehyde-3-phosphate dehydrogenase	7,49E+06	5,14E+06	5,82E+06	4,63E+06
IPI00622780	Cytoplasmic aconitate hydratase	7,14E+06	1,38E+06	5,97E+06	1,24E+06
IPI00221890	Carbonic anhydrase 3	6,85E+06	5,68E+06	6,08E+06	5,52E+06
IPI00330480	Gm5478 predicted pseudogene 5478	6,30E+06	7,55E+06	1,98E+07	5,59E+06
IPI00331241	Glutathione S-transferase A3	6,14E+06	6,59E+06	6,74E+06	7,06E+06
IPI00453673	Serine/threonine-protein kinase QSK	6,04E+06	4,37E+06	4,83E+06	2,01E+06
IPI00114209	Glutamate dehydrogenase 1, mitochondrial	5,59E+06	6,32E+06	5,04E+06	6,19E+06
IPI00121788	Peroxiredoxin-1	5,54E+06	4,48E+06	5,08E+06	6,55E+06
IPI00120451	Fatty acid-binding protein, liver	5,51E+06	1,59E+07	1,10E+07	1,04E+07
IPI00111218	Aldehyde dehydrogenase, mitochondrial	5,45E+06	4,85E+06	3,85E+06	5,38E+06
IPI00117914	Arginase-1	5,20E+06	3,33E+06	2,70E+06	2,79E+06
IPI00831055	Beta-globin	5,18E+06	4,27E+06	3,40E+06	1,35E+07
IPI00229252	Uncharacterized protein C3orf43 homolog	5,17E+06	0,00E+00	0,00E+00	0,00E+00
IPI00118384	**14-3-3 protein epsilon**	5,04E+06	6,47E+06	9,54E+06	4,11E+06
IPI00230707	**14-3-3 protein gamma**	5,03E+06	3,61E+06	9,77E+06	3,79E+06
IPI00664670	Filamin-C	5,00E+06	0,00E+00	3,38E+06	0,00E+00
IPI00222225	Protein transport protein Sec24A	4,78E+06	3,22E+06	4,72E+06	2,58E+06
IPI00169463	Tubulin beta-2C chain	4,63E+06	2,88E+06	2,46E+06	3,48E+06
IPI00649135	Glutathione S-transferase, mu 1	4,46E+06	5,31E+06	6,12E+06	3,36E+06
IPI00130589	Superoxide dismutase [Cu-Zn]	4,07E+06	3,61E+06	2,35E+06	3,28E+06
IPI00129928	Fumarate hydratase, mitochondrial	3,92E+06	3,15E+06	3,76E+06	2,40E+06
IPI00118986	ATP synthase subunit O, mitochondrial	3,71E+06	1,36E+06	1,35E+06	1,13E+06
IPI00123181	Myosin-9	3,67E+06	5,57E+06	3,53E+06	6,33E+06
IPI00228630	Fructose-1,6-bisphosphatase 1	3,65E+06	2,46E+06	1,80E+06	1,93E+06
IPI00331596	Peroxisomal trans-2-enoyl-CoA reductase	3,55E+06	2,92E+06	4,73E+06	3,31E+06
IPI00341282	ATP synthase subunit b, mitochondrial	3,48E+06	1,65E+06	4,29E+06	2,73E+06
IPI00123349	Protein transport protein Sec23A	3,29E+06	2,02E+06	3,94E+06	2,08E+06
IPI00153317	10-formyltetrahydrofolate dehydrogenase	3,25E+06	1,63E+06	2,35E+06	2,64E+06
IPI00134131	Non-specific lipid-transfer protein	3,19E+06	3,72E+06	3,08E+06	4,28E+06
IPI00117312	Aspartate aminotransferase, mitochondrial	3,17E+06	2,51E+06	1,56E+06	2,27E+06
IPI00125325	**Peroxisomal 2,4-dienoyl-CoA reductase**	3,15E+06	2,40E+06	1,83E+06	2,17E+06
IPI00114593	Actin, alpha cardiac muscle 1	3,15E+06	5,25E+06	1,27E+06	2,14E+06
IPI00133522	Protein disulfide-isomerase	3,12E+06	3,12E+06	2,84E+06	3,14E+06
IPI00323816	Selenium-binding protein 2	3,11E+06	2,48E+06	1,78E+06	1,14E+06
IPI00230440	Adenosylhomocysteinase	3,09E+06	2,42E+06	2,24E+06	2,99E+06
IPI00127417	Nucleoside diphosphate kinase B	3,08E+06	2,65E+06	9,61E+05	8,39E+05
IPI00133456	Regucalcin	3,08E+06	2,11E+06	2,17E+06	1,86E+06
IPI00126861	Protein-glutamine gamma-glutamyltransferase 2	3,04E+06	3,28E+06	4,03E+06	3,35E+06
IPI00462072	Alpha-enolase	3,01E+06	2,66E+06	2,38E+06	2,42E+06
IPI00117159	**Phosphatidylinositol 3-kinase regulatory subunit beta**	2,97E+06	2,88E+06	3,95E+06	3,43E+06
IPI00230108	Protein disulfide-isomerase A3	2,92E+06	2,20E+06	2,12E+06	2,25E+06
IPI00227299	**Vimentin**	2,92E+06	5,26E+06	3,72E+06	4,13E+06

Protein ID	Protein Name	Average Intensities			
		NCD NaCl	HFD NaCl	NCD insulin	HFD insulin
IPI00312058	Catalase	2,87E+06	3,16E+06	3,21E+06	2,91E+06
IPI00117348	Tubulin alpha-1B chain	2,65E+06	1,89E+06	1,91E+06	1,38E+06
IPI00154054	Acetyl-CoA acetyltransferase, mitochondrial	2,64E+06	2,44E+06	3,72E+06	2,39E+06
IPI00116603	Ornithine carbamoyltransferase, mitochondrial	2,58E+06	1,62E+06	2,12E+06	2,33E+06
IPI00316491	Hemoglobin subunit beta-2	2,57E+06	9,78E+05	8,48E+05	1,25E+06
IPI00123183	Aquaporin-1	2,38E+06	3,70E+06	2,13E+06	3,01E+06
IPI00626662	Retinal dehydrogenase 1	2,37E+06	2,70E+06	1,84E+06	2,83E+06
IPI00554989	Peptidyl-prolyl cis-trans isomerase A	2,20E+06	1,74E+06	1,45E+06	5,33E+05
IPI00135686	Peptidyl-prolyl cis-trans isomerase B	2,19E+06	2,40E+06	8,10E+05	2,00E+06
IPI00229080	**Heat shock protein 84b**	2,17E+06	1,34E+06	1,50E+06	1,93E+06
IPI00453777	ATP synthase subunit delta, mitochondrial	2,14E+06	9,00E+05	2,69E+06	1,16E+06
IPI00466069	**Elongation factor 2**	2,07E+06	1,75E+06	1,84E+06	9,33E+05
IPI00115862	Eukaryotic translation initiation factor 6	2,05E+06	1,83E+06	1,12E+06	1,57E+06
IPI00139780	*60S ribosomal protein L23*	2,02E+06	3,14E+06	1,63E+06	1,98E+06
IPI00109044	MCG5400	2,02E+06	3,41E+06	6,45E+05	5,84E+06
IPI00467066	Glycine N-methyltransferase	2,02E+06	1,01E+06	1,20E+06	1,17E+06
IPI00121440	Electron transfer flavoprotein subunit beta	2,01E+06	1,60E+06	1,73E+06	1,96E+06
IPI00620256	Lamin-A/C	2,00E+06	8,13E+06	3,62E+06	1,24E+07
IPI00555059	Peroxiredoxin-6	2,00E+06	2,27E+06	1,24E+06	1,68E+06
IPI00221400	Alcohol dehydrogenase 1	1,95E+06	2,30E+06	2,04E+06	1,81E+06
IPI00128518	S-adenosylmethionine synthetase isoform type-1	1,94E+06	1,55E+06	8,29E+05	1,62E+06
IPI00130280	ATP synthase subunit alpha, mitochondrial	1,88E+06	0,00E+00	1,32E+06	6,85E+05
IPI00323592	Malate dehydrogenase, mitochondrial	1,88E+06	1,36E+06	1,90E+06	1,59E+06
IPI00230507	ATP synthase subunit d, mitochondrial	1,85E+06	1,54E+06	7,76E+05	5,13E+05
IPI00653931	Fumarylacetoacetase	1,73E+06	1,22E+06	7,67E+05	1,27E+06
IPI00378063	AP-2 complex subunit beta-1	1,70E+06	2,77E+06	1,27E+06	3,03E+06
IPI00751369	L-lactate dehydrogenase	1,67E+06	1,74E+06	1,37E+06	1,75E+06
IPI00319830	Spectrin beta chain, brain 1	1,67E+06	2,78E+06	2,73E+06	5,66E+06
IPI00831626	Tpm1 tropomyosin 1, alpha	1,64E+06	2,90E+06	3,52E+06	4,18E+06
IPI00321617	Epoxide hydrolase 2	1,62E+06	2,17E+06	1,51E+06	2,18E+06
IPI00352163	Fibronectin	1,61E+06	1,76E+06	1,96E+06	2,09E+06
IPI00111950	Estradiol 17 beta-dehydrogenase 5	1,60E+06	1,50E+06	2,19E+06	1,78E+06
IPI00875416	Sorbitol dehydrogenase	1,55E+06	1,21E+06	1,21E+06	1,20E+06
IPI00112549	Long-chain-fatty-acid--CoA ligase 1	1,54E+06	1,59E+06	1,15E+06	1,63E+06
IPI00116753	Electron transfer flavoprotein subunit alpha, mitochondrial	1,51E+06	1,02E+06	9,21E+05	8,75E+05
IPI00223216	Thiosulfate sulfurtransferase	1,43E+06	8,35E+05	6,72E+05	7,29E+05
IPI00624663	Alpha-2-macroglobulin	1,41E+06	6,12E+05	9,66E+05	1,65E+06
IPI00313475	ATP synthase subunit gamma, mitochondrial	1,36E+06	4,25E+05	5,80E+05	1,51E+05
IPI00554931	4-hydroxyphenylpyruvate dioxygenase	1,35E+06	1,03E+06	1,05E+06	1,29E+06
IPI00461964	Methylmalonate-semialdehyde dehydrogenase [acylating], mitochondrial	1,35E+06	1,51E+06	1,42E+06	1,59E+06
IPI00761390	Fatty-acid-coenzyme A ligase, very long-chain 1	1,33E+06	1,19E+06	1,74E+06	1,60E+06
IPI00554834	Peroxisomal bifunctional enzyme	1,33E+06	1,43E+06	1,33E+06	8,85E+05

Protein ID	Protein Name	Average Intensities			
		NCD NaCl	HFD NaCl	NCD insulin	HFD insulin
IPI00111265	F-actin-capping protein subunit alpha-2	1,31E+06	1,93E+06	1,07E+06	1,56E+06
IPI00112322	UDP-glucuronosyltransferase 2B5	1,29E+06	1,39E+06	1,24E+06	1,19E+06
IPI00331628	Peroxisomal multifunctional enzyme type 2	1,29E+06	1,11E+06	1,65E+06	1,14E+06
IPI00129526	Endoplasmin	1,28E+06	6,32E+05	7,98E+05	8,19E+05
IPI00116498	14-3-3 protein zeta/delta	1,27E+06	1,24E+06	2,82E+06	9,51E+05
IPI00138691	Actin-related protein 2/3 complex subunit 4	1,20E+06	1,60E+06	3,93E+05	3,15E+06
IPI00317740	Guanine nucleotide-binding protein subunit beta-2-like 1	1,19E+06	1,33E+05	8,49E+05	0,00E+00
IPI00319525	Glycogen phosphorylase, liver form	1,18E+06	7,64E+05	1,09E+06	1,31E+06
IPI00405227	Vinculin	1,11E+06	1,61E+06	2,02E+06	3,80E+06
IPI00474883	CAPZB3	1,11E+06	1,59E+06	1,35E+06	2,21E+06
IPI00109293	Serine beta-lactamase-like protein LACTB, mitochondrial	1,10E+06	1,58E+06	2,07E+06	7,22E+05
IPI00381178	Liver carboxylesterase 31	1,08E+06	1,25E+06	7,67E+05	9,99E+05
IPI00848866	Myosin light polypeptide 6	1,07E+06	1,19E+06	8,12E+05	1,61E+06
IPI00387289	Carboxylesterase 3	1,07E+06	1,76E+06	1,81E+06	1,60E+06
IPI00890322	3-hydroxybutyrate dehydrogenase	1,06E+06	8,79E+05	6,20E+05	6,42E+05
IPI00136213	Sarcosine dehydrogenase, mitochondrial	1,05E+06	6,12E+05	8,90E+05	7,72E+05
IPI00120123	Dimethylglycine dehydrogenase, mitochondrial	1,05E+06	7,19E+05	1,09E+06	6,18E+05
IPI00135231	Isocitrate dehydrogenase [NADP] cytoplasmic	1,04E+06	8,69E+05	5,21E+05	6,97E+05
IPI00336324	Malate dehydrogenase, cytoplasmic	1,04E+06	8,88E+05	1,12E+06	8,20E+05
IPI00755916	Ubc protein	1,03E+06	7,30E+05	9,25E+05	1,28E+06
IPI00555069	Phosphoglycerate kinase 1	1,01E+06	9,39E+05	5,52E+05	7,38E+05
IPI00828479	Acyl-Coenzyme A oxidase 1, palmitoyl	1,01E+06	6,21E+05	5,16E+05	4,62E+05
IPI00314788	Argininosuccinate lyase	9,97E+05	6,85E+05	1,22E+06	8,66E+05
IPI00828488	*Heterogeneous nuclear ribonucleoproteins A2/B1*	9,90E+05	3,72E+06	1,49E+06	4,66E+06
IPI00177038	Actin-related protein 2	9,77E+05	1,61E+06	5,07E+05	1,48E+06
IPI00129517	Peroxiredoxin -5, mitochondrial	9,69E+05	6,75E+05	2,99E+05	9,97E+04
IPI00406302	Alpha-1-antitrypsin 1-1	9,57E+05	6,90E+05	5,21E+05	9,66E+05
IPI00129577	Apoptosis-inducing factor 1, mitochondrial	9,47E+05	7,84E+05	1,02E+06	8,70E+05
IPI00310669	Bifunctional ATP-dependent dihydroxyacetone kinase/FAD-AMP lyase (cyclizing)	9,33E+05	1,02E+06	4,53E+05	9,42E+05
IPI00885793	Fibrinogen A-alpha-chain	9,22E+05	1,31E+06	5,93E+05	3,82E+06
IPI00115627	Actin-related protein 3	8,95E+05	1,38E+06	1,02E+06	1,99E+06
IPI00274407	Elongation factor Tu, mitochondrial	8,94E+05	4,96E+05	6,02E+05	7,90E+05
IPI00406442	Succinyl-CoA ligase [GDP-forming] subunit alpha, mitochondrial	8,81E+05	6,80E+05	2,92E+05	1,67E+05
IPI00110556	Cytochrome P450 2E1	8,79E+05	6,55E+05	7,16E+05	8,68E+05
IPI00124820	Coronin-1C	8,60E+05	9,92E+05	5,51E+05	2,03E+06
IPI00622235	Transitional endoplasmic reticulum ATPase	8,59E+05	4,49E+05	7,48E+05	5,83E+05
IPI00114396	Galectin-9	8,46E+05	1,18E+06	1,03E+06	1,07E+06
IPI00466128	Alcohol dehydrogenase [NADP+]	8,45E+05	4,80E+05	7,49E+05	6,66E+05
IPI00276926	Solute carrier family 25 (Mitochondrial carrier, citrate transporter), member 1	8,41E+05	8,86E+05	9,65E+05	4,19E+05

Protein ID	Protein Name	Average Intensities			
		NCD NaCl	HFD NaCl	NCD insulin	HFD insulin
IPI00139788	Serotransferrin	8,23E+05	7,52E+05	7,29E+05	1,01E+06
IPI00308328	Cytochrome P450 2F2	7,85E+05	4,48E+05	3,97E+05	1,81E+05
IPI00754649	Myosin-Ic	7,73E+05	3,10E+06	1,52E+06	1,66E+06
IPI00310131	AP-2 complex subunit alpha-2	7,49E+05	1,18E+06	7,07E+05	1,56E+06
IPI00134961	*Medium-chain specific acyl-CoA dehydrogenase, mitochondrial*	7,47E+05	7,43E+05	5,29E+05	8,33E+05
IPI00119219	Estradiol 17-beta-dehydrogenase 12	7,37E+05	9,24E+05	6,17E+05	5,51E+05
IPI00876504	Maleylacetoacetate	7,36E+05	1,11E+06	2,68E+05	3,41E+05
IPI00124819	Coronin-1B	7,30E+05	1,66E+06	1,15E+06	2,91E+06
IPI00124829	Actin-related protein 2/3 complex subunit 3	7,29E+05	8,66E+05	4,64E+05	2,33E+06
IPI00122139	3-ketoacyl-CoA thiolase B, peroxisomal	7,23E+05	8,69E+05	4,44E+05	7,54E+05
IPI00230113	Cytochrome b5	7,07E+05	5,10E+05	3,90E+05	4,74E+05
IPI00387379	**2,4-dienoyl-CoA reductase, mitochondrial**	7,04E+05	4,68E+05	3,90E+05	2,89E+05
IPI00230084	Aldehyde dehydrogenase family 7 member A1	6,87E+05	5,92E+05	3,19E+05	7,47E+05
IPI00134344	Beta III spectrin	6,85E+05	1,41E+06	1,29E+06	2,86E+06
IPI00133549	Phenylalanine-4-hydroxylase	6,81E+05	4,85E+05	6,13E+05	6,59E+05
IPI00461427	Ig mu chain C region membrane-bound form	6,68E+05	2,60E+06	1,01E+06	1,78E+06
IPI00331436	Cytosol aminopeptidase	6,62E+05	6,87E+05	5,20E+05	7,81E+05
IPI00114416	3,2-trans-enoyl-CoA isomerase, mitochondrial	6,58E+05	5,87E+05	3,04E+05	7,64E+05
IPI00653921	Radixin	6,52E+05	9,24E+05	1,05E+06	1,12E+06
IPI00378649	Major urinary protein 24	6,51E+05	5,86E+05	2,91E+05	0,00E+00
IPI00230351	Succinate dehydrogenase [ubiquinone] flavoprotein subunit, mitochondrial	6,49E+05	3,20E+05	8,67E+05	5,97E+05
IPI00775829	Pyruvate kinase	6,48E+05	4,24E+05	5,60E+05	8,58E+05
IPI00134504	Cytochrome P450 3A11	6,46E+05	0,00E+00	5,59E+05	0,00E+00
IPI00131438	Phosphoenolpyruvate carboxykinase, cytosolic [GTP]	6,46E+05	4,09E+05	4,84E+05	3,70E+05
IPI00124771	Phosphate carrier protein, mitochondrial	6,37E+05	3,52E+05	5,73E+05	5,28E+05
IPI00467841	Calmodulin	6,35E+05	8,80E+05	9,89E+05	2,26E+06
IPI00131176	Cytochrome c oxidase subunit 2	6,06E+05	1,68E+05	2,45E+05	1,75E+05
IPI00877236	Apolipoprotein A-I	5,86E+05	8,43E+05	6,39E+05	1,06E+06
IPI00317604	Protein transport protein Sec23B	5,86E+05	2,74E+05	7,31E+05	3,76E+05
IPI00116074	Aconitate hydratase, mitochondrial	5,84E+05	4,18E+05	3,41E+05	5,08E+05
IPI00266188	Cofilin-2	5,80E+05	5,40E+05	2,05E+05	1,49E+06
IPI00125813	Dipeptidyl peptidase 4	5,74E+05	8,62E+05	6,08E+05	6,62E+05
IPI00112963	Catenin alpha-1	5,71E+05	1,05E+06	7,88E+05	1,45E+06
IPI00120233	**Glutaryl-CoA dehydrogenase, mitochondrial**	5,70E+05	3,27E+05	4,70E+05	7,13E+05
IPI00330747	*Acyl-CoA dehydrogenase family member 11*	5,62E+05	4,11E+05	6,18E+05	1,76E+06
IPI00279079	Fibrinogen beta chain	5,59E+05	9,74E+05	7,60E+05	2,95E+06
IPI00408961	3-hydroxyanthranilate 3,4-dioxygenase	5,56E+05	3,20E+05	4,45E+05	5,13E+05
IPI00117978	Cytochrome c oxidase subunit 4 isoform 1, mitochondrial	5,51E+05	1,53E+05	4,70E+05	1,89E+05
IPI00122312	Fibrinogen gamma chain	5,51E+05	6,10E+05	2,76E+05	1,42E+06
IPI00126625	Acyl-coenzyme A synthetase ACSM1, mitochondrial	5,45E+05	3,41E+05	3,02E+05	5,16E+05
IPI00648927	Clathrin light polypeptide (Lca)	5,32E+05	1,15E+06	1,00E+06	2,17E+06

		Average Intensities			
Protein ID	**Protein Name**	**NCD NaCl**	**HFD NaCl**	**NCD insulin**	**HFD insulin**
IPI00137409	Transketolase	5,32E+05	5,78E+05	5,84E+05	5,41E+05
IPI00319652	Glutathione peroxidase 1	5,28E+05	5,73E+05	3,49E+05	8,56E+05
IPI00405699	Delta-1-pyrroline-5-carboxylate dehydrogenase, mitochondrial	5,19E+05	5,69E+05	1,12E+06	9,10E+05
IPI00112339	LIM domain and actin-binding protein 1	5,13E+05	7,15E+05	3,37E+05	5,49E+05
IPI00459487	Succinyl-CoA ligase [GDP-forming] subunit beta, mitochondrial	5,09E+05	3,99E+05	2,60E+05	4,09E+05
IPI00648318	Adenylate kinase 2, mitochondrial	5,08E+05	3,42E+05	1,38E+05	4,03E+05
IPI00459279	Dihydropteridine reductase	5,03E+05	4,32E+05	2,05E+05	2,19E+05
IPI00109275	Mitochondrial glutamate carrier 1	4,93E+05	3,66E+05	5,03E+05	3,61E+05
IPI00408215	Myosin-Ib	4,74E+05	1,21E+06	8,11E+05	1,70E+06
IPI00124372	4-trimethylaminobutyraldehyde dehydrogenase	4,70E+05	3,60E+05	3,72E+05	5,47E+05
IPI00480429	UDP glucuronosyltransferase 1 family, polypeptide A1	4,67E+05	5,57E+05	9,20E+05	5,77E+05
IPI00269661	*Heterogeneous nuclear ribonucleoprotein A3*	4,63E+05	1,76E+06	4,62E+05	1,39E+06
IPI00120864	Phenazine biosynthesis-like domain-containing protein 1	4,59E+05	3,73E+05	3,99E+05	4,15E+05
IPI00331461	*60S ribosomal protein L11*	4,59E+05	7,00E+05	2,06E+05	6,81E+05
IPI00890117	Cofilin-1	4,59E+05	2,99E+05	1,84E+05	6,40E+05
IPI00338536	Succinate dehydrogenase [ubiquinone] iron-sulfur subunit, mitochondrial	4,58E+05	5,61E+05	0,00E+00	9,26E+04
IPI00131830	Serine protease inhibitor A3K	4,58E+05	1,75E+05	1,98E+05	4,16E+05
IPI00515370	Aldehyde dehydrogenase family 3, subfamily A2	4,49E+05	9,13E+05	4,23E+05	4,37E+05
IPI00454049	**Enoyl-CoA hydratase, mitochondrial**	4,48E+05	4,25E+05	4,37E+05	3,86E+05
IPI00321734	Lactoylglutathione lyase	4,47E+05	8,06E+05	1,87E+05	3,47E+05
IPI00555140	Phosphoglucomutase-1	4,47E+05	4,02E+05	3,98E+05	5,79E+05
IPI00122549	Voltage-dependent anion-selective channel protein 1	4,34E+05	2,17E+05	2,52E+05	5,82E+04
IPI00317309	Annexin A5	4,32E+05	2,07E+05	3,38E+05	1,67E+05
IPI00877205	Aspartate aminotransferase	4,31E+05	1,51E+05	2,94E+05	2,40E+05
IPI00117910	Peroxiredoxin-2	4,23E+05	2,61E+05	1,95E+05	6,04E+05
IPI00134503	Cytochrome P450 2C29	4,23E+05	1,60E+05	3,76E+05	1,72E+05
IPI00117350	Tubulin alpha-4A chain	4,22E+05	2,17E+05	2,50E+05	2,70E+05
IPI00626385	Plectin-1	4,20E+05	4,06E+05	8,56E+05	4,01E+05
IPI00874651	Imidazolonepropionate hydrolase	4,13E+05	2,80E+05	2,91E+05	4,20E+05
IPI00117167	Gelsolin	4,06E+05	5,40E+05	4,30E+05	1,35E+06
IPI00129056	Glycine N-acyltransferase	4,03E+05	4,21E+05	1,12E+05	0,00E+00
IPI00230185	Glycerol-3-phosphate dehydrogenase [NAD+], cytoplasmic	4,01E+05	4,43E+05	2,99E+05	4,03E+05
IPI00119203	**Very long-chain specific acyl-CoA dehydrogenase, mitochondrial**	3,97E+05	4,05E+05	3,51E+05	3,87E+05
IPI00111258	Major vault protein	3,96E+05	2,00E+05	3,97E+05	2,28E+05
IPI00110885	Diaphorase-1	3,88E+05	0,00E+00	3,00E+05	0,00E+00
IPI00323908	Cytochrome P450 2D10	3,87E+05	6,25E+04	1,39E+05	2,55E+05
IPI00776145	Myosin VI	3,86E+05	5,40E+05	4,88E+05	4,71E+05
IPI00132208	DnaJ homolog subfamily A member 1	3,82E+05	3,40E+05	2,09E+05	1,44E+05
IPI00138084	Adenosine kinase	3,82E+05	2,48E+05	2,12E+05	1,46E+05
IPI00132076	Catechol O-methyltransferase	3,79E+05	1,54E+05	1,96E+05	1,49E+05

Protein ID	Protein Name	Average Intensities			
		NCD NaCl	HFD NaCl	NCD insulin	HFD insulin
IPI00119114	**Long-chain specific acyl-CoA dehydrogenase, mitochondrial**	3,73E+05	3,14E+05	2,10E+05	4,17E+05
IPI00849793	*60S ribosomal protein L12*	3,71E+05	4,31E+05	2,63E+05	2,89E+05
IPI00230682	14-3-3 protein beta/alpha	3,69E+05	9,51E+05	1,67E+06	9,27E+05
IPI00320462	Valacyclovir hydrolase	3,67E+05	1,60E+05	1,71E+05	7,19E+04
IPI00309073	Microsomal triglyceride transfer protein large subunit	3,67E+05	1,26E+05	2,27E+05	2,50E+05
IPI00459493	T-complex protein 1 subunit alpha B	3,63E+05	2,24E+05	8,50E+05	1,26E+06
IPI00330323	Mannosyl-oligosaccharide glucosidase	3,61E+05	7,13E+04	3,52E+05	1,42E+05
IPI00874920	*Histone H4*	3,59E+05	3,22E+05	1,86E+05	4,65E+05
IPI00122862	C-1-tetrahydrofolate synthase, cytoplasmic	3,58E+05	7,27E+04	3,69E+05	2,27E+05
IPI00108125	Eukaryotic translation initiation factor 5A-1	3,58E+05	1,19E+05	1,09E+05	0,00E+00
IPI00229475	Junction plakoglobin	3,55E+05	6,25E+05	1,03E+06	8,32E+05
IPI00109109	Superoxide dismutase [Mn], mitochondrial	3,55E+05	3,00E+05	0,00E+00	2,29E+05
IPI00338039	Tubulin beta-2A chain	3,54E+05	1,88E+05	1,48E+05	3,53E+05
IPI00122346	Translocon-associated protein subunit delta	3,54E+05	3,44E+04	3,72E+04	0,00E+00
IPI00319973	Membrane-associated progesterone receptor component 1	3,52E+05	3,27E+05	3,31E+05	1,36E+05
IPI00465786	Talin-1	3,51E+05	3,21E+05	5,18E+05	1,25E+06
IPI00380436	Alpha-actinin-1	3,44E+05	4,91E+05	2,90E+05	4,20E+05
IPI00222546	*60S ribosomal protein L22*	3,44E+05	2,04E+05	3,68E+05	4,81E+05
IPI00132443	*Heterogeneous nuclear ribonucleoprotein M*	3,43E+05	7,11E+05	3,21E+05	1,16E+06
IPI00121522	Glycine N-acyltransferase-like protein Keg1	3,43E+05	3,31E+05	3,17E+05	1,31E+05
IPI00111885	Cytochrome b-c1 complex subunit 1, mitochondrial	3,41E+05	3,25E+05	2,88E+05	3,40E+05
IPI00119138	Cytochrome b-c1 complex subunit 2, mitochondrial	3,38E+05	2,10E+05	3,03E+05	1,82E+05
IPI00279858	DnaJ homolog subfamily A member 3, mitochondrial	3,37E+05	1,88E+05	1,84E+05	2,93E+05
IPI00130670	Serine-threonine kinase receptor-associated protein	3,35E+05	0,00E+00	1,74E+05	7,42E+04
IPI00121322	Electron transfer flavoprotein-ubiquinone oxidoreductase, mitochondrial	3,32E+05	2,41E+05	3,97E+05	3,61E+05
IPI00626790	Glutamine synthetase	3,30E+05	3,13E+05	1,33E+05	2,41E+05
IPI00137730	Phosphatidylethanolamine-binding protein 1	3,29E+05	1,98E+05	1,61E+05	1,38E+05
IPI00346073	**Heat shock 70 kDa protein 1B**	3,28E+05	3,27E+05	1,99E+05	3,08E+05
IPI00110852	Translocon-associated protein alpha, muscle specific isoform	3,23E+05	2,35E+05	3,06E+05	3,87E+04
IPI00127223	MCG1788	3,22E+05	1,32E+05	4,22E+05	1,73E+05
IPI00554961	Dimethylaniline monooxygenase [N-oxide-forming] 5	3,12E+05	2,84E+05	3,69E+05	4,52E+05
IPI00323571	Apolipoprotein E	3,10E+05	2,22E+05	4,15E+05	3,25E+05
IPI00467833	Triosephosphate isomerase	3,10E+05	1,66E+05	8,00E+04	4,24E+04
IPI00321644	Cytochrome P450 2D26	3,05E+05	1,81E+05	9,55E+04	1,47E+05
IPI00123281	Leucine-rich repeat-containing protein 59	3,04E+05	1,99E+05	2,37E+05	0,00E+00
IPI00608064	Fech protein	3,02E+05	3,02E+05	3,21E+05	3,18E+05
IPI00135651	Calcium-binding mitochondrial carrier protein Aralar2	2,99E+05	1,99E+05	3,91E+05	4,18E+05

Protein ID	Protein Name	Average Intensities			
		NCD NaCl	HFD NaCl	NCD insulin	HFD insulin
IPI00128399	Carboxylesterase ML1	2,90E+05	2,84E+05	2,90E+05	1,05E+05
IPI00469268	T-complex protein 1 subunit theta	2,89E+05	2,04E+05	3,54E+05	3,65E+05
IPI00309035	Dolichyl-diphosphooligosaccharide--protein glycosyltransferase subunit 1	2,86E+05	0,00E+00	2,58E+05	2,04E+05
IPI00553419	Desmoplakin	2,85E+05	7,93E+05	1,21E+06	6,55E+05
IPI00123639	Calreticulin	2,83E+05	2,27E+05	2,10E+05	1,46E+05
IPI00869393	Catalase	2,83E+05	1,87E+05	1,11E+05	4,91E+05
IPI00228253	Acetyl-CoA acetyltransferase, cytosolic	2,81E+05	1,42E+05	1,12E+05	2,19E+05
IPI00420363	Probable ATP-dependent RNA helicase DDX5	2,81E+05	5,52E+05	4,88E+05	5,24E+05
IPI00116192	Thioredoxin-dependent peroxide reductase, mitochondrial	2,78E+05	1,38E+05	0,00E+00	1,44E+05
IPI00221463	*Histone H2A type 3*	2,78E+05	0,00E+00	5,45E+04	1,68E+05
IPI00112822	Transcription factor A, mitochondrial	2,77E+05	8,52E+05	7,56E+05	8,36E+05
IPI00471246	Isovaleryl-CoA dehydrogenase, mitochondrial	2,77E+05	1,79E+05	2,09E+05	3,22E+05
IPI00123129	Staphylococcal nuclease domain-containing protein 1	2,75E+05	6,50E+04	2,21E+05	4,44E+04
IPI00331556	*Heat shock 70 kDa protein 4*	2,74E+05	0,00E+00	2,24E+05	2,71E+05
IPI00890309	Major urinary protein 8	2,73E+05	0,00E+00	0,00E+00	0,00E+00
IPI00313900	Lumican	2,67E+05	0,00E+00	6,96E+05	0,00E+00
IPI00127085	*60S ribosomal protein L10a*	2,67E+05	5,79E+04	8,11E+04	7,16E+04
IPI00122565	Rab GDP dissociation inhibitor beta	2,64E+05	5,08E+04	1,16E+05	1,75E+05
IPI00661414	Actin-related protein 2/3 complex subunit 2	2,64E+05	6,92E+05	4,31E+05	5,48E+05
IPI00163011	Thioredoxin domain-containing protein 5	2,61E+05	0,00E+00	5,45E+05	0,00E+00
IPI00314748	*WD repeat-containing protein 1*	2,60E+05	4,96E+05	2,90E+05	6,32E+05
IPI00118676	Eukaryotic initiation factor 4A-I	2,59E+05	1,88E+05	1,17E+05	1,40E+05
IPI00881340	*Hydroxysteroid (17-beta) dehydrogenase 13*	2,58E+05	1,78E+05	7,27E+04	1,48E+05
IPI00224575	*Heterogeneous nuclear ribonucleoprotein K*	2,57E+05	6,55E+05	2,70E+05	1,17E+06
IPI00346965	Beta-adaptin 1	2,56E+05	3,98E+05	1,92E+05	4,58E+05
IPI00122344	Cystathionine gamma-lyase	2,51E+05	0,00E+00	2,36E+05	4,62E+04
IPI00129011	Formimidoyltransferase-cyclodeaminase	2,49E+05	3,82E+05	2,15E+05	6,79E+05
IPI00460335	Aldh4a1 protein	2,45E+05	9,51E+04	1,34E+05	2,28E+05
IPI00230394	Lamin-B1	2,45E+05	7,89E+05	6,24E+05	1,88E+06
IPI00271951	Protein disulfide-isomerase A4	2,45E+05	6,26E+04	2,96E+05	1,81E+05
IPI00173179	Methyltransferase-like protein 7B	2,44E+05	7,66E+04	3,27E+04	8,18E+04
IPI00409462	Spliceosome RNA helicase Bat1	2,43E+05	8,13E+05	1,90E+05	1,01E+06
IPI00515360	Perlecan (Heparan sulfate proteoglycan 2)	2,42E+05	2,12E+05	4,16E+05	3,82E+05
IPI00116591	*Short-chain specific acyl-CoA dehydrogenase, mitochondrial*	2,41E+05	2,09E+05	1,64E+05	2,78E+05
IPI00109932	Probable ATP-dependent RNA helicase DDX6	2,37E+05	1,21E+05	1,13E+05	1,23E+05
IPI00132728	Cytochrome c1, heme protein, mitochondrial	2,35E+05	1,03E+05	0,00E+00	0,00E+00
IPI00118344	UDP-glucose 6-dehydrogenase	2,35E+05	0,00E+00	1,66E+05	4,36E+04
IPI00663627	Filamin-B	2,33E+05	3,31E+05	4,54E+05	9,23E+05
IPI00128376	3-alpha-hydroxysteroid dehydrogenase 1	2,32E+05	5,12E+04	1,00E+05	3,58E+04
IPI00114628	Indolethylamine N-methyltransferase	2,32E+05	4,10E+05	3,91E+05	1,22E+05
IPI00130018	Acyl-protein thioesterase 1	2,31E+05	1,61E+05	8,67E+04	1,70E+05

Protein ID	Protein Name	Average Intensities			
		NCD NaCl	HFD NaCl	NCD insulin	HFD insulin
IPI00227392	14-3-3 protein eta	2,31E+05	2,81E+05	4,76E+05	1,12E+05
IPI00222419	Cytochrome c, somatic	2,30E+05	3,64E+05	8,38E+05	8,68E+05
IPI00330094	Carnitine O-palmitoyltransferase 1, liver isoform	2,26E+05	2,05E+05	1,92E+05	1,72E+05
IPI00323819	*40S ribosomal protein S20*	2,22E+05	6,42E+04	0,00E+00	0,00E+00
IPI00880850	Microsomal glutathione S-transferase 1	2,21E+05	0,00E+00	0,00E+00	6,02E+04
IPI00762203	Ferritin light chain 1	2,21E+05	3,01E+04	3,68E+04	5,71E+04
IPI00130530	Glyoxylate reductase/hydroxypyruvate reductase	2,17E+05	1,27E+05	2,00E+05	4,82E+04
IPI00131204	UTP--glucose-1-phosphate uridylyltransferase	2,17E+05	2,32E+05	2,57E+05	4,62E+05
IPI00134621	**GTP-binding nuclear protein Ran**	2,15E+05	2,01E+05	4,00E+05	2,62E+05
IPI00753303	Dihydrodipicolinate synthase-like, mitochondrial	2,15E+05	1,35E+05	1,08E+05	6,39E+04
IPI00877182	F-actin-capping protein subunit alpha-1	2,14E+05	1,65E+05	4,58E+04	1,01E+05
IPI00314844	Twinfilin-1	2,12E+05	3,22E+05	4,01E+05	3,75E+05
IPI00119478	Tropomodulin-3	2,09E+05	3,18E+05	2,04E+05	7,47E+05
IPI00153143	UDP glucuronosyltransferase 2 family, polypeptide B1	2,05E+05	9,52E+04	8,85E+04	5,75E+04
IPI00314950	**60S acidic ribosomal protein P0**	2,02E+05	6,31E+04	1,31E+05	4,86E+04
IPI00313236	Bile acyl-CoA synthetase	2,02E+05	5,27E+04	3,51E+05	3,05E+05
IPI00113223	Fatty acid synthase	1,99E+05	0,00E+00	1,34E+05	1,88E+05
IPI00662342	UPF0465 protein C5orf33 homolog	1,99E+05	0,00E+00	0,00E+00	0,00E+00
IPI00344626	Glycerol-3-phosphate acyltransferase 1, mitochondrial	1,97E+05	4,49E+04	1,41E+05	6,33E+04
IPI00114818	SEC14-like protein 2	1,95E+05	1,49E+05	1,28E+05	1,28E+05
IPI00118022	AP-2 complex subunit sigma-1	1,95E+05	3,79E+05	0,00E+00	0,00E+00
IPI00114162	Fatty acid-binding protein, epidermal	1,93E+05	0,00E+00	0,00E+00	0,00E+00
IPI00153660	Dihydrolipoamide acetyltransferase component of pyruvate dehydrogenase complex	1,92E+05	5,55E+04	1,06E+05	0,00E+00
IPI00129164	Sepiapterin reductase	1,91E+05	8,04E+04	0,00E+00	3,07E+04
IPI00123223	Murinoglobulin-1	1,90E+05	5,79E+04	1,13E+05	2,86E+05
IPI00116222	3-hydroxyisobutyrate dehydrogenase, mitochondrial	1,89E+05	1,03E+05	1,01E+05	5,86E+04
IPI00110843	Agmatinase, mitochondrial	1,87E+05	0,00E+00	0,00E+00	0,00E+00
IPI00120848	Mimecan	1,87E+05	0,00E+00	2,19E+05	0,00E+00
IPI00857740	Flavin reductase	1,86E+05	1,54E+05	6,58E+04	1,21E+05
IPI00137491	Tartrate-resistant acid phosphatase type 5	1,85E+05	0,00E+00	0,00E+00	0,00E+00
IPI00119622	Cysteine sulfinic acid decarboxylase	1,80E+05	2,36E+05	1,50E+05	8,47E+04
IPI00129178	Ornithine aminotransferase, mitochondrial	1,79E+05	0,00E+00	1,28E+05	0,00E+00
IPI00874456	Dihydrolipoyl dehydrogenase, mitochondrial	1,79E+05	1,76E+05	1,36E+05	8,38E+04
IPI00132397	GTP-binding protein SAR1b	1,79E+05	5,13E+04	0,00E+00	5,16E+04
IPI00107952	Lysozyme C-2	1,78E+05	2,93E+05	8,19E+04	1,76E+05
IPI00128489	Cytochrome P450 2C50	1,77E+05	3,71E+04	1,73E+05	1,77E+05
IPI00314191	Carbonyl reductase [NADPH] 1	1,77E+05	8,29E+04	1,16E+05	2,52E+04
IPI00119755	Peroxisomal coenzyme A diphosphatase NUDT7	1,77E+05	4,96E+04	0,00E+00	0,00E+00
IPI00128287	Cytochrome P450 1A2	1,76E+05	0,00E+00	3,13E+05	5,42E+04

Protein ID	Protein Name	Average Intensities			
		NCD NaCl	HFD NaCl	NCD insulin	HFD insulin
IPI00874670	Abhydrolase domain-containing protein 14B	1,75E+05	9,94E+04	0,00E+00	2,40E+05
IPI00132762	Heat shock protein 75 kDa, mitochondrial	1,74E+05	1,28E+05	2,05E+05	1,83E+05
IPI00122633	Acyl-CoA synthetase family member 2, mitochondrial	1,74E+05	1,83E+05	1,27E+05	2,22E+05
IPI00321718	*Prohibitin-2*	1,73E+05	4,80E+04	1,12E+05	3,58E+04
IPI00133877	Cytochrome P450 4A14	1,72E+05	0,00E+00	1,76E+05	8,48E+04
IPI00330958	*Heterogeneous nuclear ribonucleoprotein D0*	1,72E+05	6,17E+05	1,77E+05	7,83E+05
IPI00621548	NADPH--cytochrome P450 reductase	1,71E+05	1,17E+05	1,91E+05	1,53E+05
IPI00108780	AP-2 complex subunit alpha-1	1,71E+05	2,03E+05	1,39E+05	3,70E+05
IPI00133440	**Prohibitin**	1,71E+05	1,03E+05	7,93E+04	4,10E+04
IPI00555036	Asialoglycoprotein receptor 1	1,70E+05	0,00E+00	0,00E+00	0,00E+00
IPI00380320	Probable D-lactate dehydrogenase, mitochondrial	1,70E+05	0,00E+00	2,55E+04	0,00E+00
IPI00222763	Splicing factor, arginine/serine-rich 7	1,68E+05	8,20E+05	2,76E+05	1,42E+06
IPI00122257	5'-nucleotidase	1,68E+05	1,35E+05	2,26E+05	1,59E+05
IPI00331442	Peptide methionine sulfoxide reductase	1,66E+05	1,54E+05	1,14E+05	5,65E+04
IPI00119685	Sterol 26-hydroxylase, mitochondrial	1,65E+05	8,50E+04	0,00E+00	3,66E+04
IPI00267407	Aldehyde dehydrogenase family 8 member A1	1,65E+05	6,94E+04	5,32E+04	1,13E+05
IPI00320241	DnaJ homolog subfamily B member 11	1,62E+05	0,00E+00	5,60E+04	0,00E+00
IPI00117705	Dolichyl-diphosphooligosaccharide--protein glycosyltransferase 48 kDa subunit	1,62E+05	4,12E+04	1,00E+05	6,49E+04
IPI00467119	Probable N-acetyltransferase CML1	1,62E+05	6,38E+04	0,00E+00	1,22E+05
IPI00154047	3-hydroxyisobutyryl-CoA hydrolase, mitochondrial	1,60E+05	9,20E+04	7,24E+04	4,99E+04
IPI00110528	Phenazine biosynthesis-like domain-containing protein 2	1,60E+05	9,15E+04	1,04E+05	4,86E+04
IPI00845652	2-oxoglutarate dehydrogenase E1 component, mitochondrial	1,58E+05	4,96E+04	1,38E+05	2,82E+04
IPI00113394	*40S ribosomal protein S15a*	1,57E+05	3,84E+05	2,33E+05	1,76E+05
IPI00123276	MOSC domain-containing protein 2, mitochondrial	1,57E+05	7,99E+04	1,11E+05	0,00E+00
IPI00313998	Sulfide:quinone oxidoreductase, mitochondrial	1,57E+05	0,00E+00	8,59E+04	0,00E+00
IPI00462802	Tripartite motif-containing protein 14	1,57E+05	2,55E+05	6,92E+04	2,44E+05
IPI00116281	T-complex protein 1 subunit zeta	1,56E+05	4,02E+04	2,42E+05	2,62E+05
IPI00856979	Sulfotransferase-like protein 2	1,55E+05	1,78E+05	1,03E+05	3,14E+04
IPI00135646	ATP-binding cassette sub-family D member 3	1,55E+05	3,87E+05	7,09E+04	1,96E+05
IPI00131138	Filamin-A	1,54E+05	6,17E+04	2,20E+05	2,04E+05
IPI00125220	Cathepsin Z	1,54E+05	3,25E+04	1,75E+05	2,84E+04
IPI00309224	**Phosphatidylinositol-4,5-bisphosphate 3-kinase catalytic subunit alpha isoform**	1,54E+05	2,98E+05	3,97E+06	2,80E+06
IPI00318750	Dehydrogenase/reductase SDR family member 4	1,52E+05	7,58E+04	6,41E+04	8,59E+04
IPI00454008	Serine hydroxymethyltransferase	1,51E+05	8,87E+04	1,75E+05	8,24E+04
IPI00125143	Actin-related protein 2/3 complex subunit 1B	1,51E+05	3,64E+05	2,32E+05	5,09E+05
IPI00653643	*Heterogeneous nuclear ribonucleoprotein L*	1,51E+05	6,66E+05	3,33E+05	8,59E+05
IPI00387282	Arylacetamide deacetylase	1,48E+05	5,41E+04	9,24E+04	5,14E+04

Protein ID	Protein Name	Average Intensities			
		NCD NaCl	HFD NaCl	NCD insulin	HFD insulin
IPI00116277	T-complex protein 1 subunit delta	1,48E+05	0,00E+00	2,56E+05	1,07E+05
IPI00112448	*40S ribosomal protein S10*	1,45E+05	8,55E+04	5,51E+04	8,27E+04
IPI00230550	Estradiol 17-beta-dehydrogenase 8	1,44E+05	3,08E+04	2,05E+05	1,01E+05
IPI00877345	Hemopexin	1,40E+05	0,00E+00	5,87E+04	0,00E+00
IPI00126191	Lamin-B2	1,40E+05	5,22E+05	3,85E+05	1,43E+06
IPI00127280	Myeloid bactenecin (F1)	1,39E+05	0,00E+00	0,00E+00	1,57E+05
IPI00277066	*Heterogeneous nuclear ribonucleoprotein A/B*	1,39E+05	5,27E+05	1,43E+05	7,08E+05
IPI00775863	Guanine nucleotide-binding protein G(I)/G(S)/G(T) subunit beta-2	1,38E+05	1,60E+05	2,36E+05	9,12E+04
IPI00421223	Tropomyosin alpha-4 chain	1,35E+05	1,91E+05	2,58E+05	4,67E+05
IPI00121833	3-ketoacyl-CoA thiolase A, peroxisomal	1,34E+05	1,48E+05	2,78E+04	9,27E+04
IPI00311682	Sodium/potassium-transporting ATPase subunit alpha-1	1,33E+05	3,90E+04	1,14E+05	1,16E+05
IPI00130144	Epoxide hydrolase 1, microsomal	1,33E+05	7,73E+04	5,81E+04	3,69E+04
IPI00226073	*Heterogeneous nuclear ribonucleoprotein F*	1,31E+05	7,26E+04	1,36E+05	3,91E+05
IPI00469380	Aldehyde oxidase 3	1,31E+05	1,71E+05	8,73E+04	1,72E+05
IPI00331146	UMP-CMP kinase	1,30E+05	1,11E+05	0,00E+00	5,14E+04
IPI00122547	Voltage-dependent anion-selective channel protein 2	1,30E+05	2,24E+04	9,08E+04	6,46E+04
IPI00154043	Carboxylesterase 6	1,29E+05	1,25E+05	7,60E+04	0,00E+00
IPI00318841	*Elongation factor 1-gamma*	1,28E+05	0,00E+00	0,00E+00	0,00E+00
IPI00222496	Protein disulfide-isomerase A6	1,28E+05	0,00E+00	8,98E+04	0,00E+00
IPI00856927	Rps19 protein	1,25E+05	9,42E+04	3,48E+04	1,21E+05
IPI00116283	T-complex protein 1 subunit gamma	1,25E+05	0,00E+00	3,33E+05	5,16E+04
IPI00316314	2-hydroxyacyl-CoA lyase 1	1,22E+05	1,78E+05	1,20E+05	6,42E+04
IPI00320217	T-complex protein 1 subunit beta	1,21E+05	9,10E+04	1,42E+05	7,44E+04
IPI00228978	Clathrin light chain B	1,21E+05	7,86E+05	2,26E+06	2,22E+06
IPI00119945	Nitrilase homolog 2	1,21E+05	6,04E+04	2,06E+04	3,51E+04
IPI00113057	Plasma kallikrein	1,20E+05	0,00E+00	2,05E+05	1,87E+05
IPI00762346	Kynurenine/alpha-aminoadipate aminotransferase mitochondrial	1,19E+05	0,00E+00	5,86E+04	0,00E+00
IPI00109823	1,4-alpha-glucan-branching enzyme	1,19E+05	0,00E+00	4,14E+04	6,66E+04
IPI00317794	Nucleolin	1,19E+05	1,04E+05	9,20E+04	3,64E+05
IPI00133034	Histidine triad nucleotide-binding protein 2	1,18E+05	0,00E+00	0,00E+00	0,00E+00
IPI00111045	Mitochondrial import inner membrane translocase subunit TIM50	1,17E+05	0,00E+00	3,18E+04	0,00E+00
IPI00121105	Hydroxyacyl-coenzyme A dehydrogenase, mitochondrial	1,17E+05	8,11E+04	1,14E+05	0,00E+00
IPI00122350	U1 small nuclear ribonucleoprotein A	1,17E+05	1,90E+05	2,82E+04	2,01E+05
IPI00122634	Cytochrome P450, family 2, subfamily a, polypeptide 12	1,16E+05	0,00E+00	8,88E+04	0,00E+00
IPI00330804	Heat shock protein HSP 90-alpha	1,15E+05	0,00E+00	1,62E+05	1,26E+05
IPI00122122	Complement component C8 gamma chain	1,14E+05	0,00E+00	0,00E+00	5,52E+04
IPI00556870	Igh protein	1,13E+05	0,00E+00	0,00E+00	0,00E+00
IPI00228633	Glucose-6-phosphate isomerase	1,12E+05	0,00E+00	2,00E+04	0,00E+00
IPI00471231	UDP-glucuronosyltransferase 2A3	1,12E+05	1,15E+05	1,90E+05	1,23E+05
IPI00115866	Hydroxyacylglutathione hydrolase	1,11E+05	2,18E+05	4,44E+05	2,36E+05
IPI00877297	Cytochrome P450 2D9	1,11E+05	2,55E+04	2,65E+04	0,00E+00

Protein ID	Protein Name	Average Intensities			
		NCD NaCl	HFD NaCl	NCD insulin	HFD insulin
IPI00261627	Succinyl-CoA ligase [ADP-forming] subunit beta, mitochondrial	1,10E+05	7,12E+04	1,21E+05	0,00E+00
IPI00310658	Aldo-keto reductase family 1 member C13	1,06E+05	0,00E+00	2,66E+04	0,00E+00
IPI00222489	Ces5 protein	1,06E+05	0,00E+00	3,41E+04	2,04E+04
IPI00131424	Carnitine O-palmitoyltransferase 2, mitochondrial	1,06E+05	1,16E+05	7,16E+04	1,82E+05
IPI00314189	3 beta-hydroxysteroid dehydrogenase type 5	1,06E+05	0,00E+00	4,84E+04	0,00E+00
IPI00113141	Citrate synthase, mitochondrial	1,05E+05	7,66E+04	1,04E+05	6,42E+04
IPI00408495	Basigin	1,05E+05	6,82E+04	1,17E+05	8,65E+04
IPI00875110	Isocitrate dehydrogenase [NADP], mitochondrial	1,05E+05	1,29E+05	8,11E+04	2,59E+04
IPI00649326	Myosin-XVIIIa	1,03E+05	1,24E+05	1,79E+05	3,94E+05
IPI00122293	Prolargin	1,00E+05	0,00E+00	4,12E+05	5,13E+04
IPI00123927	Alpha-1-antitrypsin 1-5	1,00E+05	0,00E+00	0,00E+00	0,00E+00
IPI00399943	Actin-related protein 2/3 complex subunit 5	9,94E+04	1,88E+05	5,75E+04	3,34E+05
IPI00117181	*Flotillin-1*	9,90E+04	0,00E+00	3,52E+04	1,55E+05
IPI00230035	ATP-dependent RNA helicase DDX3X	9,81E+04	7,13E+04	9,12E+04	9,71E+04
IPI00121534	Carbonic anhydrase 2	9,72E+04	0,00E+00	0,00E+00	4,47E+04
IPI00124692	Transaldolase	9,61E+04	0,00E+00	0,00E+00	0,00E+00
IPI00457898	Phosphoglycerate mutase 1	9,57E+04	0,00E+00	0,00E+00	0,00E+00
IPI00123924	Alpha-1-antitrypsin 1-4	9,56E+04	8,57E+04	1,57E+05	4,35E+04
IPI00127942	Destrin	9,56E+04	0,00E+00	0,00E+00	1,47E+05
IPI00113073	Aldehyde dehydrogenase X, mitochondrial	9,38E+04	0,00E+00	0,00E+00	0,00E+00
IPI00331555	2-oxoisovalerate dehydrogenase subunit alpha, mitochondrial	9,31E+04	0,00E+00	6,41E+04	0,00E+00
IPI00115824	Protein NipSnap homolog 1	9,26E+04	5,11E+04	0,00E+00	0,00E+00
IPI00221769	GTP:AMP phosphotransferase mitochondrial	9,22E+04	5,33E+04	0,00E+00	8,92E+04
IPI00123604	*40S ribosomal protein SA*	9,17E+04	0,00E+00	5,19E+04	0,00E+00
IPI00130343	*Heterogeneous nuclear ribonucleoproteins C1/C2*	9,07E+04	4,91E+05	1,71E+04	6,34E+05
IPI00125515	PCTP-like protein	8,96E+04	9,30E+04	1,80E+05	6,61E+04
IPI00128904	Poly(rC)-binding protein 1	8,94E+04	1,19E+05	8,02E+04	1,34E+05
IPI00762625	Anti-lipoteichoic acid light chain variable region	8,89E+04	3,44E+05	7,52E+04	1,91E+05
IPI00128271	Kynurenine 3-monooxygenase	8,88E+04	0,00E+00	3,28E+04	0,00E+00
IPI00471437	Igh protein	8,85E+04	7,85E+05	1,10E+06	2,67E+05
IPI00117741	Cytochrome P450 2J5	8,84E+04	0,00E+00	8,46E+04	3,74E+04
IPI00131584	Mitochondrial carnitine/acylcarnitine carrier protein	8,79E+04	0,00E+00	0,00E+00	2,88E+04
IPI00889811	**Ribophorin-2**	8,74E+04	0,00E+00	1,31E+05	3,85E+04
IPI00108143	*Heterogeneous nuclear ribonucleoprotein H2*	8,72E+04	8,96E+04	8,84E+04	2,31E+05
IPI00118459	Gap junction beta-1 protein	8,72E+04	5,76E+05	0,00E+00	3,29E+05
IPI00154045	Alanine aminotransferase 1	8,69E+04	0,00E+00	0,00E+00	0,00E+00
IPI00322936	Plasminogen	8,69E+04	7,90E+04	1,05E+05	1,94E+05
IPI00475378	Polypyrimidine tract binding protein 1	8,63E+04	4,34E+05	1,00E+05	7,66E+05
IPI00420972	Ig gamma-2A chain C region, A allele	8,59E+04	1,35E+05	7,36E+04	2,78E+05

Protein ID	Protein Name	Average Intensities			
		NCD NaCl	HFD NaCl	NCD insulin	HFD insulin
IPI00228617	Guanine nucleotide-binding protein G(i), alpha-2 subunit	8,59E+04	2,32E+05	1,03E+05	1,93E+05
IPI00123762	Regulator of chromosome condensation 1	8,53E+04	2,92E+05	9,62E+04	1,91E+05
IPI00121051	Glutathione S-transferase kappa 1	8,46E+04	4,80E+04	0,00E+00	3,06E+04
IPI00137471	3-beta-hydroxysteroid-Delta(8),Delta(7)-isomerase	8,44E+04	0,00E+00	0,00E+00	0,00E+00
IPI00134809	Dihydrolipoamide succinyltransferase component of 2-oxoglutarate dehydrogenase complex	8,44E+04	0,00E+00	3,40E+04	4,23E+04
IPI00226140	Amine oxidase [flavin-containing] B	8,36E+04	1,15E+05	1,34E+05	9,70E+04
IPI00121758	TAR DNA-binding protein 43	8,28E+04	1,29E+05	7,20E+04	2,92E+05
IPI00127625	Hydroxymethylglutaryl-CoA lyase, mitochondrial	8,10E+04	0,00E+00	1,11E+05	0,00E+00
IPI00123196	Decorin	8,08E+04	0,00E+00	4,35E+05	0,00E+00
IPI00111117	Actin-related protein 2/3 complex subunit 5-like protein	7,97E+04	1,30E+05	3,45E+04	6,68E+04
IPI00132958	Acyl-coenzyme A thioesterase 13	7,95E+04	0,00E+00	2,91E+04	0,00E+00
IPI00320503	Solute carrier family 25 member 42	7,84E+04	1,55E+05	0,00E+00	8,67E+04
IPI00115679	Neutral alpha-glucosidase AB	7,78E+04	0,00E+00	2,28E+04	1,16E+04
IPI00221932	Protein MAL2	7,74E+04	1,32E+05	0,00E+00	1,67E+05
IPI00124790	Receptor expression-enhancing protein 6	7,73E+04	3,64E+04	0,00E+00	0,00E+00
IPI00125853	Mitochondrial ornithine transporter 1	7,60E+04	0,00E+00	1,45E+04	0,00E+00
IPI00128378	Cystathionine beta-synthase	7,55E+04	5,21E+04	4,25E+04	0,00E+00
IPI00135085	Heme-binding protein 1	7,54E+04	0,00E+00	0,00E+00	4,45E+04
IPI00121348	L-serine dehydratase	7,43E+04	0,00E+00	0,00E+00	0,00E+00
IPI00132042	Pyruvate dehydrogenase E1 component subunit beta, mitochondrial	7,42E+04	0,00E+00	1,23E+05	0,00E+00
IPI00649763	Tyrosine-protein kinase Lyn	7,40E+04	1,41E+05	8,36E+04	2,63E+05
IPI00318577	Dihydropyrimidinase	7,40E+04	6,98E+04	2,50E+05	9,39E+04
IPI00224740	Profilin-1	7,33E+04	1,65E+05	1,23E+05	6,35E+04
IPI00322206	N-acylneuraminate cytidylyltransferase	7,31E+04	0,00E+00	1,98E+05	5,72E+04
IPI00554845	Mitochondrial inner membrane protein	7,21E+04	8,02E+04	7,34E+04	6,81E+04
IPI00408796	Splicing factor 3 subunit 1	7,12E+04	5,25E+04	3,16E+04	1,90E+05
IPI00135730	ADP-ribosylation factor 2	7,07E+04	0,00E+00	3,50E+04	0,00E+00
IPI00137145	**Polyadenylate-binding protein 1**	6,96E+04	0,00E+00	6,31E+04	1,02E+05
IPI00406193	**Ras GTPase-activating-like protein IQGAP2**	6,93E+04	0,00E+00	1,76E+05	3,11E+04
IPI00128556	Nicotinate-nucleotide pyrophosphorylase	6,82E+04	0,00E+00	9,82E+03	0,00E+00
IPI00323600	Coronin-1A	6,82E+04	4,27E+04	5,26E+04	1,19E+05
IPI00554894	Annexin A6	6,81E+04	2,55E+04	0,00E+00	6,26E+04
IPI00130535	Dihydrolipoamide branched chain transacylase E2	6,73E+04	4,88E+04	2,92E+04	0,00E+00
IPI00312468	Eukaryotic peptide chain release factor subunit 1	6,72E+04	0,00E+00	2,08E+04	2,47E+04
IPI00624210	Glycine N-acyltransferase-like protein	6,68E+04	1,19E+05	7,99E+04	1,27E+05
IPI00468203	Annexin A2	6,68E+04	0,00E+00	1,73E+05	0,00E+00
IPI00830749	Collagen alpha 3 chain type VI	6,67E+04	0,00E+00	0,00E+00	4,70E+04
IPI00458583	**Heterogenous nuclear ribonucleoprotein U**	6,61E+04	2,33E+05	3,42E+04	3,47E+05
IPI00136984	*40S ribosomal protein S7*	6,58E+04	1,77E+05	0,00E+00	5,67E+05
IPI00762185	3-mercaptopyruvate sulfurtransferase	6,57E+04	7,44E+04	6,82E+04	0,00E+00

Protein ID	Protein Name	Average Intensities			
		NCD NaCl	HFD NaCl	NCD insulin	HFD insulin
IPI00828470	Low molecular weight phosphotyrosine protein phosphatase	6,50E+04	2,13E+04	2,74E+04	0,00E+00
IPI00471081	Phospholipase B domain-containing protein 1	6,50E+04	0,00E+00	7,20E+04	0,00E+00
IPI00113427	Lysozyme C-1	6,49E+04	3,68E+04	2,12E+05	0,00E+00
IPI00136134	Protein NDRG2	6,48E+04	0,00E+00	7,93E+04	0,00E+00
IPI00877335	Putative uncharacterized protein	6,41E+04	0,00E+00	0,00E+00	0,00E+00
IPI00122557	Liver carboxylesterase 31-like	6,29E+04	0,00E+00	0,00E+00	0,00E+00
IPI00649502	Erythrocyte protein band 4.1	6,26E+04	1,38E+04	2,17E+05	3,47E+05
IPI00339468	ATP-dependent RNA helicase A	6,19E+04	3,07E+05	4,02E+04	2,19E+05
IPI00337893	Pyruvate dehydrogenase E1 component subunit alpha, somatic form, mitochondrial	6,14E+04	0,00E+00	8,42E+04	5,71E+04
IPI00135655	Vesicle-associated membrane protein-associated protein B	6,04E+04	0,00E+00	1,58E+04	3,29E+04
IPI00605187	Truncated ceruloplasmin	5,90E+04	0,00E+00	8,12E+04	7,77E+04
IPI00130102	Desmin	5,90E+04	6,70E+04	6,27E+04	4,96E+04
IPI00118625	Histidine ammonia-lyase	5,87E+04	0,00E+00	5,90E+04	7,72E+04
IPI00750595	Myosin regulatory light polypeptide 9	5,82E+04	2,18E+05	0,00E+00	2,33E+05
IPI00377351	Apolipoprotein A-IV	5,78E+04	0,00E+00	1,58E+04	0,00E+00
IPI00264501	Phosphatidylinositol-binding clathrin assembly protein	5,71E+04	1,72E+05	3,17E+04	8,51E+04
IPI00314202	Bile acid-CoA:amino acid N-acyltransferase	5,64E+04	0,00E+00	0,00E+00	0,00E+00
IPI00652925	Sec24b protein	5,61E+04	0,00E+00	1,16E+05	0,00E+00
IPI00317074	Mitochondrial dicarboxylate carrier	5,55E+04	0,00E+00	0,00E+00	3,00E+04
IPI00172146	Trans-1,2-dihydrobenzene-1,2-diol dehydrogenase	5,54E+04	0,00E+00	0,00E+00	0,00E+00
IPI00407499	4-aminobutyrate aminotransferase, mitochondrial	5,38E+04	0,00E+00	4,04E+04	0,00E+00
IPI00331490	Aflatoxin B1 aldehyde reductase member 2	5,33E+04	0,00E+00	2,73E+04	2,39E+04
IPI00119470	Probable imidazolonepropionase	5,25E+04	0,00E+00	6,21E+04	4,43E+04
IPI00134870	Peroxisomal acyl-coenzyme A oxidase 2	5,15E+04	0,00E+00	0,00E+00	1,69E+04
IPI00121514	Stress-induced-phosphoprotein 1	5,13E+04	0,00E+00	0,00E+00	0,00E+00
IPI00114331	Alpha-methylacyl-CoA racemase	5,12E+04	0,00E+00	0,00E+00	0,00E+00
IPI00123313	Ubiquitin-like modifier-activating enzyme 1	5,10E+04	0,00E+00	6,54E+04	1,44E+04
IPI00308882	NADH-ubiquinone oxidoreductase 75 kDa subunit, mitochondrial	5,04E+04	0,00E+00	0,00E+00	0,00E+00
IPI00114647	Deoxyhypusine synthase	4,95E+04	0,00E+00	0,00E+00	0,00E+00
IPI00117063	RNA-binding protein FUS	4,92E+04	2,23E+04	9,96E+04	3,01E+05
IPI00330632	Collagen alpha-1(XIV) chain	4,92E+04	0,00E+00	7,56E+04	4,72E+04
IPI00336362	Aldehyde dehydrogenase, cytosolic 1	4,79E+04	0,00E+00	4,19E+04	7,09E+04
IPI00114381	Tryptophan 2,3-dioxygenase	4,72E+04	0,00E+00	2,33E+04	0,00E+00
IPI00125091	LIM and SH3 domain protein 1	4,68E+04	0,00E+00	0,00E+00	3,06E+04
IPI00458043	Sorbin and SH3 domain-containing protein 1	4,68E+04	1,34E+05	1,81E+05	3,88E+05
IPI00918921	Ubiquitin-conjugating enzyme E2 variant 1	4,62E+04	0,00E+00	0,00E+00	0,00E+00
IPI00331174	T-complex protein 1 subunit eta	4,59E+04	0,00E+00	2,23E+05	0,00E+00
IPI00109910	Ighg protein	4,56E+04	0,00E+00	5,34E+04	2,90E+04

Protein ID	Protein Name	Average Intensities			
		NCD NaCl	HFD NaCl	NCD insulin	HFD insulin
IPI00121309	NADH dehydrogenase [ubiquinone] iron-sulfur protein 3, mitochondrial	4,55E+04	0,00E+00	0,00E+00	0,00E+00
IPI00675981	FK506-binding protein 15	4,53E+04	9,83E+04	3,82E+04	2,31E+04
IPI00133544	Pancreatic alpha-amylase	4,39E+04	1,21E+05	0,00E+00	0,00E+00
IPI00170363	Long-chain-fatty-acid--CoA ligase 5	4,36E+04	0,00E+00	1,04E+05	6,80E+04
IPI00408207	Myosin-Id	4,35E+04	1,63E+05	5,44E+04	1,26E+05
IPI00623845	Selenium-binding protein 1	4,35E+04	0,00E+00	3,09E+04	0,00E+00
IPI00226872	EF hand domain containing 2	4,34E+04	0,00E+00	2,44E+04	1,71E+05
IPI00120832	Major urinary protein 3	4,34E+04	0,00E+00	0,00E+00	0,00E+00
IPI00125899	**Catenin beta-1**	4,25E+04	2,03E+05	1,48E+05	4,07E+05
IPI00323911	Glutathione S-transferase A4	4,25E+04	5,44E+04	0,00E+00	0,00E+00
IPI00119305	Proliferation-associated protein 2G4	4,22E+04	0,00E+00	2,48E+04	0,00E+00
IPI00471091	Aspartate dehydrogenase domain-containing protein	4,19E+04	0,00E+00	3,51E+04	0,00E+00
IPI00313631	Mitochondrial 2-oxodicarboxylate carrier	4,18E+04	0,00E+00	7,67E+04	0,00E+00
IPI00153190	SEC14-like protein 4	4,15E+04	0,00E+00	3,01E+04	1,78E+04
IPI00314909	Serine--pyruvate aminotransferase, mitochondrial	4,11E+04	0,00E+00	0,00E+00	0,00E+00
IPI00108271	ELAV-like protein 1	4,05E+04	2,95E+05	5,78E+04	1,63E+05
IPI00315794	Cytochrome b5 type B	3,99E+04	0,00E+00	0,00E+00	0,00E+00
IPI00129468	Chromobox protein homolog 3	3,92E+04	6,95E+04	0,00E+00	1,27E+05
IPI00276157	Apoptosis-inducing factor 2	3,92E+04	0,00E+00	2,58E+04	2,87E+04
IPI00420807	Splicing factor, arginine/serine-rich 1	3,91E+04	2,57E+05	2,03E+05	6,17E+05
IPI00119220	Small nuclear ribonucleoprotein Sm D2	3,89E+04	4,86E+05	2,19E+05	8,52E+05
IPI00120826	Translocon-associated protein subunit gamma	3,87E+04	0,00E+00	0,00E+00	2,09E+04
IPI00850737	Methylmalonyl-Coenzyme A mutase	3,86E+04	3,57E+04	4,21E+04	3,49E+04
IPI00757790	Cingulin	3,85E+04	1,80E+05	3,19E+05	2,78E+05
IPI00115215	Thiopurine S-methyltransferase	3,79E+04	0,00E+00	0,00E+00	0,00E+00
IPI00226882	Protein transport protein Sec61 subunit alpha isoform 1	3,79E+04	0,00E+00	0,00E+00	0,00E+00
IPI00153677	Arf-GAP with dual PH domain-containing protein 2	3,78E+04	1,03E+05	3,24E+04	5,26E+04
IPI00131478	Sulfotransferase 1A1	3,77E+04	0,00E+00	0,00E+00	0,00E+00
IPI00126716	Eukaryotic initiation factor 4A-III	3,75E+04	1,10E+05	6,16E+04	1,67E+05
IPI00135635	Serine protease inhibitor A3M	3,64E+04	0,00E+00	0,00E+00	0,00E+00
IPI00313296	Ribonuclease inhibitor	3,62E+04	0,00E+00	0,00E+00	0,00E+00
IPI00124979	*Heterogeneous nuclear ribonucleoprotein G*	3,62E+04	2,25E+05	0,00E+00	3,06E+05
IPI00284816	Collagen alpha-1(XVIII) chain	3,60E+04	0,00E+00	2,91E+04	1,15E+05
IPI00886106	Ketohexokinase	3,58E+04	0,00E+00	0,00E+00	0,00E+00
IPI00137848	Splicing factor 3A subunit 3	3,54E+04	1,03E+05	0,00E+00	0,00E+00
IPI00169666	UDP glucuronosyltransferase 2 family, polypeptide B34	3,53E+04	0,00E+00	0,00E+00	0,00E+00
IPI00121271	UPF0585 protein C16orf13 homolog	3,49E+04	0,00E+00	4,24E+04	2,43E+04
IPI00114368	Vesicle-trafficking protein SEC22b	3,34E+04	2,25E+04	0,00E+00	2,56E+04
IPI00311809	Solute carrier family 2, facilitated glucose transporter member 2	3,29E+04	0,00E+00	0,00E+00	0,00E+00
IPI00271986	ATP synthase subunit f, mitochondrial	3,25E+04	0,00E+00	4,34E+05	1,36E+05
IPI00116356	AP-2 complex subunit mu-1	3,24E+04	0,00E+00	0,00E+00	5,90E+04

Protein ID	Protein Name	Average Intensities			
		NCD NaCl	HFD NaCl	NCD insulin	HFD insulin
IPI00130804	Delta(3,5)-Delta(2,4)-dienoyl-CoA isomerase, mitochondrial	3,23E+04	0,00E+00	0,00E+00	3,30E+04
IPI00673886	Sorbin and SH3 domain-containing protein 2	3,14E+04	0,00E+00	5,34E+04	1,23E+05
IPI00121493	Tetratricopeptide repeat protein 36	3,12E+04	0,00E+00	0,00E+00	2,78E+04
IPI00119808	ATP-dependent Clp protease ATP-binding subunit clpX-like, mitochondrial	3,09E+04	0,00E+00	0,00E+00	0,00E+00
IPI00120761	Band 3 anion transport protein	3,06E+04	0,00E+00	1,84E+04	4,48E+04
IPI00123557	RuvB-like 2	3,05E+04	1,98E+04	2,00E+04	5,83E+04
IPI00624896	Aspartyl/asparaginyl beta-hydroxylase	2,99E+04	4,29E+04	0,00E+00	0,00E+00
IPI00129323	Splicing factor, arginine/serine-rich 3	2,98E+04	1,28E+05	0,00E+00	3,20E+05
IPI00122743	*Aspartyl-tRNA synthetase, cytoplasmic*	2,96E+04	0,00E+00	2,26E+04	0,00E+00
IPI00877214	Peroxisomal 3,2-trans-enoyl-CoA isomerase	2,90E+04	2,60E+04	3,44E+04	5,39E+04
IPI00118963	*39S ribosomal protein L12, mitochondrial*	2,90E+04	0,00E+00	0,00E+00	3,93E+04
IPI00828590	Cytochrome P450, family 4, subfamily a, polypeptide 12a	2,84E+04	0,00E+00	2,65E+04	0,00E+00
IPI00896567	Spectrin alpha chain, erythrocyte	2,83E+04	1,51E+05	9,50E+04	4,68E+05
IPI00136012	Vitamin K-dependent gamma-carboxylase	2,81E+04	0,00E+00	0,00E+00	0,00E+00
IPI00229539	*Histone H2B type 3-B*	2,79E+04	0,00E+00	0,00E+00	0,00E+00
IPI00120457	Farnesyl pyrophosphate synthetase	2,76E+04	0,00E+00	0,00E+00	0,00E+00
IPI00117264	Protein DJ-1	2,73E+04	0,00E+00	0,00E+00	4,07E+04
IPI00347394	Protein KIAA0664	2,70E+04	0,00E+00	1,62E+04	4,56E+04
IPI00845690	Kynurenine--oxoglutarate transaminase 3	2,67E+04	0,00E+00	1,34E+04	0,00E+00
IPI00331088	Pigment epithelium-derived factor	2,65E+04	0,00E+00	0,00E+00	0,00E+00
IPI00651878	Adenylate kinase isoenzyme 4, mitochondrial	2,64E+04	3,16E+04	0,00E+00	0,00E+00
IPI00133985	RuvB-like 1	2,64E+04	0,00E+00	0,00E+00	3,25E+04
IPI00127987	Actin-related protein 2/3 complex subunit 1A	2,63E+04	0,00E+00	0,00E+00	0,00E+00
IPI00153144	Sulfite oxidase, mitochondrial	2,61E+04	0,00E+00	0,00E+00	0,00E+00
IPI00124830	Leukocyte surface antigen CD47	2,56E+04	0,00E+00	2,46E+04	2,41E+04
IPI00757372	Isochorismatase domain-containing protein 2A, mitochondrial	2,54E+04	0,00E+00	0,00E+00	0,00E+00
IPI00116432	Dimethylaniline monooxygenase [N-oxide-forming] 1	2,51E+04	0,00E+00	4,66E+04	0,00E+00
IPI00130985	Retinol dehydrogenase 7	2,49E+04	0,00E+00	5,28E+04	0,00E+00
IPI00126248	ATP-citrate synthase	2,48E+04	0,00E+00	2,32E+04	0,00E+00
IPI00666034	Apolipoprotein B	2,43E+04	0,00E+00	0,00E+00	0,00E+00
IPI00118143	Src substrate cortactin	2,41E+04	8,67E+04	2,39E+04	1,81E+05
IPI00761408	Lon protease homolog, mitochondrial	2,39E+04	0,00E+00	2,55E+04	2,97E+04
IPI00121517	Phosphotriesterase-related protein	2,39E+04	0,00E+00	0,00E+00	0,00E+00
IPI00115599	Corticosteroid 11-beta-dehydrogenase isozyme 1	2,38E+04	0,00E+00	1,54E+04	0,00E+00
IPI00123494	26S proteasome non-ATPase regulatory subunit 2	2,34E+04	0,00E+00	3,16E+04	1,01E+04
IPI00230415	Eukaryotic translation initiation factor 2 subunit 3, X-linked	2,34E+04	0,00E+00	2,92E+04	0,00E+00
IPI00111519	Fructosamine-3-kinase	2,34E+04	0,00E+00	4,35E+04	3,09E+04
IPI00856379	Fructose-bisphosphate aldolase	2,33E+04	0,00E+00	3,59E+04	0,00E+00
IPI00169543	Zymogen granule membrane protein 16	2,31E+04	0,00E+00	0,00E+00	0,00E+00

Protein ID	Protein Name	Average Intensities			
		NCD NaCl	HFD NaCl	NCD insulin	HFD insulin
IPI00761657	Galectin-8	2,16E+04	7,74E+04	0,00E+00	0,00E+00
IPI00139795	*60S acidic ribosomal protein P2*	2,15E+04	0,00E+00	0,00E+00	0,00E+00
IPI00229647	Tln2 protein	2,10E+04	4,66E+04	3,44E+04	1,88E+05
IPI00321308	*Alanyl-tRNA synthetase, cytoplasmic*	2,09E+04	0,00E+00	2,35E+04	1,45E+04
IPI00330476	Cytoplasmic FMR1-interacting protein 1	2,09E+04	0,00E+00	4,14E+04	0,00E+00
IPI00387388	BCL2-associated athanogene 3	2,09E+04	0,00E+00	1,49E+04	1,10E+05
IPI00135869	*Ras-related protein Rab-11B*	2,09E+04	0,00E+00	0,00E+00	6,70E+04
IPI00123342	Hypoxia up-regulated protein 1	2,07E+04	0,00E+00	3,82E+04	0,00E+00
IPI00129430	Splicing factor, proline- and glutamine-rich	2,07E+04	0,00E+00	1,78E+04	4,05E+04
IPI00323881	*Importin subunit beta-1*	2,05E+04	4,74E+04	2,50E+04	8,75E+04
IPI00134599	**40S ribosomal protein S3**	2,03E+04	4,34E+04	3,35E+04	0,00E+00
IPI00660980	A6 anti-[4-hydroxy-3-nitrophenyl(Phenolate form)] acetyl mAb V-L region	2,03E+04	2,07E+05	0,00E+00	0,00E+00
IPI00119239	Proteasome subunit beta type-6	2,02E+04	0,00E+00	0,00E+00	1,58E+04
IPI00116228	Peptidyl-prolyl cis-trans isomerase, mitochondrial	2,00E+04	0,00E+00	0,00E+00	0,00E+00
IPI00474446	Eukaryotic translation initiation factor 2 subunit 1	2,00E+04	0,00E+00	9,07E+04	0,00E+00
IPI00118059	Serine hydroxymethyltransferase, cytosolic	1,98E+04	0,00E+00	0,00E+00	0,00E+00
IPI00130185	*Serine/threonine-protein phosphatase PP1-alpha catalytic subunit*	1,97E+04	0,00E+00	0,00E+00	3,23E+04
IPI00114560	*Ras-related protein Rab-1A*	1,95E+04	0,00E+00	0,00E+00	1,92E+04
IPI00131376	Spectrin beta chain, erythrocyte	1,95E+04	1,16E+05	0,00E+00	3,76E+05
IPI00459033	DnaJ homolog subfamily C member 3	1,94E+04	0,00E+00	0,00E+00	0,00E+00
IPI00122428	Heat shock protein beta-8	1,89E+04	6,04E+04	0,00E+00	8,10E+04
IPI00132799	Complement component 1, q subcomponent binding protein	1,89E+04	0,00E+00	0,00E+00	3,57E+04
IPI00311072	Cysteine desulfurase, mitochondrial	1,89E+04	0,00E+00	3,07E+04	0,00E+00
IPI00118875	*Elongation factor 1-delta*	1,84E+04	0,00E+00	0,00E+00	0,00E+00
IPI00654397	Activin receptor-interacting protein 2a	1,83E+04	0,00E+00	0,00E+00	0,00E+00
IPI00170008	U2 small nuclear ribonucleoprotein A'	1,76E+04	0,00E+00	0,00E+00	0,00E+00
IPI00331573	Protein-glutamine gamma-glutamyltransferase K	1,75E+04	0,00E+00	7,96E+04	6,70E+04
IPI00406118	*Heterogeneous nuclear ribonucleoprotein Q*	1,73E+04	0,00E+00	0,00E+00	1,06E+05
IPI00132531	NADH dehydrogenase [ubiquinone] 1 beta subcomplex subunit 5, mitochondrial	1,72E+04	0,00E+00	0,00E+00	0,00E+00
IPI00124067	UPF0598 protein C8orf82 homolog	1,72E+04	0,00E+00	0,00E+00	2,76E+04
IPI00136227	Growth hormone-regulated TBC protein 1	1,70E+04	4,14E+04	0,00E+00	2,96E+04
IPI00128857	NADP-dependent malic enzyme	1,69E+04	0,00E+00	8,71E+04	0,00E+00
IPI00122362	Protein disulfide-isomerase A5	1,66E+04	0,00E+00	0,00E+00	0,00E+00
IPI00122521	Fragile X mental retardation syndrome-related protein 1	1,61E+04	3,68E+04	0,00E+00	7,72E+04
IPI00762812	Chloride channel CaCC	1,60E+04	0,00E+00	0,00E+00	0,00E+00
IPI00169925	NADH dehydrogenase [ubiquinone] flavoprotein 2, mitochondrial	1,60E+04	0,00E+00	0,00E+00	0,00E+00
IPI00331163	S-phase kinase-associated protein 1	1,53E+04	0,00E+00	0,00E+00	2,50E+04
IPI00313841	V-type proton ATPase subunit d 1	1,50E+04	0,00E+00	2,71E+04	0,00E+00

Protein ID	Protein Name	Average Intensities			
		NCD NaCl	HFD NaCl	NCD insulin	HFD insulin
IPI00115626	Lipid phosphate phosphohydrolase 3	1,45E+04	4,71E+04	1,92E+04	1,99E+04
IPI00229705	Dihydropyrimidine dehydrogenase [NADP+]	1,44E+04	0,00E+00	0,00E+00	0,00E+00
IPI00117834	Lipolysis-stimulated lipoprotein receptor	1,40E+04	0,00E+00	0,00E+00	0,00E+00
IPI00400301	Coproporphyrinogen-III oxidase, mitochondrial	1,38E+04	0,00E+00	0,00E+00	0,00E+00
IPI00457852	*60S ribosomal protein L6*	1,38E+04	0,00E+00	0,00E+00	0,00E+00
IPI00409918	Eukaryotic initiation factor 4A-II	1,38E+04	0,00E+00	0,00E+00	0,00E+00
IPI00119923	Peroxisomal Lon protease homolog 2	1,37E+04	0,00E+00	0,00E+00	0,00E+00
IPI00137142	*Transcription elongation factor A protein 3*	1,29E+04	0,00E+00	0,00E+00	0,00E+00
IPI00119618	Calnexin	1,28E+04	0,00E+00	0,00E+00	0,00E+00
IPI00229835	Cytochrome P450 CYP2C44	1,23E+04	0,00E+00	0,00E+00	0,00E+00
IPI00653398	**Flotillin-2**	1,21E+04	0,00E+00	2,70E+04	1,14E+05
IPI00127560	Transthyretin	1,21E+04	0,00E+00	7,05E+04	2,64E+04
IPI00120165	Peroxisomal carnitine O-octanoyltransferase	1,20E+04	0,00E+00	0,00E+00	0,00E+00
IPI00110588	Moesin	1,18E+04	5,92E+04	1,25E+05	1,22E+05
IPI00114246	NADH dehydrogenase [ubiquinone] 1 beta subcomplex subunit 11, mitochondrial	1,16E+04	0,00E+00	0,00E+00	0,00E+00
IPI00331598	DnaJ (Hsp40) homolog, subfamily B, member 12	1,09E+04	0,00E+00	0,00E+00	0,00E+00
IPI00317590	*40S ribosomal protein S18*	1,08E+04	0,00E+00	0,00E+00	0,00E+00
IPI00114733	Serpin H1	1,08E+04	0,00E+00	0,00E+00	0,00E+00
IPI00310091	**Serine/threonine-protein phosphatase 2A 65 kDa regulatory subunit A alpha isoform**	1,06E+04	0,00E+00	1,17E+04	6,74E+04
IPI00223714	*Histone H1.4*	1,03E+04	0,00E+00	0,00E+00	1,88E+05
IPI00136655	2-amino-3-ketobutyrate coenzyme A ligase, mitochondrial	1,01E+04	0,00E+00	0,00E+00	0,00E+00
IPI00116850	UPF0027 protein C22orf28 homolog	1,00E+04	0,00E+00	0,00E+00	2,93E+04
IPI00269265	Cytochrome P450 2C70	9,89E+03	0,00E+00	0,00E+00	0,00E+00
IPI00323660	Actin-like protein 6A	9,79E+03	0,00E+00	0,00E+00	7,08E+04
IPI00339885	Collagen alpha-1(VI) chain	9,74E+03	0,00E+00	1,37E+04	0,00E+00
IPI00121288	NADH dehydrogenase [ubiquinone] 1 beta subcomplex subunit 10	9,58E+03	0,00E+00	0,00E+00	0,00E+00
IPI00759878	Complement C3	9,09E+03	0,00E+00	5,08E+04	6,45E+04
IPI00132474	Integrin beta-1	9,09E+03	0,00E+00	0,00E+00	0,00E+00
IPI00314467	Proteasome subunit beta type-3	8,82E+03	0,00E+00	0,00E+00	0,00E+00
IPI00128818	DEAH box protein 15	8,68E+03	0,00E+00	0,00E+00	5,17E+04
IPI00136498	Lin-7 homolog C	8,54E+03	0,00E+00	0,00E+00	3,82E+04
IPI00466919	6-phosphogluconate dehydrogenase, decarboxylating	8,35E+03	0,00E+00	1,01E+04	0,00E+00
IPI00762806	Tetratricopeptide repeat protein 38	8,23E+03	0,00E+00	0,00E+00	0,00E+00
IPI00410937	RNA-binding protein 8A	8,22E+03	1,05E+04	0,00E+00	7,07E+04
IPI00221556	Acyl-coenzyme A synthetase ACSM5, mitochondrial	8,13E+03	0,00E+00	0,00E+00	0,00E+00
IPI00322218	Cytochrome P450 4A10	8,05E+03	0,00E+00	0,00E+00	0,00E+00
IPI00128945	Proteasome subunit beta type-2	8,03E+03	0,00E+00	0,00E+00	0,00E+00
IPI00111560	Protein SET	7,99E+03	0,00E+00	0,00E+00	0,00E+00
IPI00323166	NAD(P) transhydrogenase, mitochondrial	7,74E+03	0,00E+00	2,20E+04	1,13E+04

Protein ID	Protein Name	Average Intensities			
		NCD NaCl	HFD NaCl	NCD insulin	HFD insulin
IPI00756893	Retinol-binding protein 4	7,64E+03	0,00E+00	0,00E+00	0,00E+00
IPI00114781	Cytochrome P450 2C40	7,63E+03	0,00E+00	2,39E+04	0,00E+00
IPI00120197	Cytochrome P450 4V3	7,42E+03	0,00E+00	0,00E+00	0,00E+00
IPI00320399	Lamina-associated polypeptide 2, isoforms beta/delta/epsilon/gamma	7,06E+03	0,00E+00	0,00E+00	1,13E+05
IPI00119004	Isoamyl acetate-hydrolyzing esterase 1 homolog	6,98E+03	0,00E+00	0,00E+00	0,00E+00
IPI00126000	FK506-binding protein 3	6,80E+03	0,00E+00	0,00E+00	0,00E+00
IPI00649950	Elongation factor Tu GTP binding domain containing 2	6,40E+03	5,44E+04	3,00E+04	9,86E+04
IPI00387249	Regulator of microtubule dynamics protein 1	6,28E+03	0,00E+00	0,00E+00	0,00E+00
IPI00776264	Retsat protein	5,86E+03	0,00E+00	0,00E+00	0,00E+00
IPI00109311	Na(+)/H(+) exchange regulatory cofactor NHE-RF1	5,14E+03	0,00E+00	3,82E+04	0,00E+00
IPI00124181	Selenide, water dikinase 2	4,70E+03	0,00E+00	0,00E+00	0,00E+00
IPI00123619	Cytochrome P450, family 2, subfamily d, polypeptide 22	4,59E+03	0,00E+00	0,00E+00	0,00E+00
IPI00115065	Glia-derived nexin	4,22E+03	0,00E+00	0,00E+00	0,00E+00
IPI00315581	Putative uncharacterized protein	4,02E+03	0,00E+00	0,00E+00	0,00E+00
IPI00126552	U1 small nuclear ribonucleoprotein C	2,78E+03	0,00E+00	0,00E+00	4,36E+04
IPI00554933	Glutathione S-transferase theta-1	1,88E+03	0,00E+00	0,00E+00	0,00E+00
IPI00130640	Ribonuclease UK114	0,00E+00	1,07E+06	1,46E+06	1,60E+06
IPI00125929	NADH dehydrogenase [ubiquinone] 1 alpha subcomplex subunit 4	0,00E+00	0,00E+00	1,15E+06	6,98E+05
IPI00111770	ATP synthase subunit e, mitochondrial	0,00E+00	0,00E+00	1,01E+06	4,36E+05
IPI00404837	Myosin-4	0,00E+00	0,00E+00	5,77E+05	0,00E+00
IPI00230034	D-dopachrome decarboxylase	0,00E+00	4,24E+05	2,77E+05	6,04E+05
IPI00226993	Thioredoxin	0,00E+00	1,90E+05	2,69E+05	2,71E+05
IPI00129126	Claudin-3	0,00E+00	1,58E+05	2,47E+05	3,54E+05
IPI00675483	Chromodomain helicase DNA binding protein 3	0,00E+00	0,00E+00	2,20E+05	0,00E+00
IPI00677618	5-hydroxyisourate hydrolase	0,00E+00	1,44E+05	1,89E+05	5,14E+04
IPI00136110	**Phosphatidylinositol-4,5-bisphosphate 3-kinase catalytic subunit beta isoform**	0,00E+00	0,00E+00	1,88E+05	2,95E+04
IPI00116154	Cytochrome c oxidase, subunit Vb	0,00E+00	0,00E+00	1,88E+05	0,00E+00
IPI00830581	Mitochondrial ribonuclease P protein 2	0,00E+00	0,00E+00	1,73E+05	7,88E+04
IPI00377441	*40S ribosomal protein S26*	0,00E+00	0,00E+00	1,71E+05	0,00E+00
IPI00652450	Lethal(2) giant larvae protein homolog 2	0,00E+00	5,59E+04	1,02E+05	1,50E+05
IPI00130238	Adenomatous polyposis coli protein 2	0,00E+00	0,00E+00	8,84E+04	0,00E+00
IPI00853924	14-3-3 protein theta	0,00E+00	0,00E+00	6,67E+04	0,00E+00
IPI00129215	Pantetheinase	0,00E+00	5,82E+04	4,71E+04	9,49E+04
IPI00114330	Homogentisate 1,2-dioxygenase	0,00E+00	0,00E+00	4,56E+04	0,00E+00
IPI00331507	**Cullin-5**	0,00E+00	0,00E+00	4,43E+04	2,32E+04
IPI00670268	Probable phospholipid-transporting ATPase 11C	0,00E+00	0,00E+00	4,42E+04	7,43E+04
IPI00123802	Heat shock protein 105 kDa	0,00E+00	0,00E+00	3,85E+04	2,08E+04
IPI00222208	*Heterogeneous nuclear ribonucleoprotein U-like protein 2*	0,00E+00	8,53E+04	3,71E+04	6,29E+04
IPI00269662	*Heterogeneous nuclear ribonucleoprotein A3*	0,00E+00	0,00E+00	3,11E+04	5,68E+05
IPI00322562	*40S ribosomal protein S14*	0,00E+00	0,00E+00	3,02E+04	0,00E+00

		Average Intensities			
Protein ID	**Protein Name**	**NCD NaCl**	**HFD NaCl**	**NCD insulin**	**HFD insulin**
IPI00134519	Cytochrome P450 3A13	0,00E+00	0,00E+00	2,75E+04	0,00E+00
IPI00554928	Neurofilament light polypeptide	0,00E+00	0,00E+00	2,75E+04	3,01E+04
IPI00319965	26S proteasome non-ATPase regulatory subunit 6	0,00E+00	0,00E+00	2,65E+04	0,00E+00
IPI00109142	S-formylglutathione hydrolase	0,00E+00	0,00E+00	2,61E+04	0,00E+00
IPI00828412	Retinoblastoma binding protein 4	0,00E+00	0,00E+00	2,44E+04	8,11E+04
IPI00132347	Cytochrome b-c1 complex subunit 7	0,00E+00	5,43E+04	2,39E+04	0,00E+00
IPI00109672	Proto-oncogene tyrosine-protein kinase Yes	0,00E+00	0,00E+00	2,39E+04	7,21E+04
IPI00652811	Phospholipase A2 inhibitory protein	0,00E+00	0,00E+00	2,01E+04	0,00E+00
IPI00467338	Ran GTPase-activating protein 1	0,00E+00	0,00E+00	1,88E+04	1,35E+05
IPI00623030	UPF0493 protein KIAA1632	0,00E+00	0,00E+00	1,79E+04	0,00E+00
IPI00453826	Matrin-3	0,00E+00	0,00E+00	1,74E+04	1,02E+05
IPI00553777	*Heterogeneous nuclear ribonucleoprotein A1*	0,00E+00	8,78E+04	1,14E+04	1,04E+05
IPI00127707	Poly(rC)-binding protein 2	0,00E+00	0,00E+00	1,11E+04	4,20E+04
IPI00169670	Aldose 1-epimerase	0,00E+00	0,00E+00	1,08E+04	0,00E+00
IPI00125861	Disks large homolog 1	0,00E+00	0,00E+00	9,91E+03	1,77E+04
IPI00136000	Alpha-adducin	0,00E+00	0,00E+00	5,97E+03	1,59E+04
IPI00670422	NHP2-like protein 1	0,00E+00	2,25E+04	0,00E+00	0,00E+00
IPI00316740	DNA damage-binding protein 1	0,00E+00	2,47E+04	0,00E+00	0,00E+00
IPI00308077	Ectonucleotide pyrophosphatase/phosphodiesterase family member 6	0,00E+00	3,32E+04	0,00E+00	0,00E+00
IPI00378156	Rab GTPase-activating protein 1	0,00E+00	1,99E+05	0,00E+00	0,00E+00
IPI00756257	Titin	0,00E+00	2,08E+05	0,00E+00	0,00E+00
IPI00420185	Epidermal growth factor receptor substrate 15-like 1	0,00E+00	0,00E+00	0,00E+00	2,65E+03
IPI00330649	Myosin IE	0,00E+00	0,00E+00	0,00E+00	5,28E+03
IPI00125180	Uncharacterized protein KIAA0564 homolog	0,00E+00	0,00E+00	0,00E+00	5,44E+03
IPI00653270	Non-receptor tyrosine-protein kinase TYK2	0,00E+00	0,00E+00	0,00E+00	7,12E+03
IPI00755993	Ankyrin-1	0,00E+00	0,00E+00	0,00E+00	8,82E+03
IPI00762919	Huntingtin-interacting protein 1	0,00E+00	0,00E+00	0,00E+00	9,99E+03
IPI00136618	Toll-interacting protein	0,00E+00	0,00E+00	0,00E+00	1,05E+04
IPI00319509	Aminopeptidase N	0,00E+00	0,00E+00	0,00E+00	1,22E+04
IPI00125658	Glutamate--cysteine ligase catalytic subunit	0,00E+00	0,00E+00	0,00E+00	1,31E+04
IPI00415385	Bcl-2-associated transcription factor 1	0,00E+00	0,00E+00	0,00E+00	1,34E+04
IPI00310059	Polymeric immunoglobulin receptor	0,00E+00	0,00E+00	0,00E+00	1,38E+04
IPI00454050	Transcription elongation factor SPT6	0,00E+00	0,00E+00	0,00E+00	1,50E+04
IPI00453820	Ankycorbin	0,00E+00	0,00E+00	0,00E+00	1,58E+04
IPI00319933	Protein kinase C and casein kinase II substrate protein 3	0,00E+00	0,00E+00	0,00E+00	1,64E+04
IPI00133801	SAP domain-containing ribonucleoprotein	0,00E+00	0,00E+00	0,00E+00	1,66E+04
IPI00125493	Myosin light chain kinase, smooth muscle	0,00E+00	0,00E+00	0,00E+00	1,69E+04
IPI00850983	Synaptojanin-1	0,00E+00	0,00E+00	0,00E+00	2,18E+04
IPI00109482	N(G),N(G)-dimethylarginine dimethylaminohydrolase 1	0,00E+00	0,00E+00	0,00E+00	2,19E+04
IPI00263048	Nuclear mitotic apparatus protein 1	0,00E+00	0,00E+00	0,00E+00	2,23E+04

		Average Intensities			
Protein ID	**Protein Name**	**NCD NaCl**	**HFD NaCl**	**NCD insulin**	**HFD insulin**
IPI00621024	B cell antigen receptor	0,00E+00	0,00E+00	0,00E+00	2,34E+04
IPI00120719	Cytochrome c oxidase subunit 5A, mitochondrial	0,00E+00	0,00E+00	0,00E+00	2,85E+04
IPI00127172	ATP-dependent RNA helicase DDX1	0,00E+00	1,53E+04	0,00E+00	2,90E+04
IPI00130409	Pre-mRNA-processing factor 6	0,00E+00	0,00E+00	0,00E+00	2,91E+04
IPI00221767	Nuclear pore complex protein Nup107	0,00E+00	0,00E+00	0,00E+00	3,05E+04
IPI00337844	E3 SUMO-protein ligase RanBP2	0,00E+00	0,00E+00	0,00E+00	3,47E+04
IPI00115257	PC4 and SFRS1-interacting protein	0,00E+00	0,00E+00	0,00E+00	3,64E+04
IPI00114232	Histone deacetylase 1	0,00E+00	0,00E+00	0,00E+00	3,80E+04
IPI00756386	Probable 2-oxoglutarate dehydrogenase E1 component DHKTD1, mitochondrial	0,00E+00	0,00E+00	0,00E+00	3,86E+04
IPI00323748	Erythrocyte band 7 integral membrane protein	0,00E+00	0,00E+00	0,00E+00	3,88E+04
IPI00266463	Serrate RNA effector molecule homolog	0,00E+00	0,00E+00	0,00E+00	4,22E+04
IPI00377930	THO complex subunit 7 homolog	0,00E+00	0,00E+00	0,00E+00	4,77E+04
IPI00659860	Leucine-rich repeat flightless-interacting protein 2	0,00E+00	0,00E+00	0,00E+00	4,85E+04
IPI00623284	Splicing factor 3B subunit 1	0,00E+00	0,00E+00	0,00E+00	5,28E+04
IPI00331342	WD40 repeat-containing protein SMU1	0,00E+00	0,00E+00	0,00E+00	5,51E+04
IPI00848926	Peptidyl-prolyl cis-trans isomerase H	0,00E+00	0,00E+00	0,00E+00	5,62E+04
IPI00459742	SWI/SNF complex subunit SMARCC2	0,00E+00	0,00E+00	0,00E+00	5,86E+04
IPI00420329	MKIAA0788 protein	0,00E+00	0,00E+00	0,00E+00	6,30E+04
IPI00128699	Small nuclear ribonucleoprotein-associated protein N	0,00E+00	0,00E+00	0,00E+00	9,58E+04
IPI00122011	Splicing factor 3B subunit 3	0,00E+00	1,58E+04	0,00E+00	1,21E+05
IPI00606760	Splicing factor arginine/serine-rich 4 (SRp75)	0,00E+00	0,00E+00	0,00E+00	2,15E+05

7 References

1. M. M. Finucane *et al.*, National, regional, and global trends in body-mass index since 1980: systematic analysis of health examination surveys and epidemiological studies with 960 country-years and 9.1 million participants. *Lancet* **377**, 557 (Feb 12, 2011).

2. WHO, “Obesity and overweight, WHO fact sheet N°311” (2011).

3. G. B. Mensink, T. Lampert, E. Bergmann, [Overweight and obesity in Germany 1984-2003]. *Bundesgesundheitsblatt Gesundheitsforschung Gesundheitsschutz* **48**, 1348 (Dec, 2005).

4. S. Yusuf *et al.*, Obesity and the risk of myocardial infarction in 27,000 participants from 52 countries: a case-control study. *Lancet* **366**, 1640 (Nov 5, 2005).

5. G. A. Bray, Medical consequences of obesity. *J Clin Endocrinol Metab* **89**, 2583 (Jun 8, 2004).

6. K. Nanchahal, J. N. Morris, L. M. Sullivan, P. W. Wilson, Coronary heart disease risk in men and the epidemic of overweight and obesity. *Int J Obes (Lond)* **29**, 317 (Mar, 2005).

7. T. Kurth *et al.*, Body mass index and the risk of stroke in men. *Arch Intern Med* **162**, 2557 (Dec 9-23, 2002).

8. J. B. Dixon, The effect of obesity on health outcomes. *Mol Cell Endocrinol* **316**, 104 (Mar 25, 2010).

9. A. Peeters *et al.*, Obesity in adulthood and its consequences for life expectancy: a life-table analysis. *Ann Intern Med* **138**, 24 (Jan 7, 2003).

10. E. E. Calle, M. J. Thun, J. M. Petrelli, C. Rodriguez, C. W. Heath, Jr., Body-mass index and mortality in a prospective cohort of U.S. adults. *N Engl J Med* **341**, 1097 (Oct 7, 1999).

11. J. E. Manson *et al.*, Body weight and mortality among women. *N Engl J Med* **333**, 677 (Sep 14, 1995).

12. J. O. Hill, J. C. Peters, Environmental contributions to the obesity epidemic. *Science* **280**, 1371 (May 29, 1998).

13. S. O'Rahilly, Leptin: defining its role in humans by the clinical study of genetic disorders. *Nutr Rev* **60**, S30 (Oct, 2002).

14. G. S. Barsh, I. S. Farooqi, S. O'Rahilly, Genetics of body-weight regulation. *Nature* **404**, 644 (Apr 6, 2000).

15. I. S. Farooqi *et al.*, Dominant and recessive inheritance of morbid obesity associated with melanocortin 4 receptor deficiency. *J Clin Invest* **106**, 271 (Jul, 2000).

16. B. C. Martin *et al.*, Role of glucose and insulin resistance in development of type 2 diabetes mellitus: results of a 25-year follow-up study. *Lancet* **340**, 925 (Oct 17, 1992).

17. C. Heidemann, L. Kroll, A. Icks, T. Lampert, C. Scheidt-Nave, Prevalence of known diabetes in German adults aged 25-69 years: results from national health surveys over 15 years. *Diabet Med* **26**, 655 (Jun, 2009).

18. WHO, “Diabetes, WHO fact sheet N°312” (2011).

19. S. Wild, G. Roglic, A. Green, R. Sicree, H. King, Global prevalence of diabetes: estimates for the year 2000 and projections for 2030. *Diabetes Care* **27**, 1047 (May, 2004).

20. H. Kolb, T. Mandrup-Poulsen, The global diabetes epidemic as a consequence of lifestyle-induced low-grade inflammation. *Diabetologia* **53**, 10 (Jan, 2010).

21. M. A. Atkinson, N. K. Maclaren, The pathogenesis of insulin-dependent diabetes mellitus. *N Engl J Med* **331**, 1428 (Nov 24, 1994).

22. Daten und Fakten: Ergebnisse der Studie "Gesundheit in Deutschland aktuell 2009". *Robert-Koch-Institut, Berlin* **ISBN 978-3-89606-206-2**, (2011).

23. S. Lillioja *et al.*, Insulin resistance and insulin secretory dysfunction as precursors of non-insulin-dependent diabetes mellitus. Prospective studies of Pima Indians. *N Engl J Med* **329**, 1988 (Dec 30, 1993).

24. R. K. Campbell, Fate of the beta-cell in the pathophysiology of type 2 diabetes. *J Am Pharm Assoc (2003)* **49 Suppl 1**, S10 (Sep-Oct, 2009).

25. M. Prentki, C. J. Nolan, Islet beta cell failure in type 2 diabetes. *J Clin Invest* **116**, 1802 (Jul, 2006).

26. A. R. Saltiel, New perspectives into the molecular pathogenesis and treatment of type 2 diabetes. *Cell* **104**, 517 (Feb 23, 2001).

27. G. M. Reaven, Insulin-independent diabetes mellitus: metabolic characteristics. *Metabolism* **29**, 445 (May, 1980).

28. S. I. Taylor, Deconstructing type 2 diabetes. *Cell* **97**, 9 (Apr 2, 1999).

29. I. Shai *et al.*, Weight loss with a low-carbohydrate, Mediterranean, or low-fat diet. *N Engl J Med* **359**, 229 (Jul 17, 2008).

30. T. Church, Exercise in obesity, metabolic syndrome, and diabetes. *Prog Cardiovasc Dis* **53**, 412 (May-Jun, 2011).

31. O. Pedersen, H. Beck-Nielsen, L. Heding, Increased insulin receptors after exercise in patients with insulin-dependent diabetes mellitus. *N Engl J Med* **302**, 886 (Apr 17, 1980).

32. B. R. Zimmerman, Sulfonylureas. *Endocrinol Metab Clin North Am* **26**, 511 (Sep, 1997).

33. W. L. Bennett *et al.*, Comparative effectiveness and safety of medications for type 2 diabetes: an update including new drugs and 2-drug combinations. *Ann Intern Med* **154**, 602 (May 3, 2011).

34. R. S. Hundal *et al.*, Mechanism by which metformin reduces glucose production in type 2 diabetes. *Diabetes* **49**, 2063 (Dec, 2000).

35. D. F. Steiner, D. E. James, Cellular and molecular biology of the beta cell. *Diabetologia* **35 Suppl 2**, S41 (Dec, 1992).

36. F. M. Ashcroft, K(ATP) channels and insulin secretion: a key role in health and disease. *Biochem Soc Trans* **34**, 243 (Apr, 2006).

37. E. M. Bailyes *et al.*, Insulin receptor/IGF-I receptor hybrids are widely distributed in mammalian tissues: quantification of individual receptor species by selective immunoprecipitation and immunoblotting. *Biochem J* **327 (Pt 1)**, 209 (Oct 1, 1997).

38. P. R. Shepherd, B. B. Kahn, Glucose transporters and insulin action--implications for insulin resistance and diabetes mellitus. *N Engl J Med* **341**, 248 (Jul 22, 1999).

39. A. Klip, M. R. Paquet, Glucose transport and glucose transporters in muscle and their metabolic regulation. *Diabetes Care* **13**, 228 (Mar, 1990).

40. G. Sesti, Pathophysiology of insulin resistance. *Best Pract Res Clin Endocrinol Metab* **20**, 665 (Dec, 2006).

41. S. A. Kaplan, The insulin receptor. *J Pediatr* **104**, 327 (Mar, 1984).

42. A. R. Saltiel, C. R. Kahn, Insulin signalling and the regulation of glucose and lipid metabolism. *Nature* **414**, 799 (Dec 13, 2001).

43. E. M. Wright, E. Turk, B. Zabel, S. Mundlos, J. Dyer, Molecular genetics of intestinal glucose transport. *J Clin Invest* **88**, 1435 (Nov, 1991).

44. C. Nye, J. Kim, S. C. Kalhan, R. W. Hanson, Reassessing triglyceride synthesis in adipose tissue. *Trends Endocrinol Metab* **19**, 356 (Dec, 2008).

45. M. Bluher *et al.*, Adipose tissue selective insulin receptor knockout protects against obesity and obesity-related glucose intolerance. *Dev Cell* **3**, 25 (Jul, 2002).

46. D. K. Sindelar *et al.*, The role of fatty acids in mediating the effects of peripheral insulin on hepatic glucose production in the conscious dog. *Diabetes* **46**, 187 (Feb, 1997).

47. M. Pendergrass *et al.*, Insulin-induced hexokinase II expression is reduced in obesity and NIDDM. *Diabetes* **47**, 387 (Mar, 1998).

48. J. Jensen, Y. C. Lai, Regulation of muscle glycogen synthase phosphorylation and kinetic properties by insulin, exercise, adrenaline and role in insulin resistance. *Arch Physiol Biochem* **115**, 13 (Feb, 2009).

49. J. Jensen *et al.*, Muscle glycogen inharmoniously regulates glycogen synthase activity, glucose uptake, and proximal insulin signaling. *Am J Physiol Endocrinol Metab* **290**, E154 (Jan, 2006).

50. T. H. Claus, S. J. Pilkis, Regulation by insulin of gluconeogenesis in isolated rat hepatocytes. *Biochim Biophys Acta* **421**, 246 (Feb 24, 1976).

51. J. Terrettaz, F. Assimacopoulos-Jeannet, B. Jeanrenaud, Inhibition of hepatic glucose production by insulin in vivo in rats: contribution of glycolysis. *Am J Physiol* **250**, E346 (Apr, 1986).

52. F. J. Bedoya, F. M. Matschinsky, T. Shimizu, J. J. O'Neil, M. C. Appel, Differential regulation of glucokinase activity in pancreatic islets and liver of the rat. *J Biol Chem* **261**, 10760 (Aug 15, 1986).

53. K. Ito *et al.*, Exogenous insulin dose-dependently suppresses glucopenia-induced glucagon secretion from perfused rat pancreas. *Metabolism* **44**, 358 (Mar, 1995).

54. R. W. Stevenson, P. E. Williams, A. D. Cherrington, Role of glucagon suppression on gluconeogenesis during insulin treatment of the conscious diabetic dog. *Diabetologia* **30**, 782 (Oct, 1987).

55. A. D. Cherrington, The role of hepatic insulin receptors in the regulation of glucose production. *J Clin Invest* **115**, 1136 (May, 2005).

56. D. K. Sindelar *et al.*, Basal hepatic glucose production is regulated by the portal vein insulin concentration. *Diabetes* **47**, 523 (Apr, 1998).

57. A. C. Konner, T. Klockener, J. C. Bruning, Control of energy homeostasis by insulin and leptin: targeting the arcuate nucleus and beyond. *Physiol Behav* **97**, 632 (Jul 14, 2009).

58. M. Kasuga, J. A. Hedo, K. M. Yamada, C. R. Kahn, The structure of insulin receptor and its subunits. Evidence for multiple nonreduced forms and a 210,000 possible proreceptor. *J Biol Chem* **257**, 10392 (Sep 10, 1982).

59. M. P. Czech, The nature and regulation of the insulin receptor: structure and function. *Annu Rev Physiol* **47**, 357 (1985).

60. O. M. Rosen, After insulin binds. *Science* **237**, 1452 (Sep 18, 1987).

61. J. M. Backer, C. Wjasow, Y. Zhang, In vitro binding and phosphorylation of insulin receptor substrate 1 by the insulin receptor. Role of interactions mediated by the phosphotyrosine-binding domain and the pleckstrin-homology domain. *Eur J Biochem* **245**, 91 (Apr 1, 1997).

62. P. van der Geer, T. Pawson, The PTB domain: a new protein module implicated in signal transduction. *Trends Biochem Sci* **20**, 277 (Jul, 1995).

63. M. G. Myers, Jr., M. F. White, Insulin signal transduction and the IRS proteins. *Annu Rev Pharmacol Toxicol* **36**, 615 (1996).

64. A. R. Jacobs, D. LeRoith, S. I. Taylor, Insulin receptor substrate-1 pleckstrin homology and phosphotyrosine-binding domains are both involved in plasma membrane targeting. *J Biol Chem* **276**, 40795 (Nov 2, 2001).

65. M. G. Myers, Jr., X. J. Sun, M. F. White, The IRS-1 signaling system. *Trends Biochem Sci* **19**, 289 (Jul, 1994).

66. M. G. Myers, Jr. *et al.*, IRS-1 activates phosphatidylinositol 3'-kinase by associating with src homology 2 domains of p85. *Proc Natl Acad Sci U S A* **89**, 10350 (Nov 1, 1992).

67. L. C. Cantley, The phosphoinositide 3-kinase pathway. *Science* **296**, 1655 (May 31, 2002).

68. G. L'Allemain, Deciphering the MAP kinase pathway. *Prog Growth Factor Res* **5**, 291 (1994).

69. C. J. Marshall, MAP kinase kinase kinase, MAP kinase kinase and MAP kinase. *Curr Opin Genet Dev* **4**, 82 (Feb, 1994).

70. J. M. Backer *et al.*, Phosphatidylinositol 3'-kinase is activated by association with IRS-1 during insulin stimulation. *Embo J* **11**, 3469 (Sep, 1992).

71. A. Toker, Phosphoinositides and signal transduction. *Cell Mol Life Sci* **59**, 761 (May, 2002).

72. D. R. Alessi, P. Cohen, Mechanism of activation and function of protein kinase B. *Curr Opin Genet Dev* **8**, 55 (Feb, 1998).

73. B. Cheatham, C. R. Kahn, Insulin action and the insulin signaling network. *Endocr Rev* **16**, 117 (Apr, 1995).

74. Y. Li *et al.*, Protein kinase C Theta inhibits insulin signaling by phosphorylating IRS1 at Ser(1101). *J Biol Chem* **279**, 45304 (Oct 29, 2004).

75. F. Oriente *et al.*, Protein kinase C-alpha regulates insulin action and degradation by interacting with insulin receptor substrate-1 and 14-3-3 epsilon. *J Biol Chem* **280**, 40642 (Dec 9, 2005).

76. E. Y. Skolnik *et al.*, The function of GRB2 in linking the insulin receptor to Ras signaling pathways. *Science* **260**, 1953 (Jun 25, 1993).

77. E. Y. Skolnik *et al.*, The SH2/SH3 domain-containing protein GRB2 interacts with tyrosine-phosphorylated IRS1 and Shc: implications for insulin control of ras signalling. *Embo J* **12**, 1929 (May, 1993).

78. D. F. Lazar *et al.*, Mitogen-activated protein kinase kinase inhibition does not block the stimulation of glucose utilization by insulin. *J Biol Chem* **270**, 20801 (Sep 1, 1995).

79. T. G. Boulton *et al.*, ERKs: a family of protein-serine/threonine kinases that are activated and tyrosine phosphorylated in response to insulin and NGF. *Cell* **65**, 663 (May 17, 1991).

80. H. Zaid, C. N. Antonescu, V. K. Randhawa, A. Klip, Insulin action on glucose transporters through molecular switches, tracks and tethers. *Biochem J* **413**, 201 (Jul 15, 2008).

81. S. Huang, M. P. Czech, The GLUT4 glucose transporter. *Cell Metab* **5**, 237 (Apr, 2007).

82. D. Cai, S. Dhe-Paganon, P. A. Melendez, J. Lee, S. E. Shoelson, Two new substrates in insulin signaling, IRS5/DOK4 and IRS6/DOK5. *J Biol Chem* **278**, 25323 (Jul 11, 2003).

83. S. G. Gray *et al.*, Transcriptional regulation of IRS5/DOK4 expression in non-small-cell lung cancer cells. *Clin Lung Cancer* **9**, 367 (Nov, 2008).

84. C. Chakraborty, G. Agoramoorthy, M. J. Hsu, Exploring the evolutionary relationship of insulin receptor substrate family using computational biology. *PLoS One* **6**, e16580 (2011).

85. A. C. Thirone, C. Huang, A. Klip, Tissue-specific roles of IRS proteins in insulin signaling and glucose transport. *Trends Endocrinol Metab* **17**, 72 (Mar, 2006).

86. D. Sawka-Verhelle, S. Tartare-Deckert, M. F. White, E. Van Obberghen, Insulin receptor substrate-2 binds to the insulin receptor through its phosphotyrosine-binding domain and through a newly identified domain comprising amino acids 591-786. *J Biol Chem* **271**, 5980 (Mar 15, 1996).

87. H. Tamemoto *et al.*, Insulin resistance syndrome in mice deficient in insulin receptor substrate-1. *Ann N Y Acad Sci* **827**, 85 (Sep 20, 1997).

88. E. Araki *et al.*, Alternative pathway of insulin signalling in mice with targeted disruption of the IRS-1 gene. *Nature* **372**, 186 (Nov 10, 1994).

89. D. J. Withers *et al.*, Disruption of IRS-2 causes type 2 diabetes in mice. *Nature* **391**, 900 (Feb 26, 1998).

90. Y. Kido *et al.*, Tissue-specific insulin resistance in mice with mutations in the insulin receptor, IRS-1, and IRS-2. *J Clin Invest* **105**, 199 (Jan, 2000).

91. T. Ogihara *et al.*, Insulin receptor substrate (IRS)-2 is dephosphorylated more rapidly than IRS-1 via its association with phosphatidylinositol 3-kinase in skeletal muscle cells. *J Biol Chem* **272**, 12868 (May 9, 1997).

92. S. F. Previs, D. J. Withers, J. M. Ren, M. F. White, G. I. Shulman, Contrasting effects of IRS-1 versus IRS-2 gene disruption on carbohydrate and lipid metabolism in vivo. *J Biol Chem* **275**, 38990 (Dec 15, 2000).

93. C. M. Taniguchi, K. Ueki, R. Kahn, Complementary roles of IRS-1 and IRS-2 in the hepatic regulation of metabolism. *J Clin Invest* **115**, 718 (Mar, 2005).

94. R. A. Haeusler, D. Accili, The double life of Irs. *Cell Metab* **8**, 7 (Jul, 2008).

95. S. Sciacchitano, S. I. Taylor, Cloning, tissue expression, and chromosomal localization of the mouse IRS-3 gene. *Endocrinology* **138**, 4931 (Nov, 1997).

96. V. R. Fantin, Q. Wang, G. E. Lienhard, S. R. Keller, Mice lacking insulin receptor substrate 4 exhibit mild defects in growth, reproduction, and glucose homeostasis. *Am J Physiol Endocrinol Metab* **278**, E127 (Jan, 2000).

97. S. R. Keller, L. Lamphere, B. E. Lavan, M. R. Kuhne, G. E. Lienhard, Insulin and IGF-I signaling through the insulin receptor substrate 1. *Mol Reprod Dev* **35**, 346 (Aug, 1993).

98. D. LeRoith *et al.*, Insulin-like growth factors. *Biol Signals* **1**, 173 (Jul-Aug, 1992).

99. J. F. Tanti, J. Jager, Cellular mechanisms of insulin resistance: role of stress-regulated serine kinases and insulin receptor substrates (IRS) serine phosphorylation. *Curr Opin Pharmacol* **9**, 753 (Dec, 2009).

100. P. Gual, Y. Le Marchand-Brustel, J. F. Tanti, Positive and negative regulation of insulin signaling through IRS-1 phosphorylation. *Biochimie* **87**, 99 (Jan, 2005).

101. S. Boura-Halfon, Y. Zick, Phosphorylation of IRS proteins, insulin action, and insulin resistance. *Am J Physiol Endocrinol Metab* **296**, E581 (Apr, 2009).

102. C. Weigert *et al.*, The phosphorylation of Ser318 of insulin receptor substrate 1 is not per se inhibitory in skeletal muscle cells but is necessary to trigger the attenuation of the insulin-stimulated signal. *J Biol Chem* **280**, 37393 (Nov 11, 2005).

103. C. Weigert *et al.*, Interplay and effects of temporal changes in the phosphorylation state of serine-302, -307, and -318 of insulin receptor substrate-1 on insulin action in skeletal muscle cells. *Mol Endocrinol* **22**, 2729 (Dec, 2008).

104. Y. Zick, Ser/Thr phosphorylation of IRS proteins: a molecular basis for insulin resistance. *Sci STKE* **2005**, pe4 (Jan 25, 2005).

105. G. S. Hotamisligil, N. S. Shargill, B. M. Spiegelman, Adipose expression of tumor necrosis factor-alpha: direct role in obesity-linked insulin resistance. *Science* **259**, 87 (Jan 1, 1993).

106. A. L. Swislocki, Y. D. Chen, A. Golay, M. O. Chang, G. M. Reaven, Insulin suppression of plasma-free fatty acid concentration in normal individuals and patients with type 2 (non-insulin-dependent) diabetes. *Diabetologia* **30**, 622 (Aug, 1987).

107. G. M. Reaven, Y. D. Chen, Role of abnormal free fatty acid metabolism in the development of non-insulin-dependent diabetes mellitus. *Am J Med* **85**, 106 (Nov 28, 1988).

108. G. Camussi, E. Albano, C. Tetta, F. Bussolino, The molecular action of tumor necrosis factor-alpha. *Eur J Biochem* **202**, 3 (Nov 15, 1991).

109. B. B. Aggarwal, Tumour necrosis factors receptor associated signalling molecules and their role in activation of apoptosis, JNK and NF-kappaB. *Ann Rheum Dis* **59 Suppl 1**, i6 (Nov, 2000).

110. K. E. Wellen, G. S. Hotamisligil, Inflammation, stress, and diabetes. *J Clin Invest* **115**, 1111 (May, 2005).

111. V. Aguirre, T. Uchida, L. Yenush, R. Davis, M. F. White, The c-Jun NH(2)-terminal kinase promotes insulin resistance during association with insulin receptor substrate-1 and phosphorylation of Ser(307). *J Biol Chem* **275**, 9047 (Mar 24, 2000).

112. Z. Gao *et al.*, Serine phosphorylation of insulin receptor substrate 1 by inhibitor kappa B kinase complex. *J Biol Chem* **277**, 48115 (Dec 13, 2002).

113. J. M. Zabolotny *et al.*, Protein-tyrosine phosphatase 1B expression is induced by inflammation in vivo. *J Biol Chem* **283**, 14230 (May 23, 2008).

114. N. Dube, M. L. Tremblay, Involvement of the small protein tyrosine phosphatases TC-PTP and PTP1B in signal transduction and diseases: from diabetes, obesity to cell cycle, and cancer. *Biochim Biophys Acta* **1754**, 108 (Dec 30, 2005).

115. A. Bourdeau, N. Dube, M. L. Tremblay, Cytoplasmic protein tyrosine phosphatases, regulation and function: the roles of PTP1B and TC-PTP. *Curr Opin Cell Biol* **17**, 203 (Apr, 2005).

116. B. J. Goldstein, A. Bittner-Kowalczyk, M. F. White, M. Harbeck, Tyrosine dephosphorylation and deactivation of insulin receptor substrate-1 by protein-tyrosine phosphatase 1B. Possible facilitation by the formation of a ternary complex with the Grb2 adaptor protein. *J Biol Chem* **275**, 4283 (Feb 11, 2000).

117. M. R. Calera, G. Vallega, P. F. Pilch, Dynamics of protein-tyrosine phosphatases in rat adipocytes. *J Biol Chem* **275**, 6308 (Mar 3, 2000).

118. J. P. Bastard *et al.*, Adipose tissue IL-6 content correlates with resistance to insulin activation of glucose uptake both in vivo and in vitro. *J Clin Endocrinol Metab* **87**, 2084 (May, 2002).

119. R. Deepa *et al.*, Serum levels of interleukin 6, C-reactive protein, vascular cell adhesion molecule 1, and monocyte chemotactic protein 1 in relation to insulin resistance and glucose intolerance--the Chennai Urban Rural Epidemiology Study (CURES). *Metabolism* **55**, 1232 (Sep, 2006).

120. V. Rotter, I. Nagaev, U. Smith, Interleukin-6 (IL-6) induces insulin resistance in 3T3-L1 adipocytes and is, like IL-8 and tumor necrosis factor-alpha,

overexpressed in human fat cells from insulin-resistant subjects. *J Biol Chem* **278**, 45777 (Nov 14, 2003).

121. C. E. Juge-Aubry *et al.*, Adipose tissue is a major source of interleukin-1 receptor antagonist: upregulation in obesity and inflammation. *Diabetes* **52**, 1104 (May, 2003).

122. M. Straczkowski *et al.*, Plasma interleukin-8 concentrations are increased in obese subjects and related to fat mass and tumor necrosis factor-alpha system. *J Clin Endocrinol Metab* **87**, 4602 (Oct, 2002).

123. P. Sartipy, D. J. Loskutoff, Monocyte chemoattractant protein 1 in obesity and insulin resistance. *Proc Natl Acad Sci U S A* **100**, 7265 (Jun 10, 2003).

124. C. J. Carlson, M. F. White, C. M. Rondinone, Mammalian target of rapamycin regulates IRS-1 serine 307 phosphorylation. *Biochem Biophys Res Commun* **316**, 533 (Apr 2, 2004).

125. P. Gual, T. Gremeaux, T. Gonzalez, Y. Le Marchand-Brustel, J. F. Tanti, MAP kinases and mTOR mediate insulin-induced phosphorylation of insulin receptor substrate-1 on serine residues 307, 612 and 632. *Diabetologia* **46**, 1532 (Nov, 2003).

126. R. Nawaratne *et al.*, Regulation of insulin receptor substrate 1 pleckstrin homology domain by protein kinase C: role of serine 24 phosphorylation. *Mol Endocrinol* **20**, 1838 (Aug, 2006).

127. J. A. Kim *et al.*, Phosphorylation of Ser24 in the pleckstrin homology domain of insulin receptor substrate-1 by Mouse Pelle-like kinase/interleukin-1 receptor-associated kinase: cross-talk between inflammatory signaling and insulin signaling that may contribute to insulin resistance. *J Biol Chem* **280**, 23173 (Jun 17, 2005).

128. G. Solinas, W. Naugler, F. Galimi, M. S. Lee, M. Karin, Saturated fatty acids inhibit induction of insulin gene transcription by JNK-mediated phosphorylation of insulin-receptor substrates. *Proc Natl Acad Sci U S A* **103**, 16454 (Oct 31, 2006).

129. H. Sharfi, H. Eldar-Finkelman, Sequential phosphorylation of insulin receptor substrate-2 by glycogen synthase kinase-3 and c-Jun NH2-terminal kinase plays a role in hepatic insulin signaling. *Am J Physiol Endocrinol Metab* **294**, E307 (Feb, 2008).

130. T. Geetha *et al.*, Label-free proteomic identification of endogenous, insulin-stimulated interaction partners of insulin receptor substrate-1. *J Am Soc Mass Spectrom* **22**, 457 (Mar, 2011).

131. P. Langlais, L. J. Mandarino, Z. Yi, Label-free relative quantification of co-eluting isobaric phosphopeptides of insulin receptor substrate-1 by HPLC-ESI-MS/MS. *J Am Soc Mass Spectrom* **21**, 1490 (Sep, 2010).

132. M. Kruger *et al.*, Dissection of the insulin signaling pathway via quantitative phosphoproteomics. *Proc Natl Acad Sci U S A* **105**, 2451 (Feb 19, 2008).

133. S. Hanke, M. Mann, The phosphotyrosine interactome of the insulin receptor family and its substrates IRS-1 and IRS-2. *Mol Cell Proteomics* **8**, 519 (Mar, 2009).

134. R. S. Haltiwanger, M. A. Blomberg, G. W. Hart, Glycosylation of nuclear and cytoplasmic proteins. Purification and characterization of a uridine diphospho-N-acetylglucosamine:polypeptide beta-N-acetylglucosaminyltransferase. *J Biol Chem* **267**, 9005 (May 5, 1992).

135. Y. Gao, L. Wells, F. I. Comer, G. J. Parker, G. W. Hart, Dynamic O-glycosylation of nuclear and cytosolic proteins: cloning and characterization of a neutral, cytosolic beta-N-acetylglucosaminidase from human brain. *J Biol Chem* **276**, 9838 (Mar 30, 2001).

136. N. E. Zachara, G. W. Hart, Cell signaling, the essential role of O-GlcNAc! *Biochim Biophys Acta* **1761**, 599 (May-Jun, 2006).

137. S. Marshall, V. Bacote, R. R. Traxinger, Discovery of a metabolic pathway mediating glucose-induced desensitization of the glucose transport system. Role of hexosamine biosynthesis in the induction of insulin resistance. *J Biol Chem* **266**, 4706 (Mar 15, 1991).

138. M. G. Buse, Hexosamines, insulin resistance, and the complications of diabetes: current status. *Am J Physiol Endocrinol Metab* **290**, E1 (Jan, 2006).

139. D. A. Fryburg, L. A. Jahn, S. A. Hill, D. M. Oliveras, E. J. Barrett, Insulin and insulin-like growth factor-I enhance human skeletal muscle protein anabolism during hyperaminoacidemia by different mechanisms. *J Clin Invest* **96**, 1722 (Oct, 1995).

140. R. G. Bennett, F. G. Hamel, W. C. Duckworth, Insulin inhibits the ubiquitin-dependent degrading activity of the 26S proteasome. *Endocrinology* **141**, 2508 (Jul, 2000).

141. R. Zhande, J. J. Mitchell, J. Wu, X. J. Sun, Molecular mechanism of insulin-induced degradation of insulin receptor substrate 1. *Mol Cell Biol* **22**, 1016 (Feb, 2002).

142. X. J. Sun, J. L. Goldberg, L. Y. Qiao, J. J. Mitchell, Insulin-induced insulin receptor substrate-1 degradation is mediated by the proteasome degradation pathway. *Diabetes* **48**, 1359 (Jul, 1999).

143. A. M. Johnston, L. Pirola, E. Van Obberghen, Molecular mechanisms of insulin receptor substrate protein-mediated modulation of insulin signalling. *FEBS Lett* **546**, 32 (Jul 3, 2003).

144. L. Rui, M. Yuan, D. Frantz, S. Shoelson, M. F. White, SOCS-1 and SOCS-3 block insulin signaling by ubiquitin-mediated degradation of IRS1 and IRS2. *J Biol Chem* **277**, 42394 (Nov 1, 2002).

145. K. Ueki, T. Kondo, Y. H. Tseng, C. R. Kahn, Central role of suppressors of cytokine signaling proteins in hepatic steatosis, insulin resistance, and the

metabolic syndrome in the mouse. *Proc Natl Acad Sci U S A* **101**, 10422 (Jul 13, 2004).

146. D. N. Gross, M. Wan, M. J. Birnbaum, The role of FOXO in the regulation of metabolism. *Curr Diab Rep* **9**, 208 (Jun, 2009).

147. L. P. Van Der Heide, M. F. Hoekman, M. P. Smidt, The ins and outs of FoxO shuttling: mechanisms of FoxO translocation and transcriptional regulation. *Biochem J* **380**, 297 (Jun 1, 2004).

148. J. Nakae, V. Barr, D. Accili, Differential regulation of gene expression by insulin and IGF-1 receptors correlates with phosphorylation of a single amino acid residue in the forkhead transcription factor FKHR. *Embo J* **19**, 989 (Mar 1, 2000).

149. A. Brunet *et al.*, Akt promotes cell survival by phosphorylating and inhibiting a Forkhead transcription factor. *Cell* **96**, 857 (Mar 19, 1999).

150. D. Schmoll *et al.*, Regulation of glucose-6-phosphatase gene expression by protein kinase Balpha and the forkhead transcription factor FKHR. Evidence for insulin response unit-dependent and -independent effects of insulin on promoter activity. *J Biol Chem* **275**, 36324 (Nov 17, 2000).

151. R. K. Hall *et al.*, Regulation of phosphoenolpyruvate carboxykinase and insulin-like growth factor-binding protein-1 gene expression by insulin. The role of winged helix/forkhead proteins. *J Biol Chem* **275**, 30169 (Sep 29, 2000).

152. O. Puig, R. Tjian, Transcriptional feedback control of insulin receptor by dFOXO/FOXO1. *Genes Dev* **19**, 2435 (Oct 15, 2005).

153. S. D. Jordan *et al.*, Obesity-induced overexpression of miRNA-143 inhibits insulin-stimulated AKT activation and impairs glucose metabolism. *Nat Cell Biol* **13**, 434 (Apr, 2011).

154. D. E. Moller, A. Yokota, M. F. White, A. G. Pazianos, J. S. Flier, A naturally occurring mutation of insulin receptor alanine 1134 impairs tyrosine kinase function and is associated with dominantly inherited insulin resistance. *J Biol Chem* **265**, 14979 (Sep 5, 1990).

155. D. Accili *et al.*, Early neonatal death in mice homozygous for a null allele of the insulin receptor gene. *Nat Genet* **12**, 106 (Jan, 1996).

156. R. L. Joshi *et al.*, Targeted disruption of the insulin receptor gene in the mouse results in neonatal lethality. *Embo J* **15**, 1542 (Apr 1, 1996).

157. G. A. Hitman *et al.*, Insulin receptor substrate-1 gene mutations in NIDDM; implications for the study of polygenic disease. *Diabetologia* **38**, 481 (Apr, 1995).

158. A. J. McGettrick, E. P. Feener, C. R. Kahn, Human insulin receptor substrate-1 (IRS-1) polymorphism G972R causes IRS-1 to associate with the insulin

receptor and inhibit receptor autophosphorylation. *J Biol Chem* **280**, 6441 (Feb 25, 2005).

159. J. C. Bruning *et al.*, Development of a novel polygenic model of NIDDM in mice heterozygous for IR and IRS-1 null alleles. *Cell* **88**, 561 (Feb 21, 1997).

160. S. George *et al.*, A family with severe insulin resistance and diabetes due to a mutation in AKT2. *Science* **304**, 1325 (May 28, 2004).

161. H. Cho *et al.*, Insulin resistance and a diabetes mellitus-like syndrome in mice lacking the protein kinase Akt2 (PKB beta). *Science* **292**, 1728 (Jun 1, 2001).

162. P. Froguel *et al.*, Close linkage of glucokinase locus on chromosome 7p to early-onset non-insulin-dependent diabetes mellitus. *Nature* **356**, 162 (Mar 12, 1992).

163. P. Froguel *et al.*, Familial hyperglycemia due to mutations in glucokinase. Definition of a subtype of diabetes mellitus. *N Engl J Med* **328**, 697 (Mar 11, 1993).

164. O. Pedersen, Genetics of insulin resistance. *Exp Clin Endocrinol Diabetes* **107**, 113 (1999).

165. D. LeRoith, O. Gavrilova, Mouse models created to study the pathophysiology of Type 2 diabetes. *Int J Biochem Cell Biol* **38**, 904 (2006).

166. C.-O. Andersson, Mass spectrometric studies on amino acid and peptide derivatives. *Acta Chemica Scandinavica* **12**, 1353 (1958).

167. A. Pandey, M. Mann, Proteomics to study genes and genomes. *Nature* **405**, 837 (Jun 15, 2000).

168. R. Aebersold, M. Mann, Mass spectrometry-based proteomics. *Nature* **422**, 198 (Mar 13, 2003).

169. K. Schmelzle, S. Kane, S. Gridley, G. E. Lienhard, F. M. White, Temporal dynamics of tyrosine phosphorylation in insulin signaling. *Diabetes* **55**, 2171 (Aug, 2006).

170. B. Brizzard, Epitope tagging. *Biotechniques* **44**, 693 (Apr, 2008).

171. O. H. Laitinen, V. P. Hytonen, H. R. Nordlund, M. S. Kulomaa, Genetically engineered avidins and streptavidins. *Cell Mol Life Sci* **63**, 2992 (Dec, 2006).

172. A. D. Keefe, D. S. Wilson, B. Seelig, J. W. Szostak, One-step purification of recombinant proteins using a nanomolar-affinity streptavidin-binding peptide, the SBP-Tag. *Protein Expr Purif* **23**, 440 (Dec, 2001).

173. G. Rigaut *et al.*, A generic protein purification method for protein complex characterization and proteome exploration. *Nat Biotechnol* **17**, 1030 (Oct, 1999).

174. T. Burckstummer *et al.*, An efficient tandem affinity purification procedure for interaction proteomics in mammalian cells. *Nat Methods* **3**, 1013 (Dec, 2006).

175. R. Drakas, M. Prisco, R. Baserga, A modified tandem affinity purification tag technique for the purification of protein complexes in mammalian cells. *Proteomics* **5**, 132 (Jan, 2005).

176. C. J. Gloeckner, K. Boldt, A. Schumacher, R. Roepman, M. Ueffing, A novel tandem affinity purification strategy for the efficient isolation and characterisation of native protein complexes. *Proteomics* **7**, 4228 (Dec, 2007).

177. Y. Li, S. Franklin, M. J. Zhang, T. M. Vondriska, Highly efficient purification of protein complexes from mammalian cells using a novel streptavidin-binding peptide and hexahistidine tandem tag system: application to Bruton's tyrosine kinase. *Protein Sci* **20**, 140 (Jan, 2011).

178. T. Maniatis, E. F. Fritsch, J. Sambrook, *Molecular cloning : a laboratory manual*. (Cold Spring Harbor Laboratory, Cold Spring Harbor, N.Y., 1982), pp. x, 545 p.

179. F. Sanger, S. Nicklen, A. R. Coulson, DNA sequencing with chain-terminating inhibitors. *Proc Natl Acad Sci U S A* **74**, 5463 (Dec, 1977).

180. P. O. Angrand, N. Daigle, F. van der Hoeven, H. R. Scholer, A. F. Stewart, Simplified generation of targeting constructs using ET recombination. *Nucleic Acids Res* **27**, e16 (Sep 1, 1999).

181. J. P. Muyrers, Y. Zhang, G. Testa, A. F. Stewart, Rapid modification of bacterial artificial chromosomes by ET-recombination. *Nucleic Acids Res* **27**, 1555 (Mar 15, 1999).

182. A. C. Chang, S. N. Cohen, Construction and characterization of amplifiable multicopy DNA cloning vehicles derived from the P15A cryptic miniplasmid. *J Bacteriol* **134**, 1141 (Jun, 1978).

183. P. Chomczynski, P. K. Qasba, Alkaline transfer of DNA to plastic membrane. *Biochem Biophys Res Commun* **122**, 340 (Jul 18, 1984).

184. X. Mao, Y. Fujiwara, S. H. Orkin, Improved reporter strain for monitoring Cre recombinase-mediated DNA excisions in mice. *Proc Natl Acad Sci U S A* **96**, 5037 (Apr 27, 1999).

185. A. P. Feinberg, B. Vogelstein, "A technique for radiolabeling DNA restriction endonuclease fragments to high specific activity". Addendum. *Anal Biochem* **137**, 266 (Feb, 1984).

186. C. L. Stewart, Production of chimeras between embryonic stem cells and embryos. *Methods Enzymol* **225**, 823 (1993).

187. G. J. Darlington, H. P. Bernhard, R. A. Miller, F. H. Ruddle, Expression of liver phenotypes in cultured mouse hepatoma cells. *J Natl Cancer Inst* **64**, 809 (Apr, 1980).

188. G. J. Darlington, Liver cell lines. *Methods Enzymol* **151**, 19 (1987).

189. C. Kellendonk, C. Opherk, K. Anlag, G. Schutz, F. Tronche, Hepatocyte-specific expression of Cre recombinase. *Genesis* **26**, 151 (Feb, 2000).

190. U. K. Laemmli, Cleavage of structural proteins during the assembly of the head of bacteriophage T4. *Nature* **227**, 680 (Aug 15, 1970).

191. J. Rappsilber, M. Mann, Y. Ishihama, Protocol for micro-purification, enrichment, pre-fractionation and storage of peptides for proteomics using StageTips. *Nat Protoc* **2**, 1896 (2007).

192. J. Cox, M. Mann, MaxQuant enables high peptide identification rates, individualized p.p.b.-range mass accuracies and proteome-wide protein quantification. *Nat Biotechnol* **26**, 1367 (Dec, 2008).

193. J. Cox, M. Mann, Quantitative, high-resolution proteomics for data-driven systems biology. *Annu Rev Biochem* **80**, 273 (Jun 7, 2011).

194. J. Cox *et al.*, A practical guide to the MaxQuant computational platform for SILAC-based quantitative proteomics. *Nat Protoc* **4**, 698 (2009).

195. B. F. Belgardt *et al.*, PDK1 deficiency in POMC-expressing cells reveals FOXO1-dependent and -independent pathways in control of energy homeostasis and stress response. *Cell Metab* **7**, 291 (Apr, 2008).

196. R. N. Kulkarni *et al.*, Altered function of insulin receptor substrate-1-deficient mouse islets and cultured beta-cell lines. *J Clin Invest* **104**, R69 (Dec, 1999).

197. J. C. Bruning *et al.*, Role of brain insulin receptor in control of body weight and reproduction. *Science* **289**, 2122 (Sep 22, 2000).

198. S. Tanaka, L. Mohr, E. V. Schmidt, K. Sugimachi, J. R. Wands, Biological effects of human insulin receptor substrate-1 overexpression in hepatocytes. *Hepatology* **26**, 598 (Sep, 1997).

199. R. K. Dearth *et al.*, Mammary tumorigenesis and metastasis caused by overexpression of insulin receptor substrate 1 (IRS-1) or IRS-2. *Mol Cell Biol* **26**, 9302 (Dec, 2006).

200. E. Surmacz, J. L. Burgaud, Overexpression of insulin receptor substrate 1 (IRS-1) in the human breast cancer cell line MCF-7 induces loss of estrogen requirements for growth and transformation. *Clin Cancer Res* **1**, 1429 (Nov, 1995).

201. B. Draznin, Molecular mechanisms of insulin resistance: serine phosphorylation of insulin receptor substrate-1 and increased expression of p85alpha: the two sides of a coin. *Diabetes* **55**, 2392 (Aug, 2006).

202. M. A. Cornier, D. H. Bessesen, I. Gurevich, J. W. Leitner, B. Draznin, Nutritional upregulation of p85alpha expression is an early molecular manifestation of insulin resistance. *Diabetologia* **49**, 748 (Apr, 2006).

203. F. Mauvais-Jarvis *et al.*, Reduced expression of the murine p85alpha subunit of phosphoinositide 3-kinase improves insulin signaling and ameliorates diabetes. *J Clin Invest* **109**, 141 (Jan, 2002).

204. K. Ueki *et al.*, Increased insulin sensitivity in mice lacking p85beta subunit of phosphoinositide 3-kinase. *Proc Natl Acad Sci U S A* **99**, 419 (Jan 8, 2002).

205. A. Aitken *et al.*, 14-3-3 proteins: a highly conserved, widespread family of eukaryotic proteins. *Trends Biochem Sci* **17**, 498 (Dec, 1992).

206. D. H. Jones, S. Ley, A. Aitken, Isoforms of 14-3-3 protein can form homo- and heterodimers in vivo and in vitro: implications for function as adapter proteins. *FEBS Lett* **368**, 55 (Jul 10, 1995).

207. A. Craparo, R. Freund, T. A. Gustafson, 14-3-3 (epsilon) interacts with the insulin-like growth factor I receptor and insulin receptor substrate I in a phosphoserine-dependent manner. *J Biol Chem* **272**, 11663 (Apr 25, 1997).

208. A. Kosaki, K. Yamada, J. Suga, A. Otaka, H. Kuzuya, 14-3-3beta protein associates with insulin receptor substrate 1 and decreases insulin-stimulated phosphatidylinositol 3'-kinase activity in 3T3L1 adipocytes. *J Biol Chem* **273**, 940 (Jan 9, 1998).

209. T. Ogihara *et al.*, 14-3-3 protein binds to insulin receptor substrate-1, one of the binding sites of which is in the phosphotyrosine binding domain. *J Biol Chem* **272**, 25267 (Oct 3, 1997).

210. X. Xiang *et al.*, 14-3-3 facilitates insulin-stimulated intracellular trafficking of insulin receptor substrate 1. *Mol Endocrinol* **16**, 552 (Mar, 2002).

211. D. Pflieger *et al.*, Quantitative proteomic analysis of protein complexes: concurrent identification of interactors and their state of phosphorylation. *Mol Cell Proteomics* **7**, 326 (Feb, 2008).

212. E. Yamada, J. E. Pessin, I. J. Kurland, G. J. Schwartz, C. C. Bastie, Fyn-dependent regulation of energy expenditure and body weight is mediated by tyrosine phosphorylation of LKB1. *Cell Metab* **11**, 113 (Feb 3, 2010).

213. A. K. Al-Hakim *et al.*, 14-3-3 cooperates with LKB1 to regulate the activity and localization of QSK and SIK. *J Cell Sci* **118**, 5661 (Dec 1, 2005).

214. N. Horike *et al.*, Adipose-specific expression, phosphorylation of Ser794 in insulin receptor substrate-1, and activation in diabetic animals of salt-inducible kinase-2. *J Biol Chem* **278**, 18440 (May 16, 2003).

215. X. J. Sun *et al.*, The Fyn tyrosine kinase binds Irs-1 and forms a distinct signaling complex during insulin stimulation. *J Biol Chem* **271**, 10583 (May 3, 1996).

216. H. Sun *et al.*, Insulin-like growth factor I receptor signaling and nuclear translocation of insulin receptor substrates 1 and 2. *Mol Endocrinol* **17**, 472 (Mar, 2003).

217. X. Tu *et al.*, Nuclear translocation of insulin receptor substrate-1 by oncogenes and Igf-I. Effect on ribosomal RNA synthesis. *J Biol Chem* **277**, 44357 (Nov 15, 2002).

218. J. M. Boylan, P. A. Gruppuso, Insulin receptor substrate-1 is present in hepatocyte nuclei from intact rats. *Endocrinology* **143**, 4178 (Nov, 2002).

219. R. Baserga, Is cell size important? *Cell Cycle* **6**, 814 (Apr 1, 2007).

220. T. Moss, At the crossroads of growth control; making ribosomal RNA. *Curr Opin Genet Dev* **14**, 210 (Apr, 2004).

221. A. Wu, J. Chen, R. Baserga, Nuclear insulin receptor substrate-1 activates promoters of cell cycle progression genes. *Oncogene* **27**, 397 (Jan 10, 2008).

222. S. Liu *et al.*, Insulin signaling regulates mitochondrial function in pancreatic beta-cells. *PLoS One* **4**, e7983 (2009).

223. Z. Cheng *et al.*, Foxo1 integrates insulin signaling with mitochondrial function in the liver. *Nat Med* **15**, 1307 (Nov, 2009).

224. Z. A. Wood, E. Schroder, J. Robin Harris, L. B. Poole, Structure, mechanism and regulation of peroxiredoxins. *Trends Biochem Sci* **28**, 32 (Jan, 2003).

225. C. Brinkmann *et al.*, Training alters the skeletal muscle antioxidative capacity in non-insulin-dependent type 2 diabetic men. *Scand J Med Sci Sports*, (Apr 8, 2011).

226. A. Whaley-Connell, P. A. McCullough, J. R. Sowers, The role of oxidative stress in the metabolic syndrome. *Rev Cardiovasc Med* **12**, 21 (2011).

227. A. L. Nieminen, Apoptosis and necrosis in health and disease: role of mitochondria. *Int Rev Cytol* **224**, 29 (2003).

228. B. B. Lowell, G. I. Shulman, Mitochondrial dysfunction and type 2 diabetes. *Science* **307**, 384 (Jan 21, 2005).

229. R. Parish, K. F. Petersen, Mitochondrial dysfunction and type 2 diabetes. *Curr Diab Rep* **5**, 177 (Jun, 2005).

230. J. H. Lim *et al.*, Mitochondrial dysfunction induces aberrant insulin signalling and glucose utilisation in murine C2C12 myotube cells. *Diabetologia* **49**, 1924 (Aug, 2006).

231. H. J. Harwood, Jr., Treating the metabolic syndrome: acetyl-CoA carboxylase inhibition. *Expert Opin Ther Targets* **9**, 267 (Apr, 2005).

232. C. Wang, S. Rajput, K. Watabe, D. F. Liao, D. Cao, Acetyl-CoA carboxylase-a as a novel target for cancer therapy. *Front Biosci (Schol Ed)* **2**, 515 (2010).

233. M. F. Utter, D. B. Keech, Formation of oxaloacetate from pyruvate and carbon dioxide. *J Biol Chem* **235**, PC17 (May, 1960).

234. J. Lombard, D. Moreira, Early evolution of the biotin-dependent carboxylase family. *BMC Evol Biol* **11**, 232 (Aug 9, 2011).

235. F. C. Stevens, Calmodulin: an introduction. *Can J Biochem Cell Biol* **61**, 906 (Aug, 1983).

236. D. Chin, A. R. Means, Calmodulin: a prototypical calcium sensor. *Trends Cell Biol* **10**, 322 (Aug, 2000).

237. S. Liang *et al.*, Analysis of the protein complex associated with 14-3-3 epsilon by a deuterated-leucine labeling quantitative proteomics strategy. *J Chromatogr B Analyt Technol Biomed Life Sci* **877**, 627 (Mar 1, 2009).

238. G. J. Doherty, H. T. McMahon, Mediation, modulation, and consequences of membrane-cytoskeleton interactions. *Annu Rev Biophys* **37**, 65 (2008).

Acknowledgements

Performing research and writing a thesis would be impossible without the help of numerous others. First, I want to thank Prof. Jens Brüning for making this research project possible. Not only did he advance the project by his tireless quest for new scientific directions but also by creating the diverse research environment I was able to work in. Second, I would like to thank Prof. Günter Schwarz to be second chair on my thesis committee. In addition to his participation in SFB635, he was available for discussions about the TAP purification from early stages of the project onwards and shared his knowledge on streptavidin purifications with me.

For their technical skills and introduction in the CECAD mass spectrometry facility, I thank Dr. Tobias Lamkemeyer and Denise Ungrue.

Special thanks go to Dr. Marcus Krüger of the Max-Planck-Institute for Heart and Lung Research for the time-consuming data processing and quantification of mass-spectrometry results.

Within the lab, I want to thank Dr. Beatrice Coornaert for valuable discussions about biochemistry and Western blots and Sigrid Irlenbusch for guidance and assistance in cell culture experiments. Further, they both made everyday lab life more colorful for me.

All other lab members who helped out with all kinds of support, in smaller or larger issues, I want to thank a lot.

For thorough proof-reading and critical questions I want to say a big thank you to Dr. Beatrice Coornaert, Dr. Carmen Sanchez, Dr. Nora Redemann and Hayley Nicholls, PhD.

Furthermore, my project was integrated in and funded by the SFB 635, which provided an environment where I got a lot of feedback on my work, from colleagues as well as project leaders and professors. Especially, I want to thank Prof. Thomas Langer for leading the SFB and Claudia Ballweg for her continuous organization of retreats.

Finally, I want to thank my family for giving me any possible support. My parents, Linde and Klaus, my brother Timo and last but not least my husband Christoph always encouraged me to follow my greater plan for life, but also provided for manifold distractions in times when science needed to be put on hold. And yet, I thank them for not having to apologize for extensive times spent in this *unacquainted and curious world of labs and experiments.*

Statement / Erklärung

Ich versichere, dass ich die von mir vorgelegte Dissertation selbständig angefertigt, die benutzten Quellen und Hilfsmittel vollständig angegeben und die Stellen der Arbeit – einschließlich Tabellen, Karten und Abbildungen –, die anderen Werken im Wortlaut oder dem Sinn nach entnommen sind, in jedem Einzelfall als Entlehnung kenntlich gemacht habe; dass diese Dissertation noch keiner anderen Fakultät oder Universität zur Prüfung vorgelegen hat; dass sie noch nicht veröffentlicht worden ist sowie, dass ich eine solche Veröffentlichung vor Abschluss des Promotionsverfahrens nicht vornehmen werde. Die Bestimmungen der Promotionsordnung sind mir bekannt. Die von mir vorgelegte Dissertation ist von Prof. Dr. Jens C. Brüning betreut worden.

Köln, August 2011

Nina Vanessa Wegner